UNIVERSITÉ DU QUÉBEC
À CHICOUTIMI

MEMOIRE PRESENTÉ À
L'UNIVERSITÉ DU QUÉBEC À CHICOUTIMI

COMME UNE EXIGENCE PARTIELLE
DE LA MAÎTRISE EN INGÉNIERIE

PAR

HUSSEIN MOHAMED ALY ABDELSALAM BARAKAT

CHARACTERISTIQUES DE PERÇAGE ET DE TARAUDAGE DES ALLIAGES COULÉS Al-Cu ET Al-Si

Juin 2019

MASTER THESIS SUBMITTED TO THE
UNIVERSITÉ DU QUÉBEC À CHICOUTIMI

IN PARTIAL FULFILLEMENT OF THE
REQUIREMENTS FOR THE DEGREE OF
MASTER IN ENGINEERING

BY

HUSSEIN MOHAMED ALY ABDELSALAM BARAKAT

DRILLING AND TAPPING CHARACTERISTICS OF Al-Cu AND Al-Si CAST ALLOYS

June 2019

ACKNOWLEDGEMENTS

I would like to express my endless praise and gratitude to God, for his blessings and graces, who gave me this amazing opportunity from the early beginnings, and not ending by writing these words here.

I would like to express my sincere thanks and gratitude to Dr. Fawzy H Samuel, my supervisor and Professor at Université du Québec à Chicoutimi (Canada) for his continuous support and guidance along every stage of research, providing every opportunity to learn, in both academic and life aspects. I would like to express the whole gratitude also to Dr. Agnes Marie Samuel, Research Professor at Université du Québec à Chicoutimi (Canada) for her support, kindness and patience to guide, correct and tolerate with the mistakes of beginners in the research domain. I feel lucky and thankful that I had their continuous guidance, whereas it was impossible to finish this Master thesis without their support. As well, I would also like to express my sincere thanks to Dr. H. Doty and Dr. S. Valtierra for their kind interest, and valuable discussions. In addition, I would express my deep gratitude to Dr. Yasser Zedan, for his indispensable help and valuable support during the experimental phase in CTA laboratories in Montreal.

Financial support in the form of scholarships received from the Natural Sciences and Engineering Research Council of Canada (NSERC), the Centre Quebecois de Recherche et de Developpement de l'Aluminium (CQRDA), General Motors Powertrain Group (U.S.A), and Corporativo Nemak (Mexico) is gratefully acknowledged.

I would also like to express my appreciation to several colleagues in TAMLA group. A deep heartfelt gratefulness is due to Dr. Mohamed Hassan A. Abdelaziz. He is totally grace from god that he sent to me. I owe him his continuous assistance and his kind and caring attitude in each step since the first message between us in Malaysia. As well, I feel totally grateful to my colleague and my friend Marwan Hamed, for his kind and caring soul as well as his sincere support that you can count on. I would like to thank as well Abram Girgis for his help to adapt and explore the society and Mohamed Gamal for his valuable advices.

Finally and importantly, a deep and sincere heartfelt gratitude is for my family; My father the hidden hero of my life, my mother the closest consultant in my decisions, my

brother my backbone to act, my sister my wings to dream, my wife my soul to live and the whole family. I could never ever pay them back their sincere support, love, care and encouragement. Fear tells you where to go, but it is really hard to follow your fear without someone who hug you and tell you that he will be there for you.

For all of you, thank you so much..

Hussein Barakat

RÉSUMÉ

La présente étude a été réalisée sur un alliage Al-6% Cu-0,7% Si, et sur des alliages 319 et 356 après différents traitements thermiques. La tâche principale consistait à évaluer les caractéristiques de forage et de taraudage de l'alliage Al-Cu par rapport aux alliages à base d'Al-Si 319 et 356. Les travaux de forage ont été effectués sur une machine à commande numérique Huron K2X8five à 15000 tr/min avec refroidissement continu pour absorber la chaleur et nettoyer les trous des copeaux formés lors du forage. Les résultats montrent que l'addition de Si couplée au traitement de vieillissement T6 produit les forces de coupe les plus élevées (environ 360N) parmi les alliages étudiés (environ 270N) après 2500 trous. Compte tenu des alliages à base d'Al-Cu, la modification du traitement de vieillissement n'a pratiquement aucune incidence sur les forces de coupe. Apparemment, une teneur élevée en Cu joue le rôle d'autolubrifiant, facilitant le processus de forage jusqu'à 2700 trous, sans aucun signe d'usure de l'outil. Cependant, en raison du faible niveau de Si dans l'alliage à base d'Al-Cu, le BUE est plus fréquent, avec des copeaux coniques, ce qui affecterait la précision de la taille du trou foré. Les copeaux sont normalement mats et caractérisés par leurs surfaces rugueuses comparées à celles obtenues avec l'alliage A356.0. Le taraudage des trous forés a été réalisé à l'aide de taraud Guhring 971 H6 M6 6HX-Carbide. Les alliages à base de HT200 ont révélé une excellente usinabilité sans signe d'usure de l'outil après 2500 trous. En revanche, l'outil a cédé après 1600 trous dans le cas d'un alliage 356 et 2160 trous dans l'alliage 319. Ainsi, il est conclu que la présence de 3,5% de Cu dans l'alliage 319 a contribué à réduire la sévérité de l'usure due aux particules de Si eutectique. Cependant, les forces de taraudage ont atteint 120N avant la rupture, contre environ 75 N dans le cas des alliages à base de T200.

ABSTRACT

The present study was performed on an Al-6% Cu-0.7%Si alloy, and 319 and 356 alloys following different heat treatments. The main task was to evaluate the drilling and tapping characteristics of the Al-Cu alloy with respect to the Al-Si based 319 and 356 alloys. The drilling work was carried out on a Huron K2X8five CNC machine at 15,000rpm with continuous cooling to absorb the heat and to clean the holes from the chips formed during the drilling operation. The results show that addition of Si coupled with T6 aging treatment produces the highest cutting forces (about 360N) among the alloys studied (approximately 270N) after 2500 holes. Considering the Al-Cu based alloys, varying the aging treatment has practically no significant bearing on the cutting forces. Apparently, a high Cu content acts as a self-lubricant, facilitating the drilling process up to 2700 holes, with no sign of tool wear. However, due to the low level of Si in the Al-Cu based alloy, built up edge (BUE) is more frequent, with conical chips, which would affect the precision of the size of the drilled hole. The chips are normally dull and characterized by their rough surfaces compared to those obtained from A356.0 alloy. Tapping of the drilled holes was carried out using Guhring 971 H6 M6 6HX- Carbide taps. The HT200 Al-Cu based alloys revealed excellent machinability with no sign of tool wearing after 2500 holes. In contrast, the tool was failed after 1600 holes in case of 356 alloy and 2160 holes for 319 alloy. Thus, it is concluded that the presence of 3.5% Cu in the 319 alloy helped in reducing the severity of wearing due to eutectic Si particles. However, the tapping forces reached to 120N prior to failure compared to about 75 N in the case of T200 based alloys.

TABLE OF CONTENTS

LIST OF TABLES

LIST OF FIGURES

CHAPTER 1

DEFINITION OF THE PROBLEM

CHAPTER 1

DEFINITION OF THE PROBLEM

1.1 Introduction

This study aims to relate the characteristics of aluminum cast alloys with their machinability behavior when subjected to different processes of machining. It is based on an analysis of the machinability behavior of aluminum-silicon (Al-Si) and aluminum-copper (Al-Cu) cast alloys, with the focus on a new Al-Cu alloy HT200, and its machinability features, and its potential to compete with commercial Al-Si cast alloys such as the well-established A319.0 and A356.0 Al-Si type alloys.

Aluminum gains its economic importance from its abundance in addition to its unique combination of properties, which make it versatile for a wide range of applications. Aluminum is the third most common chemical element in the crust of the earth after oxygen and silicon, occupying 8% of the earth's surface [1, 2]. It exists naturally in the soil in bauxite ore associated with other elements, mainly in oxide and hydroxide forms. In addition to its abundance, three main properties of aluminum made it attractive for various industries; which are low density, high mechanical strength for its alloys and high corrosion resistance. In addition, other properties of aluminum such as thermal and electrical conductivity, reflectivity, ductility, recyclability and non-poisonous effect facilitate its use in several industries [3].

Aluminum has a low density (2.7 gm/cm^3), almost one third that of steel but contrary to steel, it resists progressive oxidation. In addition, the electrical and thermal resistance of aluminum is almost double the resistance of copper, which make it an economic material for electrical industries, with 2.65×10^{-8} Ω/m electrical resistance for pure aluminum [4]. On the other hand, despite the softness of pure aluminum, with a tensile strength of 45 MPa [5], alloying aluminum with other elements can improve its strength dramatically, and high strength commercial alloys have been developed with tensile strengths up to 505 MPa [6], with very good elongation and hardness characteristics.

The Hall–Héroult process simultaneously discovered in 1886 by American Charles Martin Hall and Frenchman Paul Héroult, provided an inexpensive method for producing pure aluminum, and paved the way for its commercialization [3]. The increasing importance of aluminum may be noted from the annual growth of production where, since 1995, primary aluminum production of the world has grown 5% annually [2] with an extraction rate of bauxite around 211 million tons annually [7].

Aluminum is used in several industries all over the world. Transportation - mainly automotive applications - consumes 40% of aluminum in the United States, followed by packaging industries which consumes 28%. The construction industry consumes 13%, consumer durables 7%, and electrical applications 5% (USGS-2007) [1]. Three major emerging markets seek Aluminium as an economic element for their equipment and products [6]:

- Electrification: in cable design and electrical towers because of low density, corrosion resistance and high conductivity properties of aluminum.

- Automotive: Mainly in engines where the low density of aluminum affects significantly vehicle performance, significant reduction in fuel consumption, engine noise and vibration.
- Aviation and aerospace industry.

Alloying aluminum is one of the most common methods to improve its properties. Aluminum is usually alloyed with copper, silicon and magnesium [8] in addition to zinc and tin. Aluminum alloys can be classified into two main categories based on the method of fabrication: wrought alloys and cast alloys [4]. Copper improves strength and hardness of the alloy at both room and elevated temperatures, and ameliorates its response to heat treatment but reduces resistance to general corrosion and hot tearing, and increases the potential for interdendritic shrinkage and solidification cracking. Thus grain refinement and chilling become necessary to avoid these casting defects.

Copper is usually used in association with magnesium and silver to give the highest strength capability for commercial casting alloys [6]. Silicon on the other hand, improves castability, fluidity, weldability, corrosion resistance and hot tearing resistance. In addition, aluminum-silicon (Al-Si) alloys show low specific gravity and low thermal expansion. These factors, together with their excellent castability of Al-Si alloys are the reasons why these alloys constitute more than 80% of all aluminum alloy castings produced [9]. The main disadvantage with the use of silicon is that it affects the alloy machinability, as the silicon phase formed in the Al-Si eutectic reaction (during solidification of the alloy) is an acicular, brittle phase, almost ten times harder than the aluminum matrix [9]. However, modification of the eutectic Si phase morphology to a fine fibrous form with the use of modifier elements such as strontium can improve the machinability characteristics [4].

Copper and/or magnesium are usually added to Al-Si alloys to improve the alloy strength. The resulting Al-Si-Cu, Al-Si-Mg or Al-Si-Cu-Mg alloys exhibit high strength and good machinability, in addition to good castability characteristics. The presence of Cu and Mg renders the alloys heat-treatable, and the strength and hardness of the alloy are improved through the formation of hardening precipitates of $CuAl_2$ and Mg_2Si following the aging stage during the heat treatment process. Binary Al-Mg alloys are used frequently in applications that require bright surface finish and corrosion resistance, while Al-Si-Mg alloys are widely used to get excellent casting characteristics as well as very good mechanical properties after heat treatment [6].

Machining is one of the most important processes undertaken in almost all industries from both technical and economical aspects, where more than 90% of manufactured parts require machining before the part is ready for use [9]. Merchant [10] mentioned that the cost of machining in industrialized countries amounts to more than 15% of the value of all manufactured products. Machining is the process of removing excessive material from a manufactured part or workpiece to achieve a specific geometry. Very tight dimensional tolerances can be obtained with machining [11], in addition to its potential to be applied on metallic and non-metallic materials [10]. Machining processes can be categorized into three main types, which are [12, 13]:

- Conventional machining: These processes which include a hard tool form a less hard work piece through the mechanical removal of chips by metal to metal friction, to achieve the desired geometry; such processes include turning, milling and drilling. Usually the cutting process forms macroscopic chips or particles with thicknesses of about 0.025mm to 2.5mm.

- Abrasive processes: which remove material by the mechanical action of abrasive particles, such as grinding. The size of chips produced in this process varies from 0.0025mm to 0.25mm.
- Non-traditional machining: where various energies are used to form the work piece by removing chips from it by non-traditional methods, such as chemical machining or electrical discharge machining. Usually the chips formed in this process are submicroscopic in size.

Whereas manufacturing process selection is based on cost, time and precision [10], the evaluation of machinability for different materials is an industrial necessity to appraise the convenience of the material to be machined under certain conditions. Machinability may thus be considered as a property of the system resulting from the interaction between workpiece, cutting tool, and cutting medium in different removal sequences and conditions to represent the relative ease of the material removal process [8, 9, 12]. Because of the wide variety of parameters associated with the process, actual machining tests are indispensable for determining machinability [11]. The major factors that affect machinability can be summarized in the machining operation, tool type and geometry, cutting conditions [11, 12] in addition to work piece characteristics such as [8, 14]:

- Alloy chemistry, additions,
- Morphology, size and volume fraction of the constituent phases,
- Microstructure (grain refining and modification),
- Porosity,
- Heat treatment, and

- Physical and mechanical properties.

Machinability is usually assessed in the majority of applications by tool life, tool wear, cutting forces, power in operation, cutting temperature and material removal rate under certain cutting conditions [12]. In addition to these tests, several tests are carried on in order to assure the precision of the process such as dimensional accuracy, chip formation and surface integrity, which is related to the study of surface roughness, wear, and fatigue [10]. In some applications, in order to facilitate assessment of the material, a standard material is chosen, usually B1112 steel, as a machining reference, for comparison purposes. The behavior of the material is compared to the reference material using a mathematical index called machinability rating [12].

Machining of pure aluminum is generally complicated and requires special techniques because of its softness and ductility [5]. This softness increases the probability of adhesion of material on the cutting edge, causing a build-up which produces a low quality surface. Alloying aluminum increases the machinability of the metal, especially with proper cold hardening or heat treatment, and reduces problems such as built-up edge (BUE), burrs, surface roughness and the formation of long chips. Moreover, elements out of the solution can also improve the machinability of aluminum alloys, because they act as chip breakers. A chip breaker improves chip control and reduces cutting resistance. Elements such as lead and bismuth in sufficient quantities provide this breakability effect for the chips, which allows increased machining speeds and reduces the cutting fluid required for machining. Intermetallic constituents such as $CuAl_2$ generally also have the same effects on machinability. On the other hand, complex intermetallics with a high level of hardness can cause a significant decrease in tool life in spite of their chip breaker effect [4].

The presence of hard phases such as the primary Si particles in hypereutectic Al-Si cast alloys is also detrimental to tool life. Using phosphorus in such alloys can refine the primary Si particles, as also modifying the eutectic Si morphology using Na or Sr and improve the machinability of Al-Si alloys [5].

1.2 Objectives

The present study was undertaken to investigate the machinability behavior of Alloy HT200, an Al-Cu based alloy, under different heat treatment conditions, to measure its comportment under different machining processes, using well-established A319 and A356 alloys as standardized references for comparison. The machining processes covered in this study are drilling and tapping. In order to measure the response of alloy HT200 to these processes, the following aspects were examined on casting blocks prepared from these alloys and used in the as-cast and heat-treated conditions.

- Cutting force measurements
- Tool life evaluation
- Built-up edge (BUE) measurements
- Chip formation

In addition to the above, microstructures were examined and tensile properties determined for the different alloys/conditions used in order to evaluate the performance of the HT200 alloy in industrial machining processes compared to the commercial alloys. The purpose of this was two-fold: (i) to improve understanding of the effects of heat treatment regime and alloying elements on the machinability behaviour of Al-Cu alloys, and (ii) optimize the alloy behavior in relation to the machining processes under specific machining conditions.

Five alloys were investigated: three HT200 alloys – used in the as-cast, T5, and T7 heat-treated condition, and A319 and A356 alloys, coded as alloys A, B, C, D, and E. The alloy codes and corresponding alloy and heat treatment condition are listed in Table 1-1.

Table 1-1 Alloys used in the study

The objectives of this study are therefore as follows:

Alloy **A**	HT200 - As Cast
Alloy **B**	HT200 – T5
Alloy **C**	HT200 – T7
Alloy **D**	A 319 – T7
Alloy **E**	356 – T6

- Investigate the general machinability behavior of Alloy HT200 under different heat treatment regimes with respect to drilling and tapping processes.
- Assess the effect of metallurgical features on the machining behavior of HT200 alloys.
- Evaluate the effect of different heat treatment regimes on the mechanical properties of HT200 alloy in comparison to heat-treated commercial alloys.
- Understand the effect of morphological and microstructural characteristics on different aspects of machinability tests, such as required cutting force, tool life, built up edge and chip formation.
- Evaluate the tool response to HT200 alloy in terms of wear, tool life and built up edge.

1.3 References

1- R.D. Harbison, M. Bourgeois and G. Johnson (2015), Hamilton & Hardy's Industrial Toxicology, 6th Edition, Wiley.

2- A. Dunsby, J. Eckstein, J. Gaspar and S. Mulholland (2008), Commodity Investing: Maximizing Returns through Fundamental Analysis, Wiley.

3- P.G. Sheasby and R. Pinner (2001), The Surface Treatment and Finishing of Aluminum and Its Alloys, 6th Edition

4-

5- J.R. Davis (Ed.) (2001), Alloying: Understanding the Basics, 1st Edition, ASM International, Metals Park, OH, pp. 351-416

6- J.E. Hatch (Ed.) (1984), Aluminum: Properties and Physical Metallurgy, ASM International, Metals Park, OH, pp. 1-24

7- J.G. Kaufman and E.L. Rooy (2004), Aluminum Alloy Castings: Properties, Processes, and Applications, ASM International, Metals Park, OH.

8- R. S. Gendron, M. Ingulstad and E. Storli (Eds) (2013), Aluminum Ore: The Political Economy of the Global Bauxite Industry, UBC Press

9- M.M. Tash (2005), Effect Of Metallurgical Parameters On The Machining Behavior Of 356 And 319 Alloys (Drilling And Tapping Study), PhD Thesis. Université du Québec à Chicoutimi 2005

10- Y. Zedan (2010), Machinability Aspects Of Heat-Treated Al-(6-Ll)% Si Cast Alloys: Role Of Intermetallics And Free-Cutting Elements, PhD Thesis. Université du Québec à Chicoutimi 2010

11- J. Paulo Davim (Ed.) (2008), Machining: Fundamentals and Recent Advances, Springer.

12- G.H. Garza-Elizondo (2010), Machinability of Al-(7-Ll%)Si Casting Alloys: Role of Free-Cutting Elements, MSc. Thesis. Université du Québec à Chicoutimi 2010

13- M.P. Groover (2010), Fundamentals of Modern Manufacturing: Materials, Processes and Systems. 4th Edition, John Wiley & Sons, Inc., Hoboken, NJ.

14- M.C. Shaw (2005), Metal Cutting Principles. 2nd Edition, Oxford University Press, New York – Oxford.

15- J. Jorstad, "Influence of Aluminum Casting Alloy Metallurgical Factors on Machinability", Society of Automotive Engineers, 400 Commonwealth Dr., Warrendale, PA, 1980 (Report, 15 pages).

CHAPTER 2

REVIEW OF LITERATURE

CHAPTER 2

REVIEW OF LITERATURE

2.1 Introduction

In this chapter, a review of the literature is carried out and is summarized, in order to clarify the concept of machinability and the different dimensions of this phenomenon, as well as the variables of the process that affect machinability. The complexity of the concept of machinability comes from the integration of workpiece metallurgical factors, tool design parameters and cutting conditions, which result in considering machinability in terms of the whole cutting system, not just the workpiece material characteristics in spite of its major participation in the machining process. Thus, in this chapter, the concept of machinability and its evaluation methods will be discussed, as well as the factors affecting the process in previous studies related to aluminum alloys as the focus of interest.

2.2 Machinability

Machining is a complex, nonlinear and multivariate process [1], and the properties of the machined material affect the machining time, quality and conditions. Therefore machinability concerns studying the phenomenon of interaction between the workpiece, the cutting tool and the cutting medium in different removal sequences and cutting conditions [2]. Machinability is defined as the relative ease with which a metal can be cut or machined in a material removal process, under specific conditions [3]. However, the term is a difficult property to quantify, because of the multi-variables and non-qualitative evaluation that includes the machining variables. Astakhov differentiates between two different meanings of machinability: (i) Machinability of the work material, (ii) and Process machinability. Machinability of the work material should be considered as a property of the work material that relates to its physico-mechanical properties, and it represents the ultimate goal of machining optimization. On the other hand, the Process machinability relates to the machining conditions, and represents the reduction of the current machining condition from the optimum machining conditions [4].

Machining of aluminum alloys is among the most common machining processes that take place industrially. Aluminum shows relatively low cutting forces in comparison to steel, with the potential to be machined at higher cutting speeds [5] (18). A brief survey of the literature on the machinability of aluminum alloys will demonstrate the role of metallurgical features, heat treatment and cutting conditions on important parameters of machinability such as tool life, surface integrity, cutting forces and chip formation. Figure 2-1 summarizes the major variables that affect the machining process and, hence, the machining results.

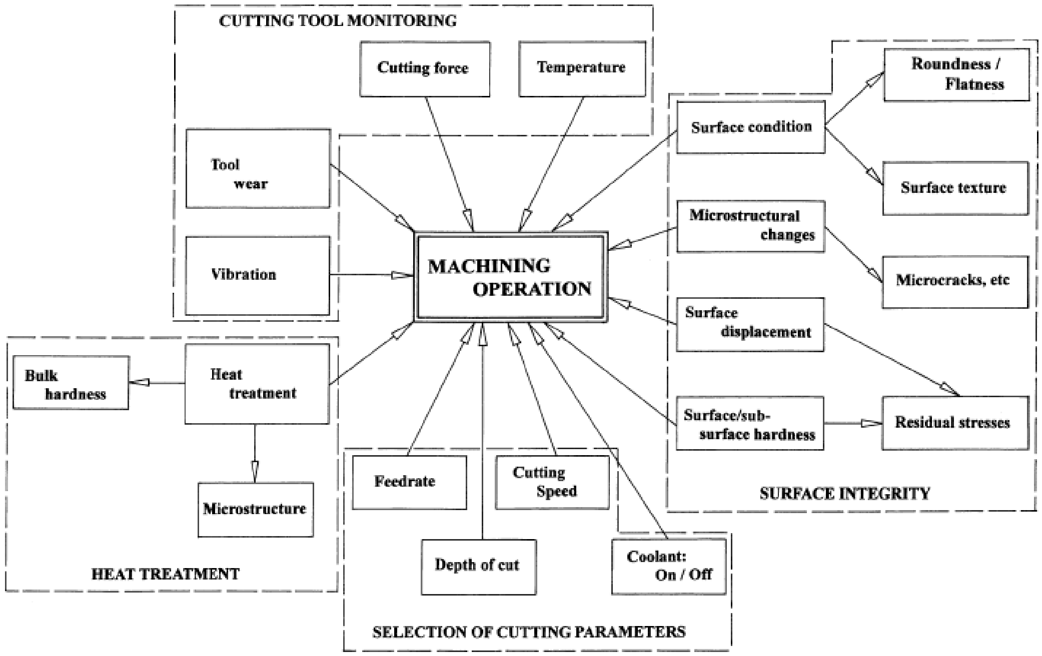

Figure 2-1 Main Variables of Machining Operation [6]

In order to assess the machinability of a specific material, several experimental tests were designed, to try to give numeric notions using these tests to describe qualitatively the relative ease of machining. According to Smith [6] as well as Mills and Redford [4, 7], these tests can be categorized into machining and non-machining testing programs. The first category is subdivided into absolute evaluation and ranking evaluation tests. The absolute evaluation machining tests include taper turning test, variable rate machining test and HSS tool wear-rate test, while ranking evaluation machining tests include rapid facing test, constant pressure test and degraded tool test. On the other hand, the non-machining testing category does not include a direct test of machinability, but measurement of factors that affect the machinability dramatically such as chemical composition, microstructure and physical properties [6]. In addition, international associations standardize different tests to evaluate machinability according to different norms, such as the ISO test based on ISO 3685, which tests tool-life with single-point turning tools and the ASTM test based on ASTM E618-07 for ferrous metals using automatic screw machine [4].

For the sake of simplification, one of the most commonly used indices to rate the machinability of the materials based on a reference material is the machinability index. This index represents the cutting speed based on 60 minutes tool life compared to the cutting speed of the reference material for the same tool life, where the reference material is SAE B111, SAE 1045, 1018, 1212 [8, 9].

$$I_m = \frac{100xV_{60\ (material)}}{100xV_{60\ (Ref.)}}\ x\ 100\ \%$$

Although experimental studies are indispensable to evaluate the machinability of a material [2], new computational techniques have been introduced in order to simulate the machining process for different alloys, thus estimating the machinability of the alloys and verifying the results by experimentation. Two major computational ways of studying machinability were developed in addition to the experimental method: physical-based modeling, and data-based modeling. In addition, hybrid algorithms are sometimes also used to simulate and predict the machinability of materials [1].

Physical based modeling depends on transforming the physical behavior into mathematical form based on cutting mechanics. Then the algorithm solves the mathematical model using computational techniques such as Finite Elements Method (FEM). This category of modeling is used to provide predictions of temperature, forces, torque, power, stresses, strain, and strain rate, such as the investigations for drilling process which were carried out by Fuh and Min et al. [10-12].

On the other hand, data based modelling develops different kind of models based on the data using soft computing tools such as artificial intelligence algorithms, neural networks and fuzzy sets. This method of simulation shows promising results with very low error margins such as the work of “Chien” to predict surface roughness, the cutting forces and tool life for 304 stainless steel, with a margin of error not exceeding 5.4% [13].

2.2.1 Criteria to evaluate the machinability of a material

Because of the complexity of evaluating machinability, various criteria were developed to transform the concept of machinability in an applicable way. The most important among these are [3, 4]:

- tool life
- cutting forces
- chip formation, and
- surface roughness.

In addition, other factors can be taken into consideration such as temperature rise, tool wear level, specific power consumed, dimensional tolerance and overall cost [14]. Although these four main criteria of evaluation simplify the study of machinability, the ease of measurability is not the same for the four criteria. While tool life can be easily evaluated by specific tool wear criteria, and cutting forces can be simply studied using dynamometry, chip formation includes chip breakability, chip morphology and built up edge. Moreover, the study of surface roughness extends to other aspects of surface integrity such as wear and stress concentration.

2.2.1.1 Tool Life

Tool life is one of the major economic issues in manufacturing processes. While the longer the tool goes, the cheaper the process becomes, however, the worse the work surface quality gets [15]. Three main kinds of failure can end the life of the tool: fracture failure, temperature failure and gradual wear. Fracture failure occurs by excessive applied forces over the cutting tool. Temperature failure takes place by excessive heat generation during the cutting process, which causes cutting point softening and deformation. Gradual wear failure occurs due to continuous interaction between the machined surface and cutting tool. Whereas the first two modes of failure are considered as premature failures, gradual wear failure is the preferred mode of failure because it represents the longest tool life for the cutting conditions [3].

While wear failure is a gradual process, the necessity to determine a specific limit to determine the end of tool life appears, especially with different areas and rates of wear taking place along the tool. In addition, tool life is not an absolute concept, but depends on the selected criteria according to the requirements of the operation [1]; so the criteria of tool life fulfill three main conditions; sustaining tolerances, maintaining surface quality and chip breakage efficiency [6]. Thus two main methods are used to evaluate tool-life capability: using tool life criteria such as burr height tolerance, or using tool life parameters such as tool life volume [16].

From a practical point of view, ISO 3685 mentions that the type of wear that is believed to contribute most shall be used as a guide of tool life criteria selection; otherwise, combined criteria can be used. Moreover, the same code mentions the specific values for flank and crater wear based on tool material, which can be summarized as follows [17]:

Table 2-1 Wear Criteria according to ISO 3685

	HSS	Sintered Carbide	Ceramics
VB_{max}	0.6 mm	0.6 mm	0.6 mm
VB_{avr}	0.3 mm	0.3 mm	0.3 mm
KT	———	0.06 + 0.3 f	———
KF	———	0.02 mm	———
Others	Catastrophic failure	Breakage of Crater at minor cutting edge	———

where VB_{max} is maximum width of flank wear, VB_{avr} is average width of flank wear, KT is depth of crater and KF is crater front distance.

Although ISO 3685 put forth a clear measurable method, the predictability of end of tool life without microscopic measurements is a practical need for industry. Thus different researches were carried out in order to assess tool life determination starting from Taylor who developed in 1907 an empirical formula to determine tool life based on time [1, 18]

$$V_c T^n = C$$

where V_c is cutting speed, T is tool life to develop a certain flank wear and n is an exponent based on cutting conditions. This formula was developed thereafter to include feed rate and depth of cut [1]:

$$V_c T^n f^a d^b = C$$

where a and b are experimentally determined. Different models and measurements were developed to avoid direct measurements of tool dimensions to evaluate tool life, such as Kovac's work to use thermal measurement to estimate tool life [19].

2.2.1.2 Cutting Forces

Among the different criteria of machinability evaluation, cutting forces have a significant role in the response of the material to the cutting process, whereas thrust forces identify the required energy to form the chips as well as tool wear. Thrust force increases significantly with wear of the cutting tool [5]. Several researches [20, 21] were carried out to predict tool life and surface roughness. Valavan [22] developed an equation to predict tool life based on cutting forces and workpiece surface temperature, while Zedan concluded that the major problem with studying cutting forces is their strong dependence on cutting conditions [5], as cutting forces depend on work piece material features, the shape of undeformed chips, as well as cutting tool geometry [23]. Thus several studies and models were published to analyse the dependence between the cutting force and these factors, such as that of Wang et al. [24] who studied the cutting forces and their relationship with cutting parameters in the reaming process and affirmed that thrust force decreases significantly with increasing cutting speed.

In drilling, cutting forces become more complex to analyse, as there are three different cutting edges: the main cutting edge, the chisel edge, and the margin cutting edge. Thus different empirical, theoretical and computational models were developed in order to have an accurate prediction based on cutting conditions and workpiece-tool interaction. While Zedan gave approximate values of participation of each cutting edge in thrust force [5], Minukhin developed an improved model focusing on the primary cutting edge as the main generator for thrust force and torque [25].

2.2.1.3 Chip Formation

Although chip layer is disposable, it gives a significant indication on the quality of the machining process. Four main mechanisms of chip formation can be distinguished: continuous formation, lamellar formation, segmented formation and discontinuous chip formation [23] as shown in Figure 2-2. Continuous chips result from high speed machining of ductile materials with small feeds and depth, while chips tend to deform discontinuously because of high brittleness [3]. The main parameters that affect the dominant mechanism of chip formation are thermo-physical properties and metallurgical features of the material and the cutting process conditions [26, 27].

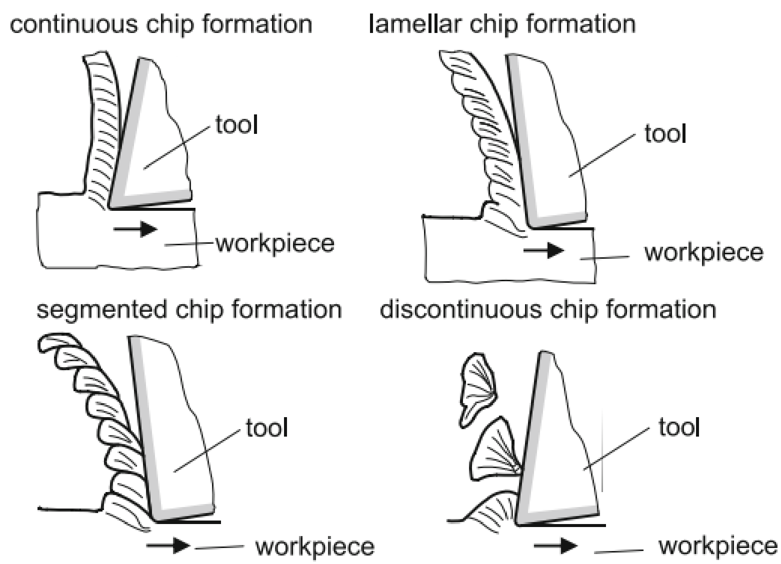

Figure 2-2 Different types of chips [23]

Moreover, measurements for chip morphology are extremely important to evaluate the quality of the machining process, such as chip volume ratio, which indicates the bulkiness of the chips. According to this measurement chips can be classified into eight classes [23]: ribbon chips, snarled chips, flat helical chips, long cylindrical helical chips, helical chip segments, spiral chips, spiral chip segments and discontinuous chips as shown in Figure 2-3. In drilling, a deeper investigation was carried out to classify six common shapes that may be generated in cast aluminum which are [28, 29]: conical chips, fan-shaped chips, chisel-edge chips, amorphous chips, needle chips and impacted chips. Elgallad [28] showed that conical chips and fan-shaped chips are in the desirable range of chip formation volume ratio, and their generation is caused by proper drilling process in aluminum cast alloys.

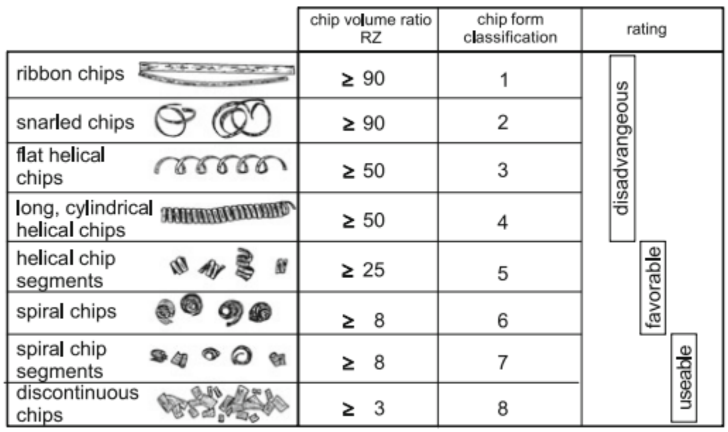

	chip volume ratio RZ	chip form classification	rating
ribbon chips	≥ 90	1	disadvangeous
snarled chips	≥ 90	2	
flat helical chips	≥ 50	3	
long, cylindrical helical chips	≥ 50	4	
helical chip segments	≥ 25	5	favorable
spiral chips	≥ 8	6	
spiral chip segments	≥ 8	7	useable
discontinuous chips	≥ 3	8	

source : Stahl-Eisen-Prüfblatt 1178-69

Figure 2-3 Chip forms (Steel Test Specification 1178-90) [23]

Built-up edge as well is an associated condition with chip formation mechanisms, in particular with continuous chip formation where chips adhere to the rake face and to cutting edges. Toenshoff summarized the conditions that cause built up edge, which are [23]:

- If the material advocates strain-hardening
- Stable and stationary chip formation
- Stagnant zone exists in front of the cutting edge in the stream of material flow
- Low temperature in chip formation zone, that does not allow recrystallization to take place

Thus hardened particles of built-up edge can adhere to the cutting edge and change the geometry of the cutting tool, which causes poor surface finish and tool wear. Usually this adherence effect can manifest in two forms: built-up edge and built-up layer [14]. In aluminum alloys the built-up edge forms in a composition close to pure aluminum, because the melting point of intermetallic particles is much higher in comparison to aluminum [30, 31]. With higher metal removal rates, a transition takes place from the built-up edge to the flow zone which can be considered as a thermoplastic shear band [14].

2.2.1.4 Surface Integrity

The differentiation between surface roughness and surface integrity was developed in 1964 by Field and Kahles [32]. The concept was developed to cover the modifications that resulted in the machined surface and near surface region due to machining in topographical, physical, mechanical, chemical, metallurgical and biological features [33]. Figure 2-4 shows the main aspects focused upon and measured from the surface and subsurface layer. In the machining of aluminum alloys, the three aspects usually considered important are the topography, mechanical and metallurgical features.

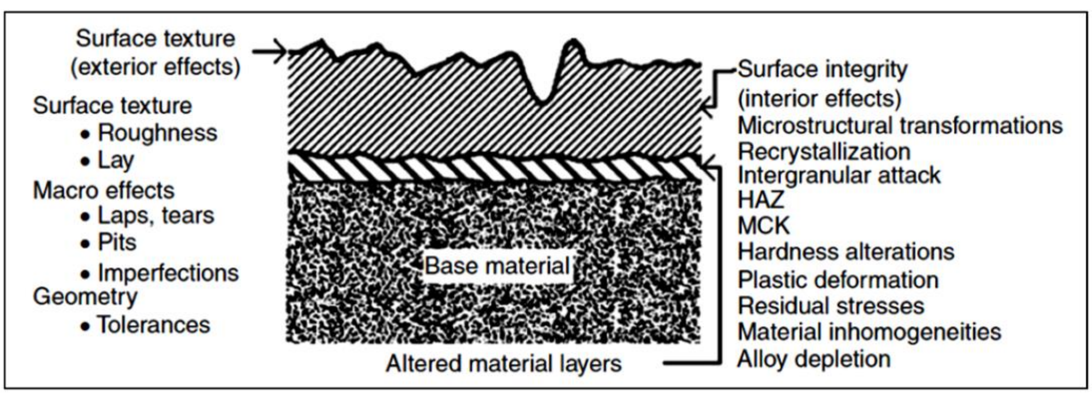

Figure 2-4 Typical machining affected layers [34]

For the surface conditions, two main aspects studied are surface topography and surface defects. For surface topography, according to El-Hofy, topographical features can be defined by roughness, waviness, lay and flaws [34]. As topographical features cannot be directly evaluated, different measuring procedures were designed to define surface characteristics based on three principles for testing [23]: tactile tests, optical tests and scanning probe microscopic tests. According to ISO 13565 four categories of parameters were selected for measurement [6, 32, 33]:

- Amplitude parameters, such as arithmetic mean roughness and maximum peak to valley height
- Spacing parameters, such as the mean spacing of the asperities at the level of the central line and peak count
- hybrid parameters, such as the root mean square slope of the profile
- waviness parameters, such as the mean value of the waviness

Surface defects include cracks, craters, scratches, inclusions and other features [35] which is not directly related to our point of research.

On the other hand, sub-surface alterations because of machining may include hardness changes, microstructure alterations, and residual stresses. The surface becomes exposed to strain hardening due to plastic deformation in the process of material removal. In addition, on the microstructural level, severe deformation can produce dislocations in the alloy matrix, and result in dynamic recrystallization and grain refinement [36, 37]. Several observations were recorded by Chen et al. [38] and Liu et al. [36] for phase formation in aluminum alloys due to machining. Internal residual stresses also can be locked in the alloy matrix after non-uniform plastic deformation because of misfit between grains due to dislocations or interface mismatching between grains [35, 39]. These residual stresses can have a positive effect if they are compressive type, or a negative effect in case of tensile type.

For surface integrity aspects in aluminum, proper cutting parameters have an advantageous effect on surface integrity. Cutting speed has a dominant effect on surface topography in comparison to the other machining factors [32]. Zedan et al. [40] investigated the drilling process in 6000 series of aluminum alloys and concluded that increasing cutting speed and feed rate also reduce the burr height significantly. Moreover, dry machining shows better surface roughness, while wet machining has a harmful effect on the diameter of the holes. But according to Shoemaker [35] in his investigation of 2024-T351 aluminum, the use of cutting fluid during machining does not have a significant effect on the residual stress profile, while other machining parameters such as cutting speed, feed rate and depth of cut have radical effect on the residual stress state [32, 41].

2.2.2 Factors affecting machinability

Based on the definition of the machinability process as the interaction between the workpiece, cutting tool and cutting medium for different removal sequences under different cutting conditions [2], the factors affecting machinability can be categorised into four categories, which are:

- Workpiece aspects, such as alloy composition, microstructural features, physical and mechanical properties and thermal and mechanical treatments
- Cutting tool aspects, which includes tool geometry, cutting tool material and tool wear studies

- Removal sequence aspects, the cutting process itself such as drilling, tapping, milling, reaming, etc.
- Cutting medium and cutting conditions to analyse the effect of cutting fluid on the process, as well as cutting parameters; cutting speed, feed rate and depth of cut.

The remainder of the literature review will follow this sequence in order to cover the main aspects influencing the machinability, to facilitate the interpretation of the results presented in Chapter 4.

2.3 Workpiece aspects

2.3.1 Introduction

In industry, it is rare to use aluminum in its pure form because of its softness, so different alloying elements and additives are added to aluminum to obtain alloys with suitable mechanical, physical and chemical properties. The major alloying elements in aluminum alloys are Silicon, Copper, Magnesium and Zinc [28, 42]. Silicon improves fluidity, castability and corrosion resistance but it reduces strength and machinability, so usually different modifiers are added to improve its properties. Copper on the other hand is used usually in both cast and wrought alloys to enhance strength and hardness at room temperature and elevated temperature, through precipitation hardening heat treatment. Magnesium is used in combination with copper to intensify age hardening process, or with silicon to improve characteristics after heat treatment in terms of strength and corrosion resistance. Zinc is usually paired with magnesium to ameliorate the response of the alloy to heat treatment [28, 43].

Metallurgical parameters that affect machinability can significantly affect the machinability of aluminium alloys. The most important metallurgical factors are [14, 44]:

- Alloying elements and additives
- Morphology, grain size and volume fraction
- Microstructure of the alloy
- Different heat and mechanical treatments
- Casting method and defects such as porosity
- Thermal, mechanical and physical properties

In terms of alloying elements, some elements can provide a degree of lubricity, while other elements increase matrix hardness or form hard intermetallic phases [14]. While copper and magnesium improve the strength characteristics through precipitation, increasing their content generally ameliorates the hardness of the alloy matrix, thereby reducing the friction with the tool, so surface quality improves significantly and decreases the possibility of built-up edge formation in addition to smaller and better chip formation. Silicon, on the other hand, is used to improve the fluidity of aluminum, but it harmfully affects the cutting tool because of its abrasive effect, causing tool wear. Thus different modifiers such as Strontium are added in order to reduce the detrimental effects of eutectic silicon by changing its morphology from acicular to fibrous [45]. Adding heavy metals to alloying elements can reduce machinability significantly because of their tendencies to form complex intermetallic phases (usually with Fe and Si) which cause hard spots in the form of sludge particles, thus increasing built-up edge. The role of morphology and effect of different phases should also be considered in studying machinability of aluminium alloys. The phases be classified based on their solubility in the aluminium matrix through heat treatment as soluble and non-soluble phases.

Usually the soluble phases include the softer particles, while the insoluble phases are hard, brittle and abrasive particles, which are usually associated with large amounts of iron. So increase of iron concentration in the alloy reduces the machinability and increases tool wear. Different techniques are used to counter the effect of iron on machinability. In addition to lowering the iron concentration in the alloy, neutralizers and modifiers may be added to the alloy in order to change the morphology of the iron intermetallics formed from platelet-like β-Fe into α-Fe script like phase, which is less harmful for cutting tools [14].

From the morphological point of view, the role of metallurgical characteristics on the machinability of the alloy (workpiece) is as follows: the finer the size of grains, the better the overall machining characteristics. In case of the presence of hard particles in the alloy, it is best to have them as spheroidized and as dispersed as possible. From the alloying elements point of view, Colwell mentioned “The dominant variables governing tool life are the silicon content, the temperatures occurring at the contact surfaces of workpiece and tool, hard-spot or sludge inclusions, and non-metallic inclusions” [46].

Material properties such as strength, ductility and hardness also affect different machinability aspects as cutting force, chip formation and surface integrity. Generally, increase in strength of the alloy improves the surface finish of the machined part, but on the other hand, it can accelerate tool wear because of bad chip formation. An enormous amount of force is necessary in order to initiate formation of chips in a material with high strength. So for this kind of material, the design of the cutting tool should be taken into consideration a less positive cutting angle and a stronger tool material [14].

Hardness also affects the machining process significantly, where the cutting speed is basically selected based on the material hardness. Low hardness allows for increased cutting speed, and hence productivity in addition to improving tool life. Increase in material hardness causes significant increase in cutting forces and extra heat generation during friction. It was reported that there is a direct relation between the unit of cutting forces and the Brinell hardness number for cast iron, copper and carbon steel [47]. In addition to cutting forces, heat generation because of friction can promote element diffusion and chemical reaction during the cutting process, which can accelerate tool damage significantly. The following sections will focus on the Al-Cu and Al-Si cast alloys and the heat treatment regimes applied to them.

2.3.2 Metallurgical aspects of Al-Cu alloys

The use of aluminium castings in automobiles has increased from non-structural demands, as it is the case of cylinder heads and engine blocks, to structural parts, such as suspension struts due to the beneficial effects that arise by combining light weight and mechanical properties [48, 49]. The Al-Cu alloy is a high strength-ductility cast alloy. It is often used to cast large structures and bearing components to realize the integrated casting structure from assembly casting parts. Al-Cu alloys substituting for some forging blank may decrease production cost. Therefore, Al-Cu alloys have been widely used in aerospace, automobile, and airplane applications [50, 51]. Figure 2-5 shows the Al-rich portion of the Al-Cu phase diagram where the gap between the solidus line and liquidus line indicates the Cu content of α-Al is much lower than that of the liquid.

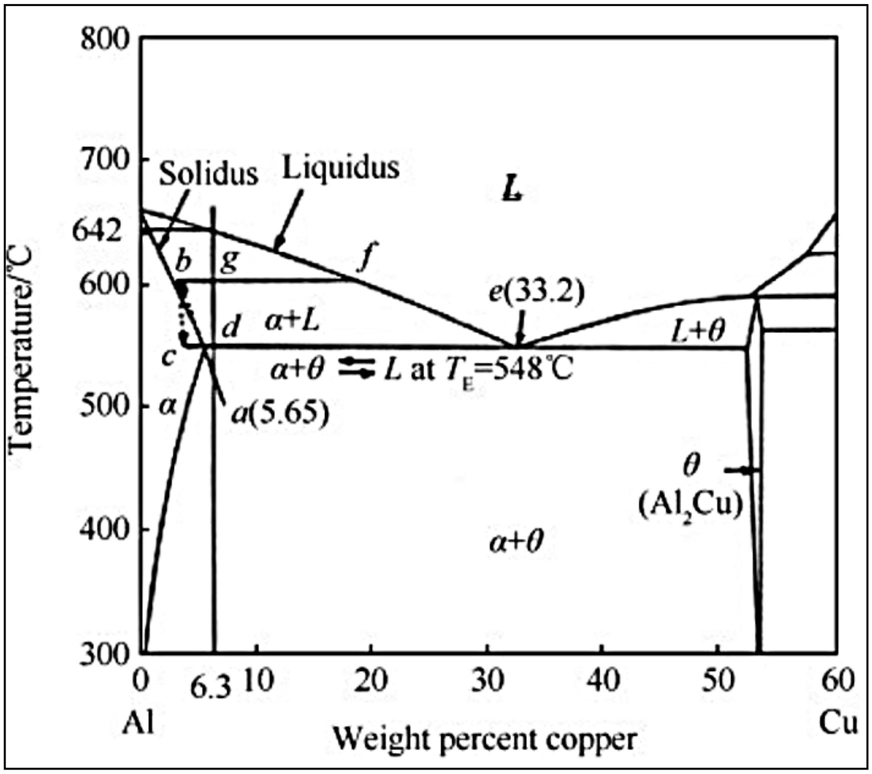

Figure 2-5 Al rich portion of the Al-Cu binary phase diagram [108]

A computer model used to predict the formation and the amount of microporosity in directionally solidified Al-4.5 wt pct Cu alloy was established by Poirier et al. [52]. The calculations show that for an initial hydrogen content less than approximately 0.03 ppm, no interdendritic porosity results. For initial hydrogen contents in the range of 0.03 to 1 ppm, there is interdendritic porosity. The amount is sensitive to the thermal gradient and solidification rate; an increase in either or both of these variables decreases the amount of interdendritic porosity. Samuel et al. [53] studied microstructural aspects of the dissolution and melting of Al_2Cu phase in Al-Si alloys during solution heat treatment. They observed that ultimate tensile strength (UTS) and elongation to fracture (%EL) show a linear increase when plotted against the amount of dissolved copper in the matrix, whereas the yield strength (YS) is not affected by the dissolution of the Al_2Cu phase. Melting of the copper phase is observed at 540 °C solution temperature; the molten copper-phase particles transform to a shiny, structureless phase upon quenching. Coarsening of the copper eutectic can occur prior to melting and give rise to massive eutectic regions of (Al + Al_2Cu). Unlike the eutectic, fragments of the blocky Al_2Cu phase are still observed in the matrix, even after 24 hours at 540 °C [54].

T6 temper is one of the important thermal treatments used for automotive components made from Al foundry alloys, which generally induces higher alloy strengthening. The T6 thermal cycle consists of a solution heat treatment followed by water quenching and then age hardening (or precipitation hardening). The solution heat treatment leads to the dissolution of intermetallic phases and the spheroidization of eutectic Si with a resulting improvement in alloy ductility [55, 56]. The time for solution treatment is strongly dependent on the microstructure [57], ranging from few minutes up to several hours [58, 59]. In general, too short a solution treatment does not guarantee that all alloying elements are dissolved in the α-Al matrix and made available for further precipitation hardening; in contrast, too long a solution treatment shows economic limitations because it uses more energy and time than necessary. Age hardening at room temperature (natural aging) or elevated temperature (artificial aging, AA) increases the alloy strength because of the ultra-fine particles which precipitate from the supersaturated solid solution and act as obstacles to dislocation movement.

The microstructure of 206 Al-Cu alloy was assessed by measuring the secondary dendrite arm spacing (DAS), grain size and porosity [60]. It was found that these three parameters increased as the average solidification rate decreased. Copper is used in Al-Cu based alloys to increase strength and hardness, which are influenced mainly by precipitation of $CuAl_2$ phase during the heat treatment. This phase has a tetragonal structure and forms also during rapid solidification [15]. Liu et al. [61] reported that for the 206 Al-Cu cast alloys at Fe higher than 0.15 pct in the T7 condition, it is difficult to meet the minimum requirement of the ductility (7%) for automotive applications due to its rapid drop at high iron content. Further work using a more overaged T7 treatment may be shown to be useful. However, with treatment in the current T4 condition, for the alloys with well-controlled alloy chemistry and microstructure, the upper iron limit can be extended to 0.3 pct, or even 0.5 pct, to meet the 7% elongation combined with good tensile strength properties, indicating the potential of developing new high-iron 206 cast alloys. Development of as-cast high strength aluminum alloys with Ni and Sr addition was carried out by Fang [62] using A380 alloy as the base alloy. The results of the tensile testing at high temperatures up to 300 ^{0} C showed that 2 wt.% Ni additions increased the UTS and YS by 27.4% and 11.7% over those of A380 alloy. The Sr addition had a similar effect on the high temperature tensile strength.

Caceres et al. [63] studied the effect of aging on the quality index of 201 alloy, an Al-Cu casting alloy containing Al–4·6%Cu–0·31%Mg–0·29%Mn– 0·55%Ag–0·23%Ti. Their findings show that when the alloy is aged up to the peak-aged condition, it exhibits a monotonic increase in yield strength and a continuous decrease in ductility such that the quality index is high and remains nearly constant. When overaged the alloy shows a high strain-hardening rate at low strains, but at strains beyond 3–4% the strain hardening saturates, which limits the tensile strength and ductility, causing the quality index to fall. The circular pattern shown by the quality index results from the transition from the high quality index (Q) value in the underaged and peak aged conditions to the lower Q value associated with the overaged condition. Mechanical characterization of aluminium alloys for high temperature applications were investigated by Molina et al. [64]. Among the aluminum alloys studied, the AlCu5 alloy showed the better performance at both room and high temperature and could provide adequate strength (UTS around 140 MPa) even at 250 °C. Basak and Babu [65] studied the aging behaviour of Cu-containing Al-Si alloy. The authors concluded that the addition of Cu in Al-6 wt% Si-2wt%Fe alloy improves the YS, UTS and hardness, with marginal loss in ductility. After solutionizing and aging for 86.4 ks, the alloy with 6 wt% Cu addition offers the same ductility as that of as-cast Al-6wt%Si-2wt%Fe alloy but with almost 50% increase in yield strength.

2.3.3 Metallurgical aspects of Al-Si alloys

Al-Si alloys have the potential to be used in tribological applications such as internal combustion engines, plain bearing, compressors and refrigerators. It was found that Al-Si-Mg alloy with 3.67% Si and 4.9%Mg shows the best wear resistance due to the precipitation of Al_4Si phase. Since the eutectic Al-Si and Al-Cu phases are favorable to the alloy strength and the subsequent heat treatment process, they have been widely applied in the structural parts of the aerospace and auto industries [66, 67]. The binary Al-Si phase diagram was initially studied by Fraenkel of Germany in 1908. It is a relatively simple binary diagram where there is very little solubility at room temperature for Si in Al and for Al in Si. Thus, the terminal solid solutions are nearly pure Al and Si under equilibrium conditions. The currently accepted diagram, Figure 2-6, is based on the study by Murray and McAlister in 1984 [68]. Figure 2-7 shows the microstructure development with the addition of Si to pure Al.

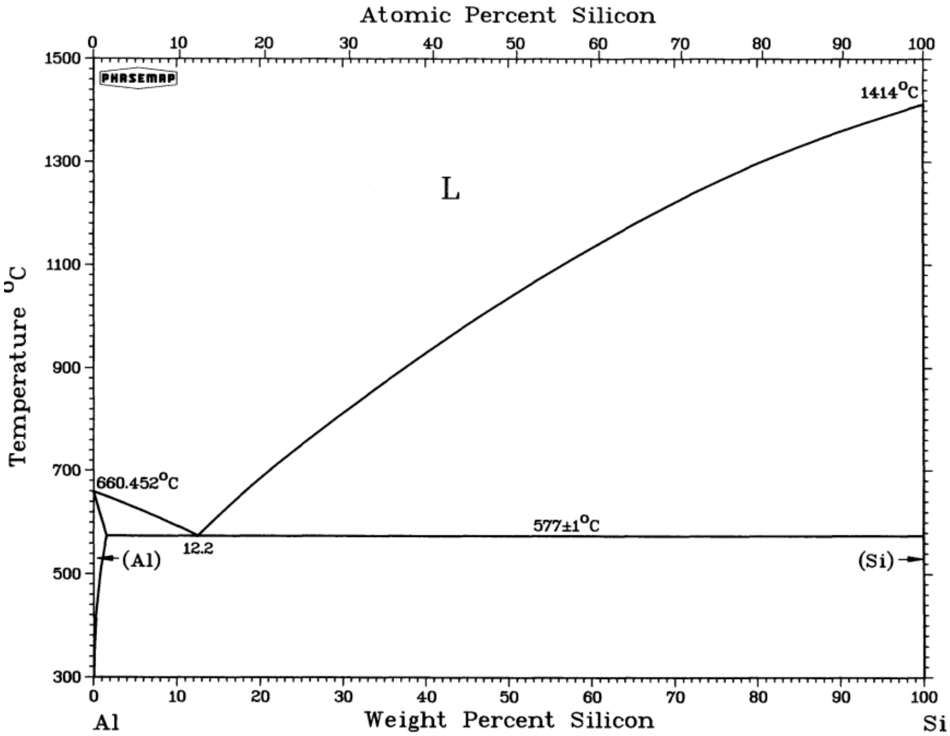

Figure 2-6 Al-Si binary diagram [108]

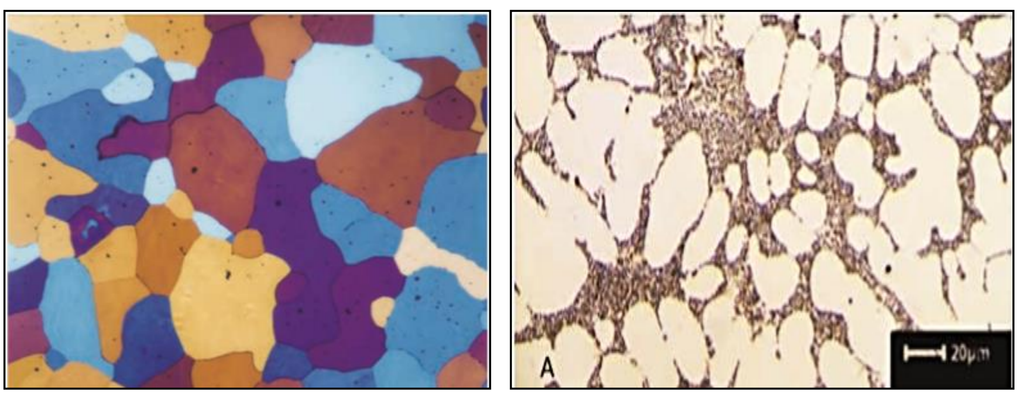

Figure 2-7 Development of Al-7%Si alloy: (a) pure Al, (b) Al-7%Si alloy [109]

According to Sigworth [69] and other researchers [70, 71] an unmodified alloy contains large flakes of brittle silicon, which cause the casting to have poor ductility. Unmodified alloys often have elongations no more than a few percent and the fracture surface is primarily brittle. With a successful modification treatment, the silicon assumes a fine, fibrous structure. These fibers appear to be small individual particles on a polished surface, but etching some of the aluminum from the surface shows that silicon is connected in a seaweed- or coral-like structure. Eutectic Si is usually chemically modified by Na, Sr or Be. The modification of plate–like Si into finer shapes was first reported by Pacz [72]. The mechanism of refinement has been well established. Hamilton and Seidensticker [73] proposed the twin plane re-entrant edge (TPRE) mechanism and held that Si growth occurs more readily at the re-entrant edge. Modifier atoms that are adsorbed on the TPRE sites can retard the growth of eutectic Si. According to Wang et al. [74], compared to the unmodified Al-Si eutectic alloy, the tensile strength and elongation of the alloy modified with 0.4wt.% Al-3P at 740 °C increased by 7% and 74%, respectively. The modification effect of hypoeutectic AlSi6Cu4 cast alloy on the microstructure and mechanical properties (tensile strength and hardness) was systematically investigated by Farkašová et al. [75]. The results reveal that transition of eutectic Si morphology involving impurity modification may be independent of the frequency and mode of eutectic nucleation. Addition of 1000 ppm Sb reduces the size of eutectic cells about 84% by improving the nucleation.

Grain refinement of casting aluminum alloys has significant influence on the improvement in mechanical performance. The addition of Al-5Ti-IB master alloy seems to be the most studied technique and also the most industrially employed [76]. The fundamental purpose of using master alloys based on the AI-Ti-B ternary system is the possibility to have TiB_2 and Al_3Ti particles, which act as heterogeneous nucleation sites and dissolve in the melt, respectively [77-80].

Optimization of Al-Si-Cu-Mg alloy heat treatment was investigated by Toschi [81]. The author concluded that over-aging curves highlighted the superior thermal stability of the quaternary A354 alloy in comparison to the ternary A356 alloy on account of the beneficial effect of Cu addition. Such behavior is related to the presence of Cu-based Q quaternary precipitates induced by heat treatment in Al-Si-Cu-Mg alloys, which are reported in the literature to possess higher coarsening resistance in comparison to β-Mg_2Si and θ-Al_2Cu phases found in ternary alloys. Singh et al. [82] investigated the microstructure and mechanical properties of Al-Si alloy (LM 25 alloy) in as-cast and heat treated conditions. Their results show that the ultimate tensile strength, yield strength and elongation of LM25 alloy after T6 heat treatment reaches 229 MPa, 196 MPa and 3.3%, respectively, and they are improved by 49%, 73% and 18%, respectively, compared to the as-cast condition.

2.4 Cutting tool aspects

2.4.1 Tool material and coating

Tool material is one of the main parameters that affect the machinability of different alloys. A well-selected material for the tool can effectively reduce cutting forces, improve tool life significantly and reduce the overall machining cost. A wide range of materials can be used for tool production, such as high carbon steel and diamond. Selecting the proper material depends on its task, in order to fit the requirements of speed, efficiency and economic production. In general, there are common characteristics of materials which are used as tool materials, which are: [14]

- Higher hardness than the work piece
- High strength (or hardness) at high temperature
- High impact toughness
- High thermal shock resistance
- Low adhesion (to prevent wear and diffusion)
- Low coefficient of friction

- Low diffusivity to workpiece material

Although characteristics of cutting materials are well determined, a trade-off always takes place in order to adjust a convenient cutting material to the workpiece. According to Astakhov [1] as shown in Figure 2-8, materials that show high hardness have poor toughness and vice versa.

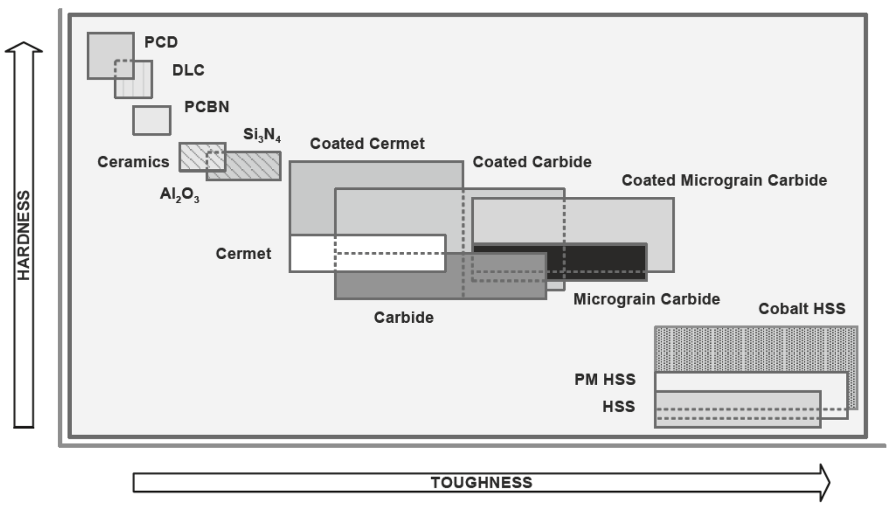

Figure 2-8 Hardness and toughness for different tool materials [4]

The commercial materials used as tool materials are: High speed steel, Cermets, Ceramic Tools, Cast Carbides, Cemented Carbides, Polycrystalline Cubic Boron Nitride (PCBN) and Polycrystalline Diamond (PCD) [14]. The selection of material varies according to the process and the work piece to optimize the suitable characteristics of the cutting material. For example, solid carbide drills are being increasingly used for machining the less abrasive wrought alloys for economic considerations, whereas a very long tool operating life, in addition to the high cutting speeds attainable, more than compensate for the higher price of solid carbide drills [2].

On the other hand, aluminum alloys with high content of abrasive elements such as silicon challenge conventional cemented carbide inserts from having a reasonable tool life.

A comparison between different designs for cemented carbide and polycrystalline diamond tools based on function and geometrical design was carried out by Soares. This comparison showed generally that low cutting forces and better surface roughness is associated with uncoated cemented carbide tools, with simpler chip breakers and flat rake face PCD tool, while efficient chip control is obtained for inserts with small grooves with high cutting forces and power consumption. In addition to the tool material, the purpose of the machining process also affects tool selection. For example, for finishing operations feed rate < 0.14 mm/rev PCD with chip breaker showed a very good control on chip formation but with higher cutting forces and power consumption. Also a flat face PCD insert showed much lower tendency toward Built-up formation because of its low chemical affinity [83].

The main function of coating can be summed up as providing a means to protect the cutting edge from deterioration because of cutting conditions. The right coating can significantly reduce the effects of friction and heat during high speed machining, reducing rate of wear, and thus increasing tool life [84]. Diamond usually is the ideal coating for dry machining of aluminum alloys because of its very high resistance to wear [14].

Coating of cutting tools by single or multi-layer coatings have provided industry with highly wear-resistive cutting tools with lower friction coefficients. Four main categories of coating include: titanium based coatings, ceramic-type coatings, super hard coatings and solid lubricant coatings [1]. On the other hand, the residual stresses induced by machining using coated tools became a point of interest for several researchers, where it was affirmed that residual stresses in plain carbon steel after machining with coated cutting tools are higher [85]. As well, Juturu investigated the effect of coating of cutting tool on residual stresses and surface quality for several aluminum alloys and reported that grooved TiN coated cutting tools showed the highest residual stresses for 7075-T6 alloy under minimum quantity lubricant conditions [25].

2.4.2 Tool geometry

Tool geometry and coating participate significantly to enhance the machinability of alloys, whereas the right tool design can improve effectively the quality of the machining process in terms of power, built-up edge and tool life.

Tool geometry affects the main machinability aspects, such as chip formation, cutting forces, productivity, surface quality and tool life. The geometry of the tool determines chip flow direction, breakage and evacuation. In addition to that, tool angles contribute significantly to direction and magnitude of cutting forces, and thus the tool life. Four parameters affect the direction and magnitude of cutting force components, which are the rake angle, the tool cutting edge angle, the tool minor cutting edge angle and the inclination angle. The productivity of the machining process is also affected, in terms of feed rate, which is adjustable according to the tool cutting edge angle. The influence of tool geometry on surface integrity and residual stresses can be remarked by defining the deformation zone according to the geometry [1]. According to the Merchant model of orthogonal cutting, the clearance angle and rake angle define the cutting tool. These angles affect the shear angle, thus the chip formation mechanism, as shown in Figure.2-9.

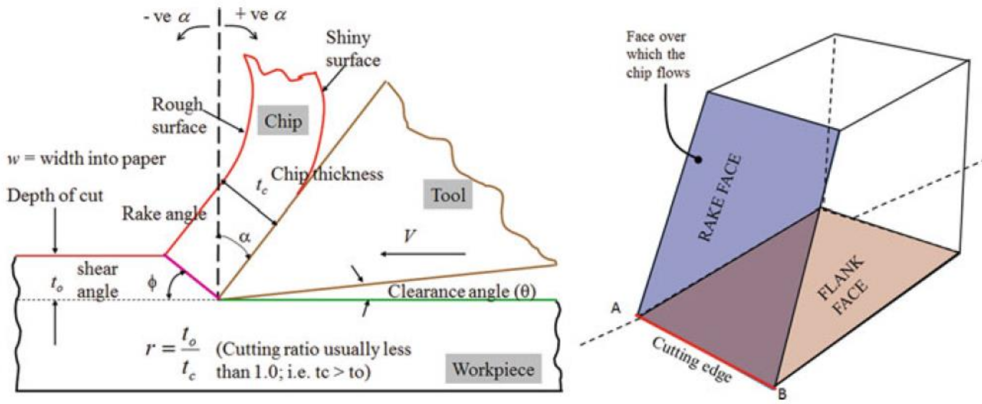

Figure 2-9 Machining nomenclature [107]

Many researches were undertaken in order to analyse the role of the geometrical parameters on the machinability of different alloys under different cutting conditions for different machining processes. In turning Fang introduced a new model to predict chip formation in chamfered and honed tools for aluminum alloys and concluded that the ratio between thrust force and cutting force varies according to the thickness of the uncut chip. And thrust force can exceed cutting force if the uncut chip thickness is less than the critical thickness which can be determined by cutting speed and tool geometry [86]. On the other hand, in drilling Schneider mentioned that in casting alloys with high abrasive materials, it is preferable to use solid carbide drills with twist drills to make the edges more resistant to wear at higher speeds [84]. Smaller helix angles and thicker webs is a convenient way to improve the rigidity of these drills, which also ultimately helps to preserve the carbide [2]. Soares and coworkers discussed different chip breaker systems in different tools made from Cemented carbide and PCD in order to evaluate their quality in machining of aluminum alloys. They concluded that inserts with big grooves and a high angle of the entrance in chip breaker showed good results in power consumption, surface roughness and chip control for roughing operations ($f > 0.14$ mm/rev) for high silicon content aluminum alloys [83]. As well, Wang et al. [87] reported that the specific energy consumption increases with the decrease of the tool rake angle.

2.4.3 Tool wear

Tool wear is the primary factor that controls tool life. It takes place as a gradual process because of continuous interaction between the cutting edge and workpiece under specific cutting conditions till failure of the tool. The wear process depends on tool material and geometry, workpiece material and cutting parameters and medium. The process occurs naturally because of loads of wear surfaces and the fast movement of cutting chips and workpiece, which subject the tool to these loads under conditions of high temperature because of friction. These mechanical factors are unavoidable because of their necessity for material removal process, so wear is an unavoidable production problem in manufacture [5, 88].

Tool wear zones vary along the tool according to different variables. Two zones were studied as the most important zones for wear measurements: flank wear and crater wear. Flank wear is the most commonly measured wear in tool life evaluation using toolmaker microscopes or a stylus instrument [1]. Opitz in 1956 defined a mathematical formula in order to predict the principle zones of tool wear according to the two main factors affecting them: cutting speed (V) and un-deformed chip thickness (t):

$$Opitz\ Factor = Vt^{0.6}$$

The resulting value of the Opitz Factor provides an indication of the predominant tool wear zone as shown in Figure 2-10. At low values for the formula, tool wear consists predominantly of rounding of the cutting point and loss of sharpness. As the value increases, the predominant zone of tool wear shifts up toward the tool body [89].

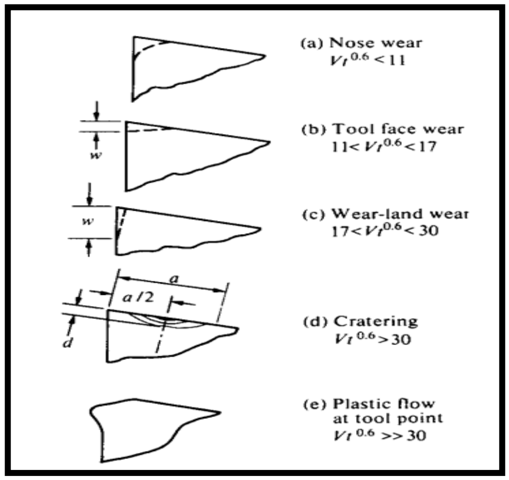

Figure 2-10 Types of predominant tool wear [1, 4]

Although tool wear is still not fully understood [5], general mechanisms causing and accelerating tool wear can be identified. The major contributing mechanisms in tool wear are:

- Abrasion due to cutting action in hard particles
- Diffusion for atoms between the two surfaces specially at high temperatures
- Fatigue
- Adhesion of the particle between the contacting surfaces
- Delamination wear, in which subsurface micro-cracks join up to produce laminar wear particles [89]

Moreover, other mechanisms play a significant role in tool wear such as microchipping, gross fracture and plastic deformation of the tool. The dominance of a particular mechanism in a specific process depends on the cutting conditions. It is reported that abrasive wear is the main wear type in low speed conditions. Otherwise, with increased speed of cutting, diffusive and adhesive wear play a predominant role in tool wear. This can be interpreted by the magnitude of the tool-chip interface temperature, which causes increase in material transfer toward the chip under high speed conditions. This can form an adhesive layer and built up edge at high speed (adhesive wear), or lead to the formation of a crater on the tool rake face (diffusion wear) at extreme cutting speeds [90].

The wear evolution process can be divided into three main regions. The first region is primary wear, where a high rate of wear takes place due to accelerated wear of damaged external layers because of manufacturing or re-sharpening of the tool. After the initial wear passes, a steady state phase of wear takes place, which is the normal operation region for the tool. After this second region a third region starts which is known as the tertiary or accelerated wear region, as shown in Figure 2-11 [1]. Operation of the tool in this region is associated with getting close to tool failure. Several indicators may be noted in this phase such as:

- Significant increase in flank wear size, crater depth and width in the rake face
- Increase in power consumption, cutting forces and vibrations
- Worse dimension control and surface roughness
- Change in chip formation because of excessive heat generation [14]

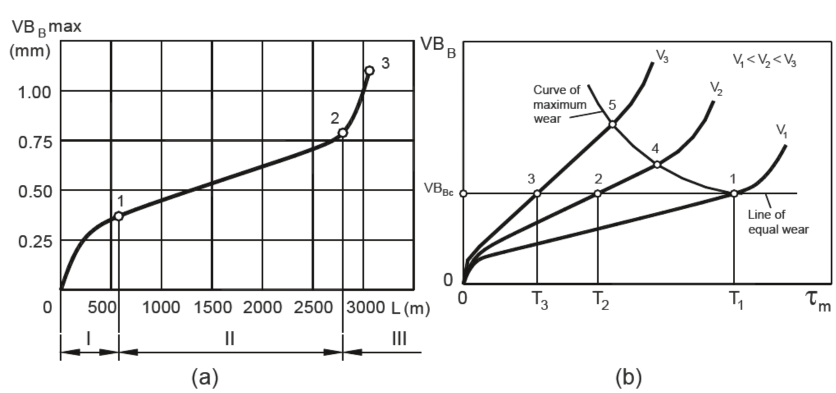

Figure 2-11 Tool wear evolution [1, 4]

Thus it is not recommended to use the cutting tool in the third operating region because of unsuitable operating conditions and high vibration.

2.5 Machining process

2.5.1. Introduction

Machining generally can be defined as the broad term used for the process of material removal from a workpiece in order to obtain a desired geometry [1]. It can be classified under three categories: conventional machining, abrasive processes, and non-traditional machining. A conventional process is one in which a mechanical tool is used to remove the excess material in order to obtain the designed geometry, which includes turning, milling, drilling and their related processes. Abrasive processes can be defined as those processes in which material is mechanically removed by the action of hard, abrasive particles such as grinding, honing and lapping. On the other hand, non-traditional machining uses different forms of energy rather than direct cutting to remove material, such as electrochemical, thermal and chemical energy [3].

The basic principles in all metal cutting operations are almost the same in mechanics, but geometry and kinematics can differ from one to the other [8, 91]. Two methodologies are used to study machining processes: the trial and error experimental method, and the mechanistic approach in metal cutting that allows applying simulation methods in metal cutting mechanics. A brief review of the literature is presented in the next sections for the drilling and tapping operations studied, for a better understanding of the cutting mechanisms in these processes.

2.5.2. Cutting mechanics

A study of cutting mechanics is essential to understand the interaction between tool and workpiece and to facilitate computational modeling using finite elements. The different models of cutting aim to calculate the cutting forces and power using the thermomechanical processes involved during the cutting process. These models can be separated into two main types: orthogonal cutting and oblique cutting. The orthogonal cutting model is the simplest, because it reduces the analysis to two dimensions. The main difference between the two models is the perpendicularity of the cutting edge to the direction of movement [92]. Merchant was the pioneer for the orthogonal model, using force diagrams to analyse the cutting process, where he resolved the resultant cutting force into two main forces, based on the chip movement direction: tool face–chip friction force, and normal force; while the same force was divided into a shear force and a normal force relative to the shear plane, and to a cutting force and thrust force based on the direction of motion as shown in Figure 2-12 depicting the Merchant circle. Thus he presented his formula for cutting force based on shear force as [1]:

$$F_s = \frac{\tau_y A_c}{\sin \varphi} \qquad\qquad F_c = \frac{F_s \cos(\mu - \gamma)}{\cos(\varphi + \mu - \gamma)}$$

where τ_y is the shear strength, A_c is the area of shear and φ is the shear angle.

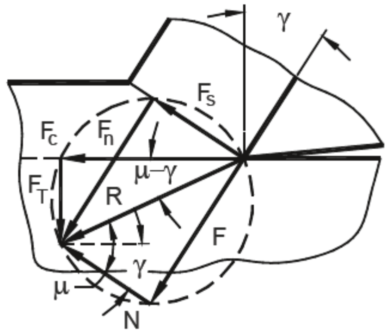

Figure 2-12 Merchant Circle and main cutting Forces [1]

More complex and advanced models were designed for computational simulation as well as elaboration of the process of cutting. While Shaw [89] introduced an advanced model for orthogonal cutting analysis, Astakhov [1, 93] introduced a more advanced model based on conservation of energy, where he assumed that the cutting power is equal to the summation of several powers: (i) power consumed in plastic deformation (P_{pd}), (ii) power consumed in tool-chip interface (P_{fR}), (iii) power consumed in tool-workpiece interface (P_{fF}) and (iv) power consumed in new surface formation (P_{ch}), as shown in the following equation. He carried out further analysis for each component of cutting power. Several studies were carried out in order to integrate the effect of minor cutting edges and integrate their effect, such as that of Zorev [94].

$$P_c = F_c v = P_{pd} + P_{fR} + P_{fF} + P_{ch}$$

2.5.3. Drilling process

Drilling is one of the most time-consuming machining processes in industry, where it consumes around 36 - 40% of all machining hours [95]. Moreover, drilling is one of the complex machining processes due to the complex geometry of the cutting tool and the variable cutting speed and variable cutting angles along the cutting edge. The drill may be defined as a rotary end-cutting tool with one or more cutting lips, with helical or straight flutes to pass chips and cutting fluid [2]. Drills can be divided into two main categories according to the helix angle into straight flute drills and twist drills [95]. The main characteristic of the drilling process can be identified in the combined behavior of metal cutting and chip extrusion through the chisel edge [14]. Three cutting edges can be identified in drills: the main cutting edge or the drill point, the central chisel edge, and the marginal cutting edge [28].

Drills consist of three basic parts: shank, body and point. While the shank is a point of holding, the body is rounded by flutes to facilitate chip removal and lubrication. The flutes are edged by the land, which is the peripheral portion of the cutting tooth between adjacent flutes. The intersection between flutes and the flanks forms the lips of the drill, which form the point with the face of the flutes. The point is the direct part of contact between drill and cutting material, which consists of cutting lips, face and flank. The web thickness decreases gradually along the tool to end with the chisel edge, which connects the cutting lips to each other. Body clearance exists between the margin and the flank, which intersect with the face of the flute forming the heel of the drill. A detailed design showing the twist drill is presented in Figure 2-13. In the straight flute drills, as well, the same parameters exist, except some particular angles that differ between the twist drill and the straight flute drill. The geometry of the drill facilitates understanding the machining process, where the undeformed chip width is equal to the length of the drill lip, while the thickness of the undeformed chip differs from the feed per lip based on the point angle [14].

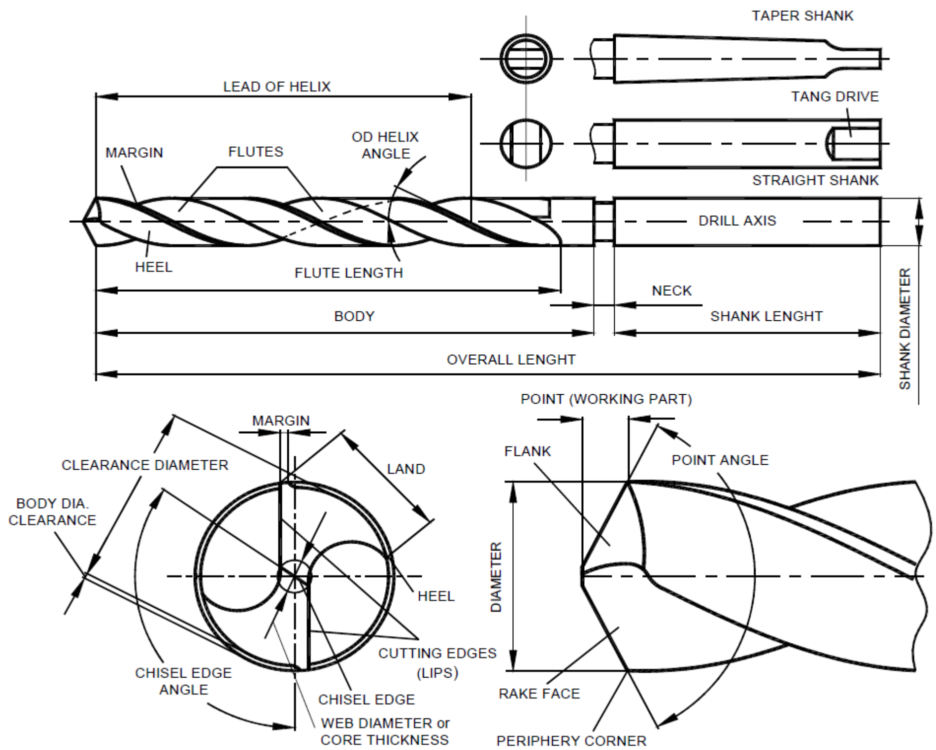

Figure 2-13 Terms applied to twist drills [94]

Four angles are often used to characterise the drills. Firstly, the helix angle is the angle between the leading edge and the axis of drilling. In case of straight flute drills, this angle is equal to zero. The chisel edge angle is the angle between the chisel edge and cutting lips; Point angle is the angle between the flanks of the drill; and the lip relief angle is the angle between the flank and the line normal to the drill axis. This characterisation of drill angles facilitates understanding cutting mechanics; whereas mechanical analysis of the drilling process based on normal orthogonal cutting mechanics is not convenient. In drilling, normal cutting angles such as rake angle and clearance angle vary across the radius of the drill. Thus, there is neither one rake angle nor one clearance angle for the tool. Therefore, the drilling process is analysed as a double oblique cutting process based on the cutting lips, using varying inclination angles and geometry along the cutting edges [14]. Figure 2-14 clarifies the complexity of cutting mechanics. Then empirical formulas may be used in order to facilitate analysis. Smith [6] mentions the following formulas to calculate the axial force and torque in solid drilling:

$$F = C_F d^{bF} s^{uF} K_H$$

$$M = C_M d^{bM} s^{uM} K_H$$

where C_F and C_M are constants, d is the nominal drill diameter, bF and bM are exponents that characterise the influence of the drill diameter, S is the feed rate corrected by uM and uF exponents, and K_H is the workpiece correction coefficient.

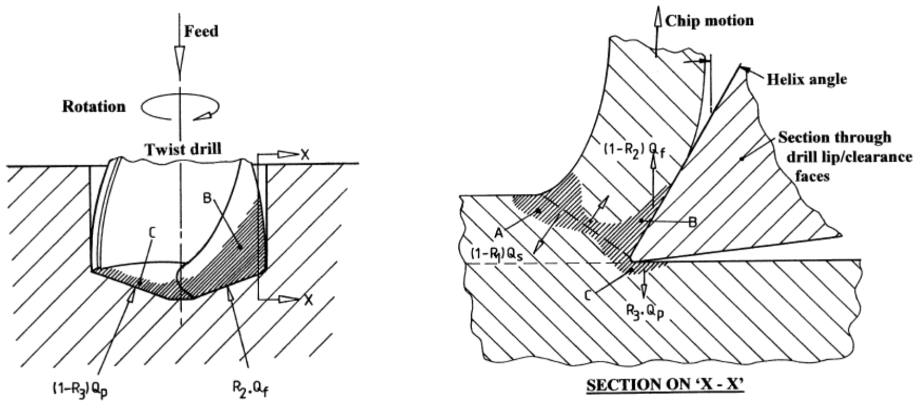

Figure 2-14 Cutting mechanics in drilling process [6]

2.5.4. Tapping process

Tapping is one of the machining processes that aim to form internal threads for the holes. The tap is a teeth-shaped tool that combines rotary and axial motion to form the internal threads by material cutting and plastic deformation mechanisms. Taps can be categorised into three most common types: tapered tap, plug tap and bottoming tap. These types can be with helical flutes, straight flutes, or fluteless taps. Because of susceptibility of the teeth to be damaged by heat and the potential for chip trapping in the flute, conservative cutting conditions are often used to avoid catastrophic failure [96, 97], as well as the cooling during the tapping process which is more vital in tapping than in other machining processes [5].

The complexity in geometry comes from the multi-cutting edge process as shown in Figure 2-15. The main cutting edges of the taps are on the conical surface and the crest of the first full thread, while minor cutting edges are on the flank surfaces of the tap. For the sake of simplification, V-form screw threads are based on triangular teeth with truncated crests and roots. Pitch of the taps is defined by the distance between two adjacent teeth of the thread, while lead is defined based on the axial advance of the screw for 360-degree rotation. Flank angle is the angle between the flank and the line normal to the axis of the screw. Chen and Smith developed an advanced mathematical model to facilitate the modeling of the tapping process for three main tapping modes: long through holes, short through holes and blind holes [97].

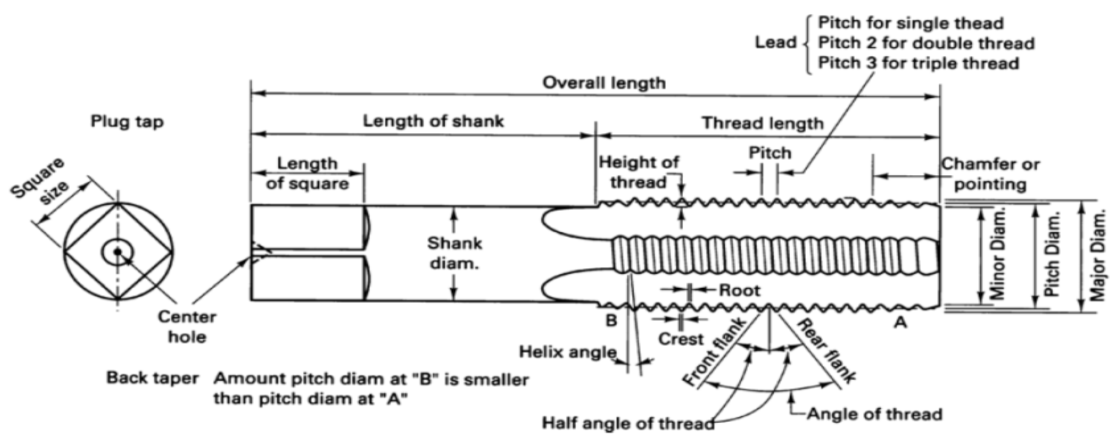

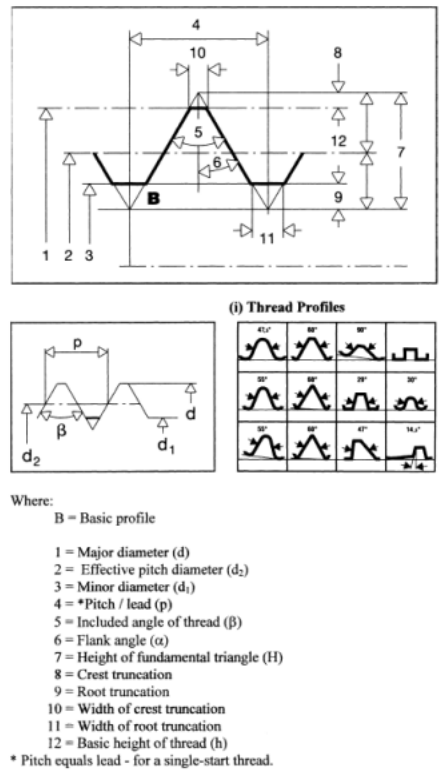

Figure 2-15 Nomenclature of tapping process [6]

Variations in tap parameters can significantly affect the tapping torque. Lorenz [98] investigated the effect of cutting speed, rake angle, thread relief and chamfer relief for Carbon steel, and reported that the interaction between cutting speed and chamfer relief has a strong influence on the tapping torque. In addition, he affirmed that the torque is a quadratic function of the logarithm of cutting speed. As well, Agapiou [99] discussed the effect of high speed tapping for A319 Al-Si alloy for different tap geometries, and concluded that the effect of the speed on the steady state torque was not clear in contrast to the peak torque which increased with speed.

2.6 Cutting parameters

2.6.1. Cutting fluids

Excessive heat generation in cutting processes is a major problem in cutting mechanics in terms of surface integrity and tool life. The wear mechanism can be shifted from one mechanism to another according to tool-chip interface temperature [14]. Thus different fluids are used during the cutting process for the sake of cooling and lubrication as primary functions, in addition to surface quality improvement and tool life extension [6]. Kronenberg mentioned in 1966 that 18% of heat generated dissipates to the cutting tool during the cutting process. A wide variety of cutting fluids exist in order to adjust the balance between the lubricating effect and cooling effect, which is influenced by the machining process and the workpiece. Thus, cutting fluids are subdivided into four main categories: straight oils, soluble oils, synthetic fluids and semi-synthetics [100]. Machining processes can also be classified according to the fluid type used, into wet machining, dry machining and semi-dry or MQL, where the last two categories are mainly of interest for industry for economic and environmental reasons. A series of studies [100-102] were conducted to adjust, simulate and optimize the machining processes of steel and aluminum alloys in terms of cutting fluid and dry machining in normal and high speed machining conditions. However, a detailed discussion is out of the scope of this thesis.

2.6.2. Cutting kinematic factors

Three main parameters in the cutting process dominate the cutting forces, power consumption, surface integrity as well as the need of cutting fluids, which are cutting speed, feed rate and depth of cut. The combination of these three factors in addition to the cutting environment creates a challenge with regard to optimization. Thus, several studies were made in order to determine a model to study, simulate and optimize the cutting process using mathematical, experimental and computational tools. Astakhov [1] affirmed a good match between cutting parameter analysis using his mathematical model (mentioned in section 2.5.2) and experimental results for steel and aluminum alloys. As well, Carrilero et al. [103] experimentally investigated the behavior of Al-Cu alloys and the effect of cutting kinematics in turning, and affirmed that the best quality of surface is obtained with lower feed rates and higher cutting speeds, but optimization was to be followed to reduce energy cost and machining time. Davoodi and Tazehkandi [104] also used experimental investigations for aluminum alloy 5083 to optimize cutting parameters when using dry machining. Jomaa [32] reported that in the machining of AA7075 aluminum alloys the built-up edge (BUE) increased proportionally with the increase of the cutting feed; but increase in cutting speed reduced it and promoted the built up layer (BUL) on the rake face. Several researches have been carried out to optimize the cutting parameters computationally using finite element methods, and using genetic algorithms in neural network models such as the work of Majeed et al. in FED modelling [10], Solimanpur [105] and Chien [13] in neural networks.

Applying high-speed cutting enhances both the quality and productivity of machining. It is reported that high speed machining gives better surface roughness because of short contact time between the tool and the part, thus a lower time of exposure to heat and, in consequence, less effect on surface quality [14, 106]. Farid et al. [107] reported that the surface roughness improves with increase in machining time and cutting speed for A383 cast alloys using HSS tools.

2.7 References

1. J. Paulo Davim, *Machining: Fundamentals and Recent Advances*. 2008, London: London: Springer London.

2. Guillermo Hernan Garza Elizondo, *Machinability of Al-(7-11%)Si casting alloys : role of free-cutting elements*, in *Aspects de l'usinabilité des alliages de fonderie Al-(7-11)%Si*. 2010, Université du Québec à Chicoutimi: Chicoutimi]. p. xii, 151 f.

3. Mikell P. Groover, *Fundamentals of modern manufacturing : materials, processes, and systems*. 4th ed. ed. 2010, Hoboken, N.J.: J. Wiley & Sons. xii, 1022 p.

4. J. Paulo Davim, *Machinability of Advanced Materials*. 2014: Wiley-ISTC ISBN: 978-1-848-21396-8.

5. Yasser Zedan, *Machinability aspects of heat-treated Al-(6-11)%Si cast alloys : role of intermetallics and free-cutting elements*, in *Aspects de l'usinage des alliages de fonderie Al-(6-11)%Si traités thermiquement rôle des intermétalliques et des éléments de décolletage*. 2010, Université du Québec à Chicoutimi: Chicoutimi]. p. xiv, 217 f.

6. Graham T. Smith, *Cutting Tool Technology*. Cutting Tool Technology : Industrial Handbook. 2008: Springer London.

7. Redford A.H. Mills B., *Machinability of Engineering Materials*. 1983, London: Applied Science Publishers.

8. Osama Elfasi, *Machinability of stainless steel alloys*. 2018, École de technologie supérieure.

9. David A. Stephenson and John S. Agapiou, *Metal cutting theory and practice*. 2nd ed. ed. 2006, Boca Raton, Flor.: CRC , Taylor and Francis. xvii, 846 p.

10. Arfan Majeed, Asif Iqbal, and Jingxiang Lv, *Enhancement of tool life in drilling of hardened AISI 4340 steel using 3D FEM modeling.* The International Journal of Advanced Manufacturing Technology, 2018. **95**(5): p. 1875-1889.

11. Kuang-Hua Fuh, *COMPUTER AIDED DESIGN AND MANUFACTURING FOR MULTIFACET DRILLS (CAD).* 1987, ProQuest Dissertations Publishing.

12. Sangkee Min, et al., *FINITE ELEMENT MODELING OF BURR FORMATION IN METAL CUTTING.* Machining Science and Technology, 2001. **5**(3): p. 307-322.

13. Wen-Tung Chien and Chung-Yi Chou, *The predictive model for machinability of 304 stainless steel.* Journal of Materials Processing Tech., 2001. **118**(1): p. 442-447.

14. Mahmoud Tash, *Effect of metallurgical parameters on the machining behavior of 356 and 319 alloys (drilling and tapping study)*. 2005, ProQuest Dissertations Publishing.

15. Asif Iqbal, Khalid A. Al-Ghamdi, and Ghulam Hussain, *Effects of tool life criterion on sustainability of milling.* Journal of Cleaner Production, 2016. **139**: p. 1105-1117.

16. Ingo G. Reichenbach, et al., *Tool-life criteria and wear behavior of single-edge ultra-small micro end mills.* Precision Engineering, 2019. **55**: p. 48-58.

17. International Organization for Standardization.1993.ISO 3685: Tool-life testing with single-point turning tools.

18. W. Taylor Fred, *The Art of Cutting Metals.* Scientific American, 1907. **63**(1619supp): p. 25942.

19. Pavel Kovac, et al., *Using the temperature method for the prediction of tool life in sustainable production.* Measurement, 2019. **133**: p. 320-327.

20. A. Thangaraj and P. K. Wright, *Drill wear sensing and failure prediction for untended machining.* Robotics and Computer Integrated Manufacturing, 1988. **4**(3): p. 429-435.

21. E. Brinksmeier, *Prediction of Tool Fracture in Drilling.* CIRP Annals - Manufacturing Technology, 1990. **39**(1): p. 97-100.

22. Jamal Seikh-Ahmad and Uvanandan Valavan, *Tool life prediction based on cutting forces and surface temperature in edge trimming of multidirectional CFRP composites*. 2007, ProQuest Dissertations Publishing.

23. Hans Kurt Toenshoff and Berend Denkena, *Basics of Cutting and Abrasive Processes*. 2013, Berlin, Heidelberg: Springer Berlin Heidelberg, Berlin, Heidelberg.

24. Yongguo Wang, et al., *Cutting force analysis in reaming of ZL102 aluminium cast alloys by PCD reamer.* The International Journal of Advanced Manufacturing Technology, 2013. **67**(5): p. 1509-1516.

25. Igor Minukhin, *An Improved Method of Cutting Forces Prediction for the Primary Cutting Edges of Twist Drills*. 2013: M. Appl. Sc. Thesis, Concordia University, Montreal, Canada.

26. Mohsen Marani Barzani, *Machinability of Al-20Mg2Si-Cu metal matrix composite modified with bismuth or barium*. 2019, École de technologie supérieure.

27. U. A. Dabade and S. S. Joshi, *Analysis of chip formation mechanism in machining of Al/SiCp metal matrix composites.* Journal of Materials Processing Technology, 2009. **209**(10): p. 4704-4710.

28. Emad-Eldin Elgallad, *Effect of additives on the mechanical properties and machinability of a new aluminum-copper base alloy*. 2010, ProQuest Dissertations Publishing.

29. S. A. Batzer, et al., *Chip morphology and hole surface texture in the drilling of cast Aluminum alloys.* Journal of Materials Processing Tech., 1998. **79**(1): p. 72-78.

30. A. Gómez-Parra, et al., *Analysis of the evolution of the Built-Up Edge and Built-Up Layer formation mechanisms in the dry turning of aeronautical aluminium alloys.* Wear, 2013. **302**(1-2): p. 1209-1218.

31. M. S. Carrilero, et al., *A SEM and EDS insight into the BUL and BUE differences in the turning processes of AA2024 Al–Cu alloy.* International Journal of Machine Tools and Manufacture, 2002. **42**(2): p. 215-220.

32. Walid Jomaa, *Contributions to understanding the high speed machining effects on aeronautic part surface integrity*. 2015, ProQuest Dissertations Publishing.

33. J. Paulo Davim (Ed), *Surface Integrity in Machining*. 2010, London: London: Springer London.

34. Helmi A. Youssef and Hassan El-Hofy, *Machining technology : machine tools and operations*. 2008, Boca Raton: CRC Press. xxxvi, 633 p.

35. Trevor Shoemaker, *Developing and applying a surface integrity framework to metal cutting on 2024-T351 aluminum with wiper cutting tools*. 2015, ProQuest Dissertations Publishing.

36. Bing Liu, et al., *Machining introduced microstructure modification in aluminium alloys.* Journal of Alloys and Compounds, 2018. **757**: p. 233-238.

37. F. J. Humphreys and M. Hatherly, *Recrystallization and related annealing phenomena*. 2nd ed. ed. 2004, Amsterdam: Elsevier. xxx, 628 p.

38. Yanxia Chen, et al., *Surface gradient nanostructures in high speed machined 7055 aluminum alloy.* Journal of Alloys and Compounds, 2017. **726**: p. 367-377.

39. P. J. Withers and H. K. D. H. Bhadeshia, *Residual stress. Part 1 – Measurement techniques.* Materials Science and Technology, 2001. **17**(4): p. 355-365.

40. Srichand Hinduja, Lin Li, and Conference International Matador, *Proceedings of the 37th International MATADOR Conference*. 2013 ed. 2013, London: London: Springer London.

41. Balkrishna Rao and Yung C. Shin, *Analysis on high-speed face-milling of 7075-T6 aluminum using carbide and diamond cutters.* International Journal of Machine Tools and Manufacture, 2001. **41**(12): p. 1763-1781.
42. Aluminum Association, American Society for Metals, and John E. Hatch, *Aluminum : properties and physical metallurgy*. 1984, Metals Park, Ohio: American Society for Metals. 424 p.
43. J. G. Kaufman and Elwin L. Rooy, *Aluminum alloy castings : properties, processes, and applications*. 2004, Schaumburg, Ill. : AFS Materials Park, Ohio: ASM International. viii, 340 p.
44. J. L. Jorstad, *Influence of Aluminum Casting Alloy Metallurgical Factors on Machinability.* SAE Transactions, 1980. **89**: p. 1892-1906.
45. G. Sigworth and K. Whaler D. Apelian, *Assessment of Grain Refinement and Modification of Al-Si Foundry Alloys by Thermal Analysis.* AFS Transactions, 1984. **92**: p. pp. 297-307.
46. O.Tichy D.L.Colwell, *Machinability of Aluminum Die Castings.* AFS Transactions, 1956. **64**: p. pp. 236-241.
47. M. Kronenberg, *Machining Science and Application*. 1966, London: Pregamon.
48. W.E. Kosak, 2003.*Cast Aluminum rear subframe control arm articulations*.
49. W.E. Kosak, 2004.*Cast aluminum vehicle subframe with tension/compression struts*.
50. Zhao Xin Yu Guilin, *The casting process of large closed annular castings made of high strength Al-Cu alloy.* Journal of Materials Engineering, 2000. **9**: p. 42-45.
51. X.Bin Hongji, N. Yuchao, W. Weimin, S. Bailai, *Effects of different pouring conditions on the microstructure of Al-Cu alloy.* Special Casting and Nonferrous Alloys, 2006. **26 (1)**: p. 10-13.
52. D. Poirier, K. Yeum, and A. Maples, *A thermodynamic prediction for microporosity formation in aluminum-rich Al-Cu alloys.* Metallurgical Transactions A, 1987. **18**(11): p. 1979-1987.
53. A. Samuel, J. Gauthier, and F. Samuel, *Microstructural aspects of the dissolution and melting of Al 2 Cu phase in Al-Si alloys during solution heat treatment.* Metallurgical and Materials Transactions A, 1996. **27**(7): p. 1785-1798.
54. F. H. Samuel, *Incipient melting of Al5Mg8Si6Cu2 and Al2Cu intermetallics in unmodified and strontium-modified Al–Si–Cu–Mg (319) alloys during solution heat treatment.* Journal of Materials Science, 1998. **33**(9): p. 2283-2297.

55. E. Ogris, et al., *On the silicon spheroidization in Al–Si alloys.* Journal of Light Metals, 2002. **2**(4): p. 263-269.
56. E. Sjölander and S. Seifeddine, *Optimisation of solution treatment of cast Al–Si–Cu alloys.* Materials and Design, 2010. **31**(1): p. S44-S49.
57. D. L. Zhang, L. H. Zheng, and D. H. Stjohn, *Effect of a short solution treatment time on microstructure and mechanical properties of modified Al–7wt.%Si–0.3wt.%Mg alloy.* Journal of Light Metals, 2002. **2**(1): p. 27-36.
58. Y. Han, et al., *Optimizing the tensile properties of Al–Si–Cu–Mg 319-type alloys: Role of solution heat treatment.* Materials and Design, 2014. **58**: p. 426-438.
59. M. A. Talamantes-Silva, et al., *Characterization of an Al–Cu cast alloy.* Materials Characterization, 2008. **59**(10): p. 1434-1439.
60. Elina Huttunen-Saarivirta and Jyrki Vuorinen, *Preparation and characterisation of melt-spun Al–Cu–Fe quasicrystals.* Intermetallics, 2005. **13**(8): p. 885-895.
61. K. Liu, X. Cao, and X. G. Chen, *Tensile Properties of Al-Cu 206 Cast Alloys with Various Iron Contents.* Metallurgical and Materials Transactions A, 2014. **45**(5): p. 2498-2507.
62. Li Fang, *Development of As-Cast High Strength Aluminum Alloys with Ni and Sr addition*. 2018, ProQuest Dissertations Publishing.
63. C. H. Cáceres, et al., *Effect of aging on quality index of an Al–Cu casting alloy.* Materials Science and Technology, 1999. **15**(6): p. 711-716.
64. P. Amalberto R. Molina, M. Rosso, *Mechanical characterization of aluminium alloys for high temperature applications Part 2: Al-Cu, Al-Mg alloys.* Metallurgical Science and Technology, 2011. **29**: p. pp 5-13.
65. C. Basak and N. Babu, *Influence of Cu on modifying the beta phase and enhancing the mechanical properties of recycled Al-Si-Fe cast alloys.* Sci Rep, 2017. **7**(1): p. 5779-5779.
66. M. Okayasu, et al., *A study of the mechanical properties of an Al–Si–Cu alloy (ADC12) produced by various casting processes.* Materials Science & Engineering A, 2012. **543**: p. 185-192.
67. E. M. Elgallad, et al., *Microstructural characterisation of Al–Si cast alloys containing rare earth additions.* Philosophical Magazine, 2018. **98**(15): p. 1337-1359.

68. A. M. A. Mohamed, F. H. Samuel, and Saleh Al kahtani, *Microstructure, tensile properties and fracture behavior of high temperature Al–Si–Mg–Cu cast alloys.* Materials Science & Engineering A, 2013. **577**: p. 64-72.

69. G. Sigworth, *The Modification of Al-Si Casting Alloys: Important Practical and Theoretical Aspects.* International Journal of Metalcasting, 2008. **2**(2): p. 19-40.

70. L.F. Mondolfo. P.B. Crosley, *The Modification of Aluminum-Silicon Alloys.* Modern Castings, 1966: p. pp. 89-100

71. J.E. Grusleski F. Paray, *Factors to Consider in, Modification.* AFS Transactions, 1994. **102**: p. 833-842.

72. A. Pacz, 1921.*US Patent No. 1387900A.*

73. D. R. Hamilton and R. G. Seidensticker, *Growth Mechanisms of Germanium Dendrites: Kinetics and the Nonisothermal Interface.* Journal of Applied Physics, 1963. **34**: p. 1450-1460.

74. Shuo Wang, et al., *Microstructure and mechanical properties of Al–Si eutectic alloy modified with Al–3P master alloy.* Journal of Materials Processing Tech., 2018. **255**: p. 105-109.

75. M. Farkašová, E. Tillová, and M. Chalupová, *Modification of Al-Si-Cu cast alloy.* FME Transactions, 2013. **41**(3): p. 210-215.

76. A. M. Samuel, et al., *Some aspects of grain refining of Al-Si cast alloys.* International Journal of Cast Metals Research, 2019. **32**(1): p. 1-14.

77. Haizhi Ye, *An overview of the development of Al-Si-Alloy based material for engine applications.* Journal of Materials Engineering and Performance, 2003. **12**(3): p. 288-297.

78. S. A. Kori, B. S. Murty, and M. Chakraborty, *Development of an efficient grain refiner for Al–7Si alloy.* Materials Science & Engineering A, 2000. **280**(1): p. 58-61.

79. D. Qiu, et al., *A mechanism for the poisoning effect of silicon on the grain refinement of Al–Si alloys.* Acta Materialia, 2007. **55**(4): p. 1447-1456.

80. Geoffrey Sigworth and Timothy Kuhn, *Grain Refinement of Aluminum Casting Alloys.* International Journal of Metalcasting, 2007. **1**(1): p. 31-40.

81. S. Toschi, *Optimization of A354 Al-Si-Cu-Mg Alloy Heat Treatment: Effect on Microstructure, Hardness, and Tensile Properties of Peak Aged and Overaged Alloy.* Metals, 2018. **8**(11).

82. Raj Kumar Singh, Amit Telang, and Mohammad Mohsin Khan, *Effect of T6 Heat Treatment on Microstructure, Mechanical Properties and Abrasive Wear Response of Fly Ash Reinforced Al-Si Alloy.* Materials Today: Proceedings, 2017. **4**(9): p. 10062-10068.

83. R. Soares, et al., *Comparison Between Cemented Carbide and PCD Tools on Machinability of a High Silicon Aluminum Alloy.* Journal of Materials Engineering and Performance, 2017. **26**(9): p. 4638-4657.

84. G. Schneider. *Cutting Tool Applications*. 2002; Available from: www.toolingandproduction.com.

85. J.C. Outeiro, Dias, A.M., Lebrun, J.L., Astakhov, V.P. , *Residual stresses induced by machining of a plain carbon steel using coated and uncoated commercial tungsten carbide tools.* Key Engineering Materials, 2002. **Vol. 230-232**: p. pp. 118-121.

86. N. Fang and Q. Wu, *The effects of chamfered and honed tool edge geometry in machining of three aluminum alloys.* International Journal of Machine Tools and Manufacture, 2005. **45**(10): p. 1178-1187.

87. Bing Wang, et al., *Proper selection of cutting parameters and cutting tool angle to lower the specific cutting energy during high speed machining of 7050-T7451 aluminum alloy.* Journal of Cleaner Production, 2016. **129**: p. 292-304.

88. B. Mubaraki, et al., *Drilling studies of an Al 2 O 3 -Al metal matrix composite - Part I Drill wear characteristics.* Journal of Materials Science, 1995. **30**(24): p. 6273-6280.

89. Milton C. Shaw, *Metal cutting principles*. 2nd ed. ed. 2005, New York: Oxford University Press. xix, 651 p.

90. M. Nouari, et al., *Effect of machining parameters and coating on wear mechanisms in dry drilling of aluminium alloys.* International Journal of Machine Tools and Manufacture, 2005. **45**(12): p. 1436-1442.

91. Y. Altintas and A. A. Ber, *Manufacturing Automation: Metal Cutting Mechanics, Machine Tool Vibrations, and CNC Design.* Applied Mechanics Reviews, 2001. **54**(5): p. B84.

92. Andrew Y. C. Nee and A. Y. C. Nee, *Handbook of Manufacturing Engineering and Technology*. 2015 ed. 2015, London: London: Springer London.

93. Astakhov, *Metal Cutting Mechanics*. 1998, USA: CRC.

94. N.N. Zorev, *Metal Cutting Mechanics*. 1966, Oxford, UK: Pergamon.

95. D. T. Pham and Viktor P. Astakhov, *Geometry of Single-point Turning Tools and Drills*. 2010: Springer London.

96. T. J. Wick Drozda, C. (Ed), *Tool and Manufacturing Engineers Handbook, Machining*. 4 ed. Vol. 1. 1983, Dearborn, MI: Society of Manufacturing Engineers.

97. N. M. Chen and A. J. R. Smith, *Modelling of straight-flute machine tapping.* Proceedings of the Institution of Mechanical Engineers, Part B: Journal of Engineering Manufacture, 2011. **225**(9): p. 1552-1567.

98. G. Lorenz, *On Tapping Torque and Tap Geometry.* CIRP Annals - Manufacturing Technology, 1980. **29**(1): p. 1-4.

99. J. S. Agapiou, *Evaluation of the effect of high speed machining on tapping.* Journal of engineering for industry, 1994. **116**(4): p. 457-462.

100. A. K. Balaji and Anshu Jayal, *An experimental investigation of the effects of cutting fluid application on machining performance*. 2006, ProQuest Dissertations Publishing.

101. Amir Mahyar Khorasani, et al., *Investigation on the effect of cutting fluid pressure on surface quality measurement in high speed thread milling of brass alloy (C3600) and aluminium alloy (5083).* Measurement, 2016. **82**: p. 55-63.

102. Anshu D. Jayal, et al., *Machining Performance and Health Effects of Cutting Fluid Application in Drilling of A390.0 Cast Aluminum Alloy.* Journal of Manufacturing Processes, 2007. **9**(2): p. 137-146.

103. M. S. Carrilero, M. Marcos, and V. M. Sanchez, *Feed Cutting Speed and Cutting Forces as Machinability Parameters of Al-Cu Alloys.* Journal of the Mechanical Behavior of Materials, 1996. **7**(3): p. 167-178.

104. Behnam Davoodi and Ahmadreza Hosseini Tazehkandi, *Experimental investigation and optimization of cutting parameters in dry and wet machining of aluminum alloy 5083 in order to remove cutting fluid.* Journal of Cleaner Production, 2014. **68**: p. 234-242.

105. M. Solimanpur and F. Ranjdoostfard, *Optimisation of cutting parameters using a multi-objective genetic algorithm.* International Journal of Production Research, 2009. **47**(21): p. 6019-6036.

106. M. Nouari, et al., *Experimental analysis and optimisation of tool wear in dry machining of aluminium alloys.* Wear, 2003. **255**(7): p. 1359-1368.

107. A. Akhavan Farid, S. Sharif, and M. H. Idris, *Surface integrity study of high-speed drilling of Al–Si alloy using HSS drill.* Proceedings of the Institution of Mechanical

Engineers, Part B: Journal of Engineering Manufacture, 2011. **225**(7): p. 1001-1007.

108. J.L. Murray and A.J. McAlister, *Bull. Alloy Phase Diagrams,* Vol. 5, No. 1, Feb. 1984.

109. J. Asensio-Lozano and G.V. Voort, *Tech Notes*, Buehler, Illinois Tool Works, 2015, Vol. 5, Issue 1.

CHAPTER 3

EXPERIMENTAL PROCEDURES

CHAPTER 3

EXPERIMENTAL PROCEDURES

3.1 Introduction

In this chapter, the methodology used in this research study will be discussed, through a description of the experiments that were carried out, the techniques used to obtain the results, and processing and analysis of the data, to determine the machinability characteristics of the new HT200 Al-Cu alloys in comparison with those of the well-established Al-Si alloys.

The methodology can be divided into four main parts, covering preparation and casting of the alloys studied, heat treatment, mechanical and machining tests, and data analysis. The material preparation part includes the procedures followed to prepare melts of the Al-Cu and Al-Si alloys investigated, the alloying additions made, and the melt treatments used (grain refining and Sr modification) to achieve the required chemical compositions, and the casting procedures for preparation of test bar samples for tensile testing and blocks for machinability tests, as well as samplings for chemical analysis. The heat treatment phase describes the different heat treatment conditions that were used to heat treat the cast samples, for investigating the influence of the resulting microstructure, phases and precipitates formed on the tensile properties. The different testing procedures are described thereafter, and include microstructural analysis, tensile testing, cutting force analysis, built-up edge measurement, tool life evaluation and chip characterisation. The fourth part describes the algorithm followed in order to calculate the different components of the cutting forces, and the mean and resultant forces in drilling and tapping processes using data processing functions, so as to provide a clearer insight into the machinability characteristics of the alloys investigated with respect to these processes.

3.2 Preparation of Alloys and Casting

3.2.1. Materials preparation

The alloy HT200 was supplied by Nemak; the chemical composition is shown in Table 3.1. The alloy HT200 contains a lower concentration of Silicon in comparison to the A319.0 and A356.0 alloys which were used as reference alloys for comparison purposes in the same domain of commercial applications. The remarkable element in alloy HT200 is its high Copper content (6 wt%) with minor percentages of additives such as Manganese, Magnesium and Titanium. The alloy HT200 was prepared as received from Nemak, while the A319 and A356 alloys were grain refined and modified using Al-5%Ti-1%B and Al-10%Sr master alloys, respectively.

Table 3-1 Chemical Analysis of the alloys studied

Chemical Analysis (wt%)										
Alloy	**Elements**									
	Cu	Si	Fe	Mn	Mg	Ti	Zr	V	Zn	Al
HT200	6.0	0.69	0.17	0.38	0.015	0.102	0.19	0.013	0.19	Balance
A319.0	3.323	7.97	0.418	0.245	0.266	0.131	-	-		Balance
A356.0	0.12	7.19	0.12	-	0.32	0.12	-	-		Balance

In order to identify the alloys, a nomination system was used, where alloy A was used to indicate HT200 alloy in the as-cast condition. Alloy B was used to identify HT200 alloy subjected to T5 heat treatment, while Alloy C was used to indicate HT200 alloy subjected to T7 heat treatment, and the reference alloys A319 and A356 were termed Alloy D and Alloy E, respectively.

3.2.2. Casting procedures

The alloys used in this study were provided in the form of ingots, cut into smaller pieces, dried and melted in a SiC crucible of 120-kg capacity at a temperature of 750 ± 5º C, using an electric resistance furnace. Measured amounts of additives were calculated by weight for each composition, and added to the melt using a perforated graphite bell, plunged deep into the melt to ensure homogeneous distribution.

Figure 3-1 Casting Furnace

The melt was degassed by injecting dry argon gas at a constant rate for 15-20 minutes by means of a degassing impeller, rotating at a speed of 120-130 rpm to ensure homogeneity and minimize the absorbed gases in the melt. After degassing, the melt surface was carefully skimmed to remove the dross and oxide inclusions from the molten metal. The molds used to prepare the castings for this study were preheated to 450º C. Then the melt was poured at 740 ºC into waffle-shaped graphite-coated metallic molds to cast blocks for machining tests, and into an ASTM B-108 permanent mold for preparing tensile test bar samples, each casting providing two test bars.

Figure 3-2 Waffle-Shaped Permanent Mold

The geometry of the waffle block casting is designed with initial dimensions of 300 mm length, 200 mm width, and 30 mm thickness, with five ribs with an average width of 1 in or 25.4 mm. A facing process was applied to improve the surface quality of the block after casting. For tensile tests, standard bar samples were cast with 50 mm gauge length and 12.7

mm cross-sectional diameter. Seventy blocks were produced for machining tests, fourteen blocks for each alloy, in addition to 25 test bar castings, for tensile testing, five for each alloy.

3.3 Heat treatment

After casting, the HT200 blocks were divided into three groups, coded A, B and C. Together with the group of A319.0 and the group of A356.0 blocks, coded D and E, five groups of alloys were used. These were subjected to different heat treatment processes or tempers as follows.

- Group corresponding to Alloy A (HT200) was used in the as-cast condition.
- Group corresponding to Alloy B (HT200) was subjected to T5 heat treatment which consisted of heating the blocks to 250 ºC through 1 hour, soaking for 5 hours at this temperature, then reducing the temperature gradually using air cooling.
- Group corresponding to Alloy C (HT200) was subjected to T7 heat treatment where the blocks were heated to 530 ºC through 2.5 hours, then soaked for 8 hours at the same temperature, followed by quenching in hot water (60 ºC), and then aging at 250 ºC by heating to this temperature for 1 hour, then soaking at this temperature for 5 hours, followed by air cooling.
- Group corresponding to Alloy D (A319.0) was also subjected to T7 heat treatment by heating to 510 ºC through 2.5 hours, followed by 8 hours of soaking, then quenching in hot water (60 ºC), followed by aging at 250 ºC using the same procedure as outlined above.

- Group corresponding to Alloy E (A356.0) was subjected to T6 heat treatment by heating to 540º C through 2.5 hours, soaking the alloy for 8 hours, then quenching in hot water, followed by aging at 180 ºC for five hours, followed by air cooling.

The different heat treatment schemes for the five alloys are summarized in Table 3.2. All heat treatments were carried out using a forced-air Blue M electric furnace as shown in Figure 3.3 with a high accuracy programmable temperature controller (± 2 ºC) for solution heat treatment and aging processes. The tensile test bars were also subjected to the same heat treatments.

Table 3-2 Heat Treatments Used in the Present Study

Alloy Code	Alloy Type	Heat Treatment				
		Type	SHT* Temperature	SHT* Time	Aging Temperature	Time
A	HT 200	As-Cast	—	—	—	—
B	HT 200	T5	—	—	250º C	5 hrs
C	HT 200	T7	530º C	8 hrs	250º C	5 hrs
D	A 319	T7	510º C	8 hrs	250º C	5 hrs
E	A 356	T6	540º C	8 hrs	180º C	5 hrs

* SHT: Solution Heat Treatment

Figure 3-3 Heat Treatment Furnace

3.4 Microstructural examination

In order to study the microstructural characteristics, specimens were sectioned from test bar samples obtained from the five alloys. The specimens (about 10 mm thick) were sectioned about 10-15 mm below the fracture surface, and individually mounted in bakelite using a Struers Labopress-3 Mounting Press. The mounted samples were subjected to successive grinding and polishing procedures to achieve the desired mirror-like surface finish for metallographic examination.

The grinding and polishing process was carried out using a Struers Tegrapol-35 Grinder-Polisher. Grinding was carried out employing SiC abrasive papers with grit sizes of # 120, # 240, # 320, # 400, # 600, # 800, using water as a lubricant. A significantly high pressure was applied on the specimens during the grinding process to assure the quality and the rate of the grinding process, without excessive heat generation or tear of the abrasive.

Polishing was carried out using Struers diamond suspension, with diamond particle sizes of 6 µm and 3 µm, successively. Struers DP-lubricant was used as the lubricant for these polishing steps. The third stage of polishing was carried out using a Mastermet colloidal silica suspension, SiO_2, having a particle size of 0.6 µm. Water was used as lubricant in this final polishing stage. After polishing, the samples were washed in alcohol, and then dried by compressed air. A summary of the grinding and polishing procedure is given in Table 3.3.

Table 3-3 Grinding and Polishing Procedure

Stage	Abrasive	Particle Size (µm)	Coolant	Pressure(lb)	Time (min)
1	SiC (120)	100	Running Water	15	2:30
2	SiC (240)	50	Running Water	15	3:45
3	SiC (320)	35	Running Water	15	4:00
4	SiC (400)	26	Running Water	15	4:45
5	Diamond	6	Special Oil	32	3:30
6	Diamond	1	Special Oil	32	3:30
7	Diamond	0.25	Special Oil Running Water	25 1	2:30 5:00

The polished samples were examined using an optical microscope-Clemex Vision PE 4.0 image analyzer system, as shown in Figure 3.4. Microstructural characterization included grain size measurements and eutectic Si particle measurements (particle area, length roundness and density). Phase identification and examination of precipitates was carried out using a Hitachi S-4700 field emission scanning electron microscope (FESEM). The purpose of the FESEM was to assess the distribution, size and density of the hardening precipitates in the alloys with the different heat treatments applied.

Figure 3-4 Optical microscope-Clemex Vision PE 4.0 image analyzer system

3.5 Tensile testing

Five bundles of test bars from the different alloys were cast using the ASTM B-108 mold, and heat treated, using the same procedures applied to the blocks. Each bundle consists of five test bars with standard dimensions (70 mm gauge length and 12.7 mm cross-sectional diameter) that were tested to evaluate the average tensile properties at ambient temperature. (25ºC). The average ultimate tensile strength (UTS), yield strength (YS) at 0.2% offset strain and percent elongation (%El) values were obtained from each set of five bars tested for each alloy. The average values obtained over the five tests were taken to represent the average tensile properties for the specified alloy/condition.

A Servohydraulic MTS Mechanical Testing machine was used to carry out the tests, using a strain rate 4 x 10^{-4} s^{-1} as shown in Figure 3-5. A strain gauge extensometer (with a 50.8 mm range) attached to the gauge length of the test bar was used for elongation measurements. The data acquisition system of the machine with Test Works 4 software records and provides the yield strength, ultimate tensile strength and the percentage elongation values.

Figure 3-5 MTS Mechanical Testing Machine

3.6 Machining procedures

A preparation process was applied to the blocks before machining, by surfacing both sides and drilling four fixation holes for installation purposes. After that, a Huron K2X8five CNC machine located at the Centre technologique en aérospatiale (CTA) in Montreal was used to carry out the different machining processes on the blocks as shown in Figure 3-6.

Figure 3-6 Drilling & Tapping by Huran CNC machine

Drilling was carried out using a Guhring 16101256 M6 drilling tool made from Carbide steel at a cutting speed of 240 m/min (15000 rpm) and 0.2 mm/rev feed rate, to fit the designed cutting conditions. This tool has two step straight flutes with coolant-fed carbide "G" type drills with dimensions of 5.08 mm and 7 mm diameter and a minimum length of 30 mm. The coolant used while cutting was Hocut 4549, which is suitable for high speed processes. The CNC machine was programmed to drill 180 M6 holes with 22.5 mm depth for each block or workpiece. These 180 holes are distributed in ten rows with eighteen holes each, two rows per rib, over the five ribs of the workpiece, with a constant spacing between holes.

After drilling, a tapping process was carried out at a cutting speed of 45 m/min to create a standard thread for the holes with 18 mm depth, using a Guhring 971 Carbide tool. The criterion set for the machining process was to devote a tool for each alloy to machine 2700 holes in both drilling and tapping processes. The cutting conditions and tools used in the two processes are summarized in Table 3-4.

Table 3-4 Machining Conditions for Drilling and Tapping

Machine	Huron K2X8 machine
Coolant	Hocut 4549
Drilling	
Drilling Tool	Guhring 16101256, PT14A 10328, T01008, ID2187851 5.1 x 7.0mm
Drilling Speed	240 m/min
Feed rate	0.2 mm/rev
Diameter	M6 Standard Hole
Depth	22.5 mm ± 0.5
Tapping	
Tapping Tool	Guhring 971 H6 M6 6HX, HM K/P 15.0/70.3, 33442
Drilling Speed	45 m/min
Feed rate	By pitch
Depth	18 mm ± 0.5

In order to evaluate the machinability of the different alloys, four major aspects were examined and analyzed: Cutting forces, tool wear, built up edge and chip characterization.

3.6.1 Cutting force measurements

In order to calculate the cutting forces on the tool, the machining process was carried out in two stages to analyze the forces on the cutting tool. The first stage was to install a hardware configuration on the machine to measure and record the cutting forces in both drilling and tapping processes, while the second stage was to analyze the force components, filter them, and calculate the main cutting forces and moments.

3.6.2 Output recording phase

In order to measure the forces, a specific configuration was used, where a four 6-component piezoelectric quartz crystal dynamometer was installed on the base plate on which the workpiece is installed over the four sensors using installation studs. These dynamometers transform the acting forces into proportional electric charge, which can be transformed in terms of Newtons according to the charge intensity.

Figure 3-7 Distribution of holes over the block

Eight charges are generated by these four dynamometers in the different directions, which are Fx_{12}, Fx_{34}, Fy_{14}, Fy_{23}, Fz_1, Fz_2, Fz_3, Fz_4 with a sampling rate 10MHz, which means that there are eight recorded readings for every 0.0001 s along the whole machining processes. Charges are converted into forces by passing the charges through amplifiers in order to magnify the signal then convert them by analog to digital circuit, then representing the data and recording it through special interface on LabView, in order to use them to calculate the major force components through the next phase of the experiment. Figure 3-8 shows the analogue to digital unit that used to transform the electric sensor signals in force units.

Figure 3-8 Hardware Configuration and Analogue-to-Digital Unit

3.6.3 Force calculation phase

In order to calculate the main components over the drilling tool and the tapping tool, a specific algorithm was designed on MATLAB using signal processing libraries. The algorithm will be explained in details in Section 3.7 in this chapter. This algorithm transforms the recorded signals into the basic components of forces Fx, Fy, Fz and Fr, taking into consideration the effects of rotation and noise; following which it calculates the maximum and average value of each force component for each hole to summarize the behavior of the alloy.

3.6.4 Tool Life and Built-Up Edge

Tool life is one of the most important factors to consider in terms of economics and quality, as it significantly affects the surface finish and tolerance of the machined workpiece. A restricted criterion was designed for evaluating tool life for drilling and tapping processes.

The criterion of the experiment is to devote a tool for each alloy to machine 2700 holes. In case of tool failure before achieving this number of holes (representing tool life) tool life is recorded for the alloy as the number of holes till breakage. In order to define failure in a measurable way, periodic measurement of flank wear was carried out at a rate of 5 times per plate at corners during the machining test. In order to evaluate the wear of the cutting tools, three types of wear limits were considered as representing tool failure; these are:

- full margin width in the outer corner of the cutting tool is worn
- flank wear achieves 0.015 inches
- the tool fails to gauge or gets broken

According to this criterion, the life of each tool was measured by the number of holes drilled, and the failure of the tool recorded accordingly.

In addition to tool life measurement, a specific plan was followed to evaluate built-up edge (BUE) by measuring it periodically after drilling a specific number of holes in each alloy, for the five alloys studied. A digital microscope type Keyence 2000 was used with a magnification of 100X to have clear measurements for wear and built-up accumulation as shown in Figure 3-9. The measurements included the height and the width of built up edge over the three involutes of the tool. The maximum and the average value of built up edge were considered for each alloy to evaluate the alloy behavior.

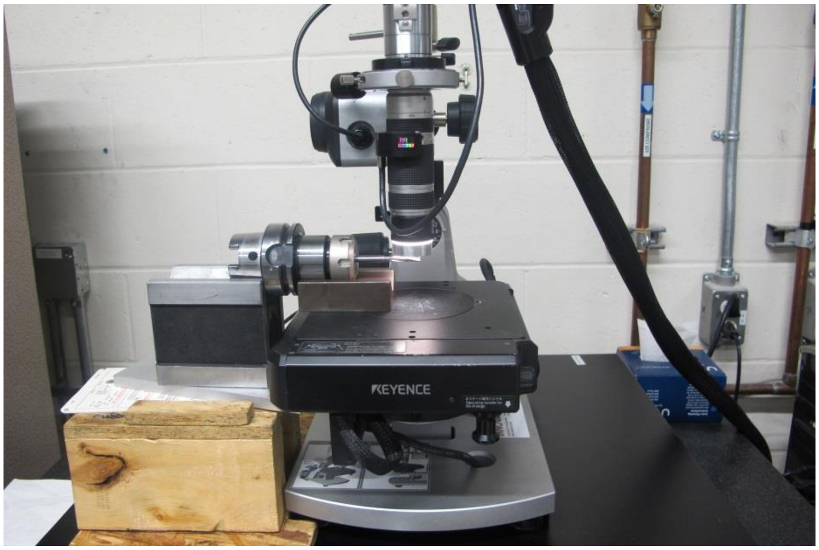

Figure 3-9 Microscope used for BUE measurements

3.6.5 Chip characterization

Chip characterization is an appropriate means for estimating the surface integrity after machining, by evaluating the morphology of the generated chips, chip size and the rate of chip formation. Thus, in addition to tool wear and built up edge (BUE) evaluation, chip characterization was also included to assure the quality of the surface. The plan followed to study chip morphology and BUE is summarized in the Table 3-5.

Table 3-5 BUE and Chip Morphology Testing Plan

Block	No. of drill	No. of Tap	Microscope & Chip Inspection	Holes
Alloy A				
A1	1	1	√	180
A3	1	1	√	540
A5	1	1	√	900
A7	1	1	√	1260
A9	1	1	√	1620
A11	1	1	√	1980
A13	1	1	√	2340
A15	1	1	√	2700
Alloy B				
B1	2	2	√	180
B2	2	2	√	360
B3	2	2	√	540
B4	2	2	√	720
B5	2	2	√	900

B7	2	2	√	1260
B9	2	2	√	1620
B11	2	2	√	1980
B13	2	2	√	2340
B15	2	2	√	2700
Alloy C				
C1	3	3	√	180
C2	3	3	√	360
C3	3	3	√	540
C4	3	3	√	720
C5	3	3	√	900
C7	3	3	√	1260
C9	3	3	√	1620
C11	3	3	√	1980
C13	3	3	√	2340
Alloy D				
D1	4	4	√	180
D2	4	4	√	360
D3	4	4	√	540
D4	4	4	√	720
D5	4	4	√	900
D9	4	4	√	1620
D12	4	4	Tap Failure	2160
D13	4	—	√	2340
Alloy E				
1	10	10	√	180
2	5	10	√	360
3	5	10	√	540
4	5	10	√	720
5	5	10	√	900
8	5	5	Tap Inspection	1260
9	5	5	Tap Inspection	1440
10	5	5	√	1620
11	5	5	Tap Inspection	1800
12	5	5	Tap Inspection	1980
14	5	5	Drill Inspection	2340

3.7 Data analysis phase

The recorded data after the machining process were imported in the form of mdt extension files to be processed on MATLAB. A sophisticated code was written in order to read, represent, and process the data using specialized libraries. The raw data were the forces recorded between each two sensors for the horizontal forces, and the recorded values from each sensor for the vertical forces, at a high frequency rate of recording (10 MHz). So the data input were Fx_{12}, Fy_{23}, Fx_{34}, Fy_{14}, Fz_1, Fz_2, Fz_3, Fz_4 in addition to the timing of each record.

The algorithm imports the data and calculates the main force components in the three directions (Fx, Fy, Fz) in order to get the raw forces using the following equations:

$$Fx = Fx_{12} + Fx_{34} \;, \quad Fy = Fy_{14} + Fy_{23} \;, \quad Fz = Fz_1 + Fz_2 + Fz_3 + Fz_4$$

The main force components for drilling and tapping are shown in the Figures 3.10 and 3.11. These forces were studied in order to recognise the patterns of forces and identifying the timing of holes. These figures show that in drilling there is no clear sign to distinguish the holes by Fx and Fy components. But Fz and Fr clearly show a periodic cycle pattern, which enables us to identify the timing of the holes, while in tapping the force components reveal clear periodic patterns which are distinguishable as holes.

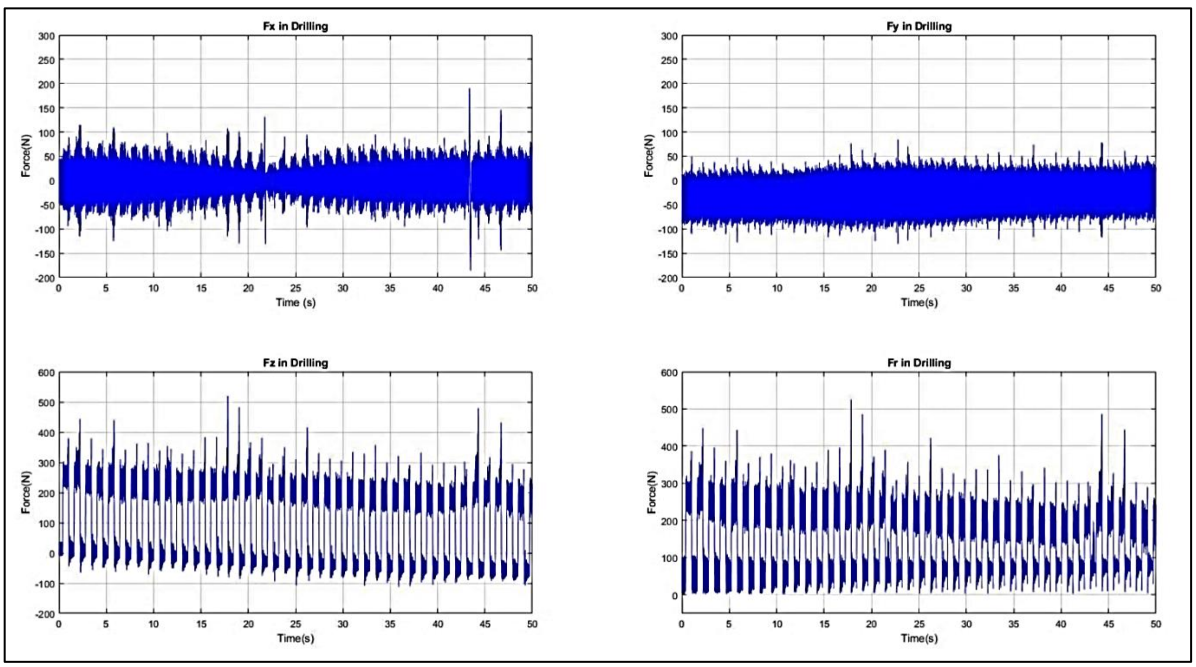

Figure 3-10 Basic Force Components in Drilling

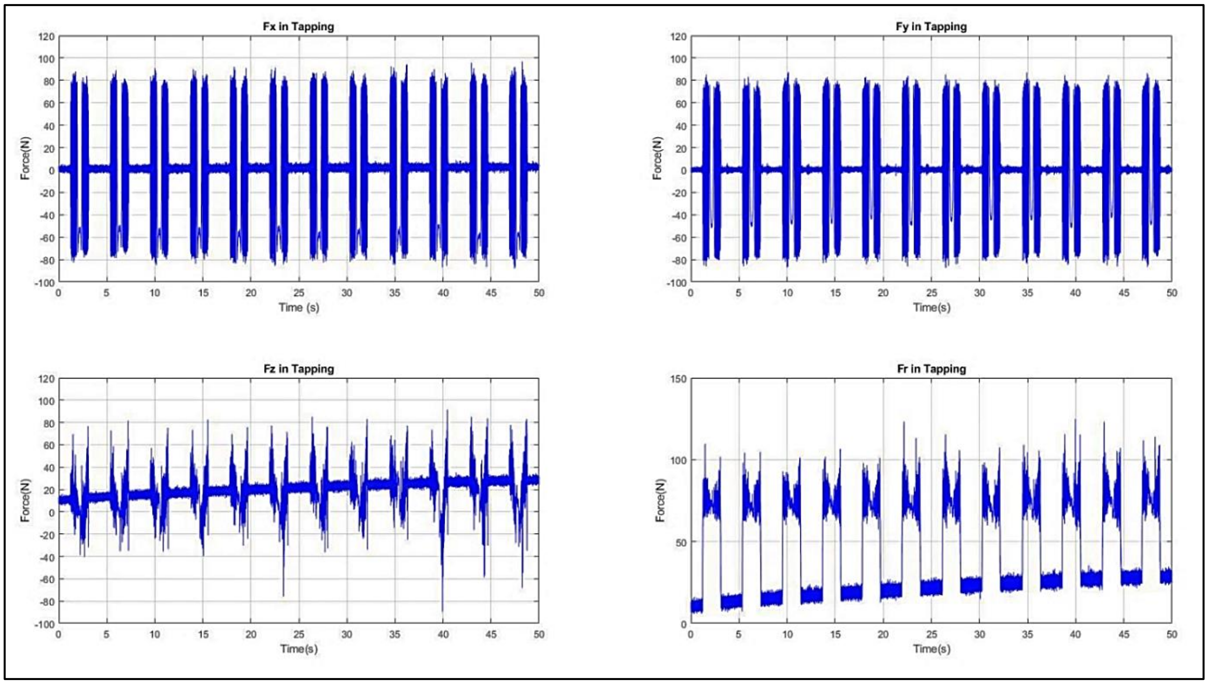

Figure 3-11 Basic Force Components in Tapping

After this step, frequency analysis was applied on the cutting force components in order to identify the basic frequencies of the forces and eliminate the effect of noise from the recorded data. This step was carried out by calculating Fourier series for the data to evaluate the power of each frequency in the system. As Figure 3.12 reveals, two dominant frequencies for the forces could be distinguished: the forces resulting from the feed rate movement, and the forces resulting from the effect of cutting speed.

After identifying the dominant frequencies and noise frequencies, several types of filters were designed in order to identify convenient filtration criteria for the forces. For this, median filters, digital filters, dynamic average and Savetsky-Golay filters were tested to evaluate their convenience, and a digital low pass filter was optimized to filter the forces to get a clear behavior for the drilling and tapping cycles with 1000 Hz passband frequency for drilling and 1000 Hz passband frequency for tapping as shown in Figure 3.12.

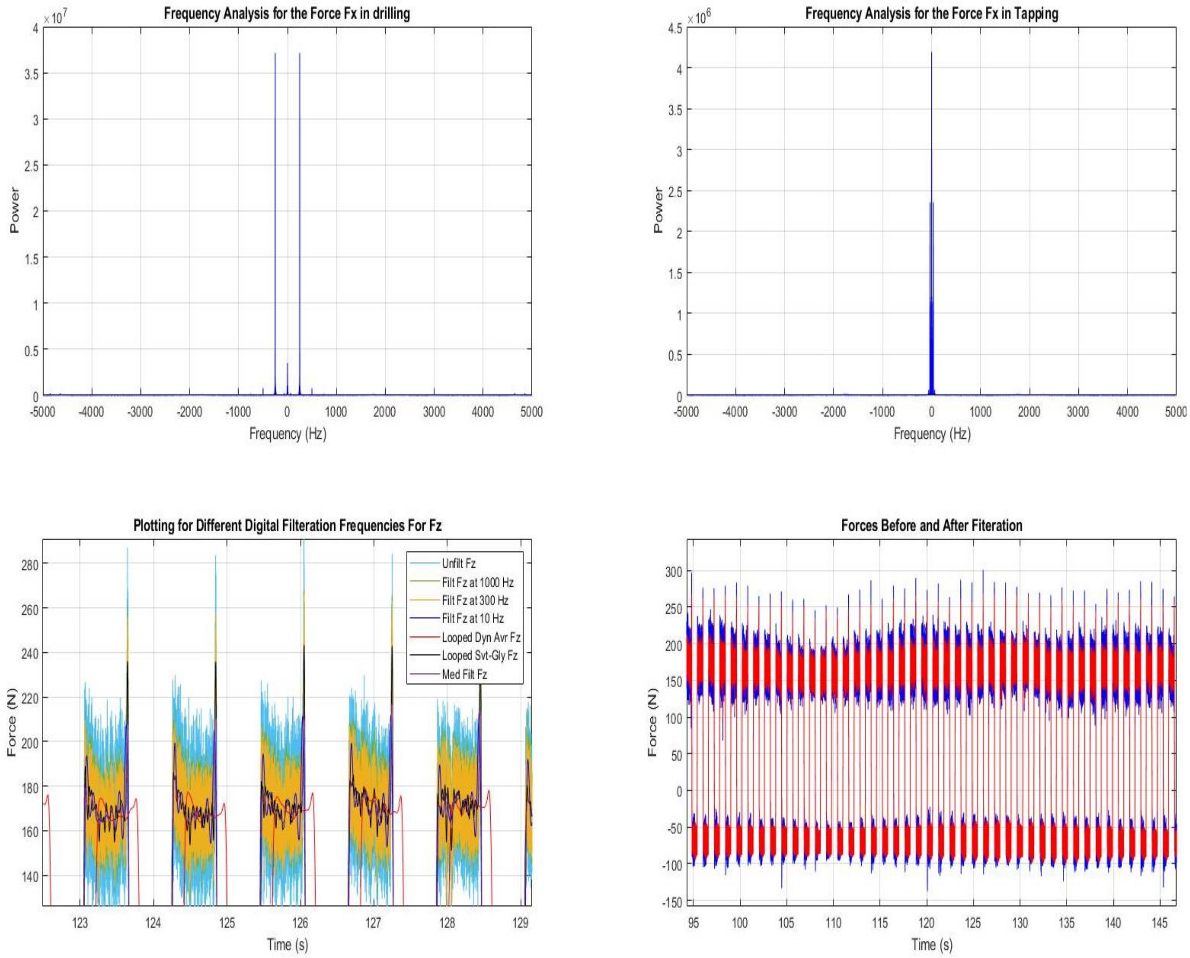

Figure 3-12 Different applied filters and the force before and after filtration

Besides filtration, the vertical force Fz showed an augmented deviation from the zero point. This augmented error deviates each cycle toward starting from negative values (tension) instead of zero in drilling and tapping. Therefore, the axial force requires re-adjustment to represent real values. Therefore, a MATLAB function was designed using a signal-processing toolbox in order to re-calibrate the recorded axial force. This function involves three main steps: cycle recognition to calibrate each hole separately, then defining reference for the cycle, after that cycle shifting was applied on each cycle to start from the reference. Cycle recognition function was designed using a combination of (findpeak) built-in function in MATLAB and derivatives analysis for the signal for a very finely filtered version of the recorded signal, where the first derivative indicates maxima and minima. After that, cycle shifting was applied using a simple mathematical function to obtain the corrected version of the signal, as shown in the Figure 3-13, without affecting the readings of the peaks of the forces.

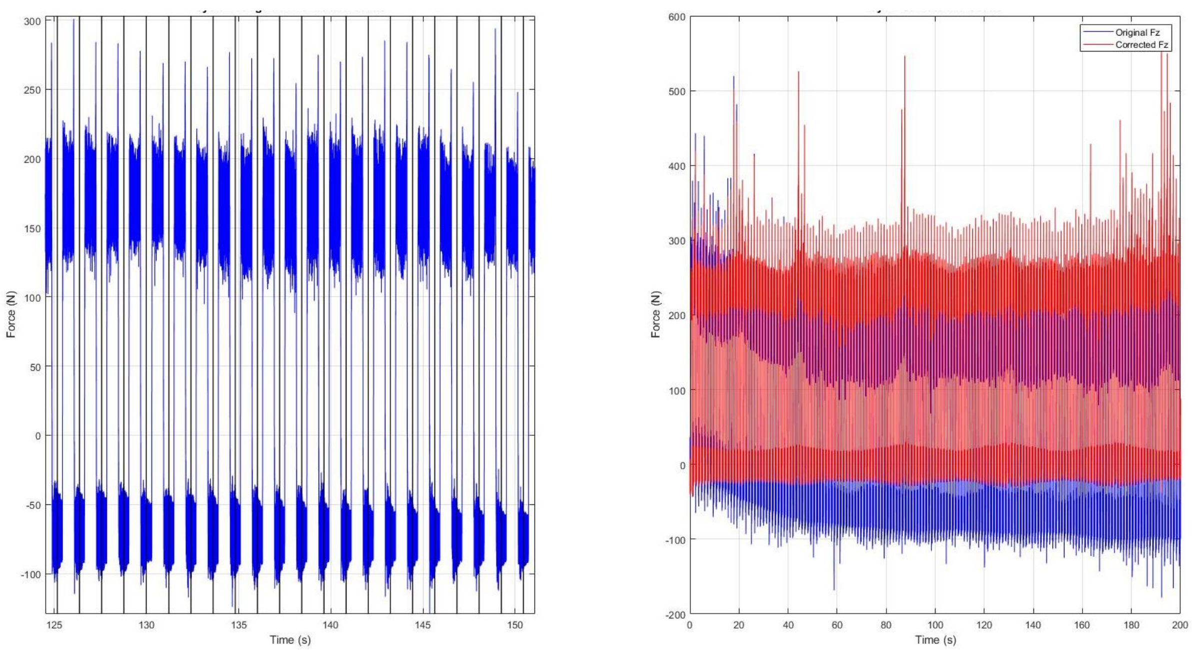

Figure 3-13 Cycle recognition and error correction

After the cycle adjustment step, the shear force and resultant force were calculated from their components according to the following equations:

$$Fs = \sqrt{Fx^2 + Fy^2} \quad , \qquad Fr = \sqrt{Fx^2 + Fy^2 + Fz^2}$$

Following these calculations, a peak extraction function was designed to evaluate the maximum and average forces for the different stages of the drilling and tapping processes, namely, engagement, cutting and disengagement and getting the average of these forces as the required force for cutting procedure. The average is used in this function in order to normalize the effect of mechanical shock through the engagement and disengagement stages.

After peak extraction for the different components of cutting forces for each hole, a merging function was designed to accumulate, merge and present the behavior of the whole alloy as shown in Figure 3-14. Therefore, a continuum of the 2500 holes of each alloy was merged by this function to represent the change in force components with the aging of the cutting tool.

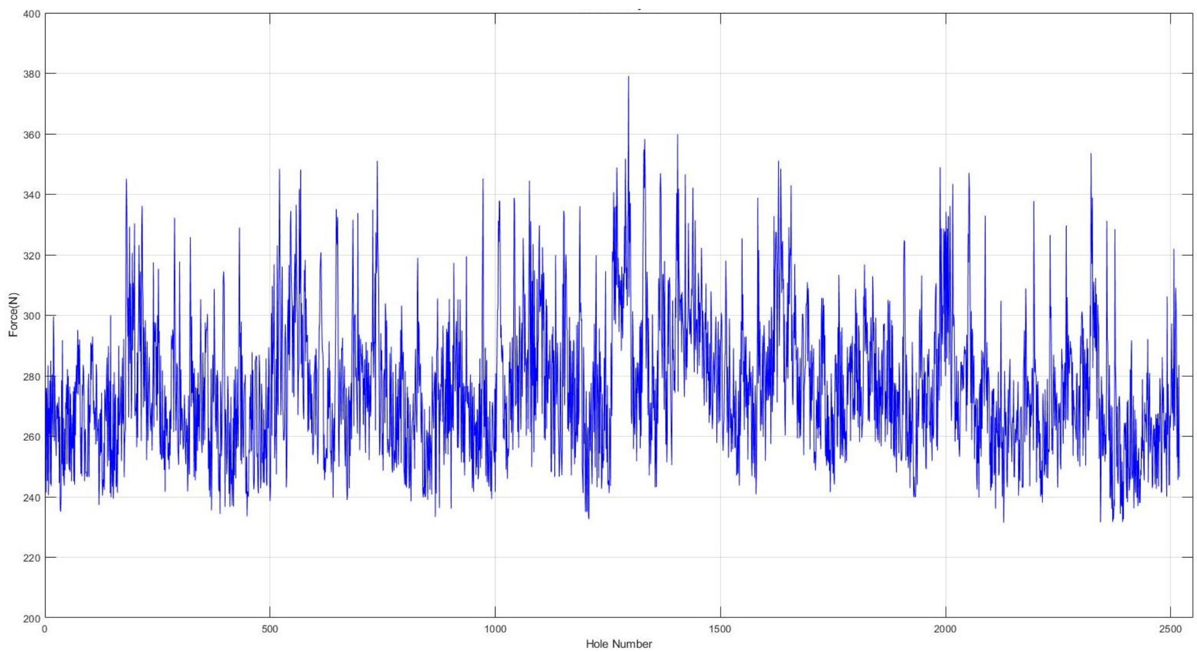

Figure 3-14 Force across the Alloys

After merging the data of the different alloys in order to obtain a full picture of each alloy, different curve fitting functions were used to understand the alloy behavior. Smoothing functions and curve fitting functions were applied over the resulting graph, to get the best fit for the obtained results and to find a suitable mathematical formula to represent these results

.

CHAPTER 4

RESULTS AND DISCUSSION

CHAPTER 4

RESULTS AND DISCUSSION

4.1.Introduction

Machinability is the phenomenon which represents the ease, cost and quality of the metal removal process of a work piece for shaping the work piece by the cutting tool. As the material response toward different operations and different cutting conditions is different, in the industrial domain it is preferable to define it as a property of the system than as a property of the material. Considering machinability as a system property allows us to define machinability as an interactive phenomenon between the workpiece, cutting tool (tool material and geometry) and cutting medium (wet or dry cutting) for different removal sequences such as turning, drilling, tapping, milling and sawing under different cutting conditions which include cutting speed, feed rate and depth of cut [1, 2].

Many research investigations were undertaken in order to analyze the role of the tool geometry on the machinability of different alloys under different cutting conditions for different machining processes. In the case of turning, Fang et al. [3] introduced a new model to predict chip formation in chamfered and honed tools for aluminum alloys and concluded that the ratio between thrust force and cutting force varies according to the thickness of the uncut chip. Also, that the thrust force can exceed the cutting force if the uncut chip thickness is less than the critical thickness, which can be determined by the cutting speed and tool geometry [4-6]. On the other hand, with respect to drilling, Schneider [4] reported that in casting alloys with high abrasive materials, it is preferable to use solid carbide drills with twist drills to make the edges more resistant to wear at higher speeds [5, 7]. Soares et al. [5]

investigated chip breaker systems in different cemented carbide and PCD diamond cutting tools, in order to evaluate their quality in the machining of aluminum alloys. They reported that inserts with big grooves, with a high angle of entrance in the chip breaker, showed good results in power consumption, surface roughness and chip control for roughing operations ($f > 0.14$ mm/rev) in high silicon-containing aluminum alloys [6].

Tool wear is the main factor that controls tool life. It takes place as a gradual process because of continuous interaction between the cutting edge and workpiece under specific cutting conditions, till failure of the tool. The wear process depends on tool material and geometry, workpiece material, and the cutting parameters and medium. This process occurs naturally because of the loads of wear surfaces and the fast movement of cutting chips and workpiece which subject the tool to these loads under conditions of high temperature because of friction. These mechanical factors are unavoidable in the material removal process, so wear is an unavoidable production problem in manufacture [2, 8].

Material properties such as strength, ductility and hardness also affect different machinability aspects as cutting force, chip formation and surface integrity. Generally, increase in strength of the alloy improves the surface finish of the machined part; on the other hand, it can accelerate tool wear because of bad chip formation. An enormous amount of force is necessary in order to initiate formation of chips in a material with high strength. In this case, the design of the cutting tool should take into consideration a less positive cutting angle and a stronger tool material [9].

The principal aim of the work presented in this chapter was to optimize the alloy composition and heat treatment conditions on drilling and tapping characteristics of the newly developed Al-6% Cu alloy (coded HT200). In addition, to compare the performance of the Al-Cu alloy with the widely used Al-Si based 319 and 356 commercial alloys [10]. The study also investigates the tensile properties, microstructure and machinability behavior of the HT200 alloy castings under different heat treatment conditions, to include these important aspects of the production process.

4.2. Drilling characteristics

4.2.1. Microstructure and tensile properties

Figure 4-1 shows the optical microstructures of samples of the three alloys A, D and E sectioned from their as-cast tensile bars. The large amount of Cu in the alloy A (or HT200 alloy) is reflected in the precipitation of coarse Al_2Cu phase throughout the entire matrix along with a few α-$Al_{15}(Fe,Mn)_3Si_2$ phase particles as presented in Figure 4-1(a). As reported earlier [11], modification with Sr would lead to a divorced eutectic reaction, where the Al-Si eutectic is observed separated from the Al-Al_2Cu eutectic, as seen in Figure 4-1 (b) for alloy D (i.e. 319 alloy). In addition, the α-Fe phase particles are also rejected in front of the advancing Al-Si eutectic-Figure 4-1(c). Pucella et al. [12] reported on the inverse precipitation of α-Fe in Sr-modified alloys. In this case, the α-Fe phase precipitates within the α-Al during solidification of the alloy-Figure 4-1(d). In other words, the α-Fe precipitates prior to the formation of the α-Al dendrite network. The importance of this reaction is to harden the soft α-Al leading to more-or-less uniform strength over the entire alloy. Figure 4-1(e) is an enlarged micrograph of alloy E (i.e. 356 alloy) revealing partial transformation of β-Al_5FeSi phase to π-Al_8Mg_3FeSi phase at ~560°C followed by the precipitation of Mg_2Si phase at about 545°C-Figure 4-1(f) [13].

Table 4-1 lists the tensile properties of the five used alloys following the heat treatments described in Table 3-2. The as-cast HT200 alloy itself shows relatively good characteristics, with almost 96% of the ultimate tensile strength of the 319 alloy after T7 treatment, but with a significantly low yield tensile strength and elongation, whereas Alloy E exhibits the highest ductility, thus it may indicate higher sensitivity to burr formation mechanisms [14].

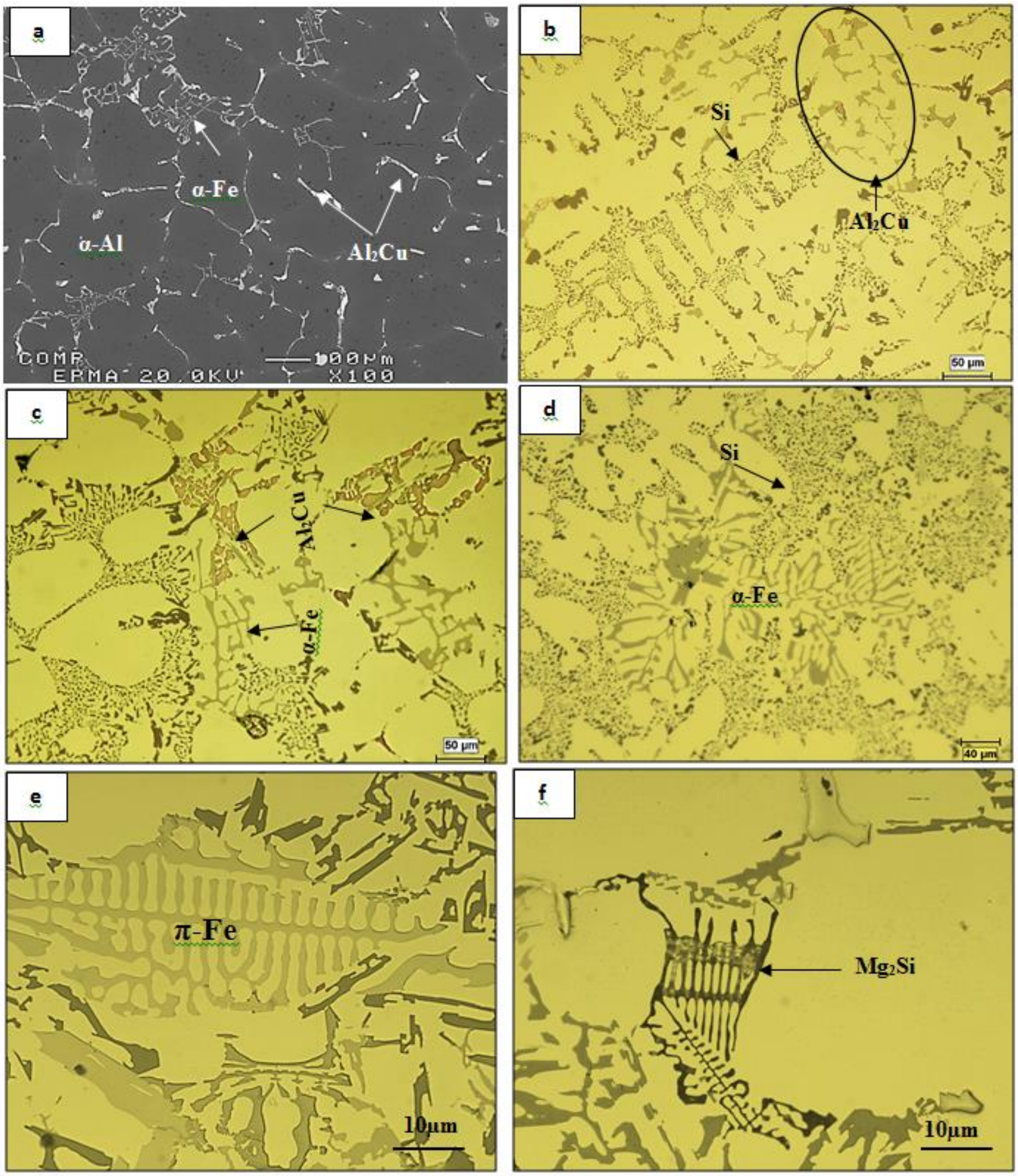

Figure 4-1 Optical microstructures of alloys in the as-cast condition: (a) alloy A, (b, c) alloy D, (d-f) alloy E

Table 4-1 Tensile properties of the studied alloys

Alloy	UTS (MPa)	YS (MPa)	EL%
Alloy A	285	212	2.2
Alloy B	298	235	3.4
Alloy C	331	247	5.3
Alloy D	295	244	3.8
Alloy E	355	310	6.9

The T5 heat treatment of alloy B for 5 hours increased its elongation by 1.2%, coupled with a slight improvement in its ultimate tensile strength by about 5% and better improvement in the alloy yield strength, by about 12%, from the original as-cast value (alloy A). In comparison, alloy C (in the T7 treated condition) showed real improvement in all three properties: the elongation increased by about 3% and both the yield strength and the ultimate tensile strength increased by about 17 % above the values obtained from alloy A.

In terms of comparison between alloy HT200 and the commercial alloys, it can be noted that the T7 heat-treated HT200 alloy (coded alloy C) reveals a comparable performance to the 319 alloy - also T7 heat-treated, in terms of yield strength but with a higher elongation. On the other hand, alloy C exhibits lower yield strength compared to the 356 alloy (T6 heat-treated) despite its comparable ultimate tensile strength and ductility values. Figure 4-2 demonstrates the effect of heat treatment on the size and distribution of Al_2Cu phase particles in HT200 alloys, as confirmed from the associated EDS spectrum shown in Figure 4-2(d).

The backscattered electron images in Figure 4-3 reveal dense precipitation of hard eutectic Si particles (1000 VHN) in the matrix during the solidification process as shown in Figure 4-3(a) and (b), and Mg_2Si phase particles in alloy E in the T6 condition, as seen in Figure 4-3(d), confirmed by the corresponding EDS spectrum in Figure 4-3(e). In a previous study, the Si particle density was determined to be approximately 41,500 particles/mm^2 [11]. Considering the cross section area of the drill used (approximately 36mm^2), the tool is instantaneously passing through some 2 million hard Si particles.

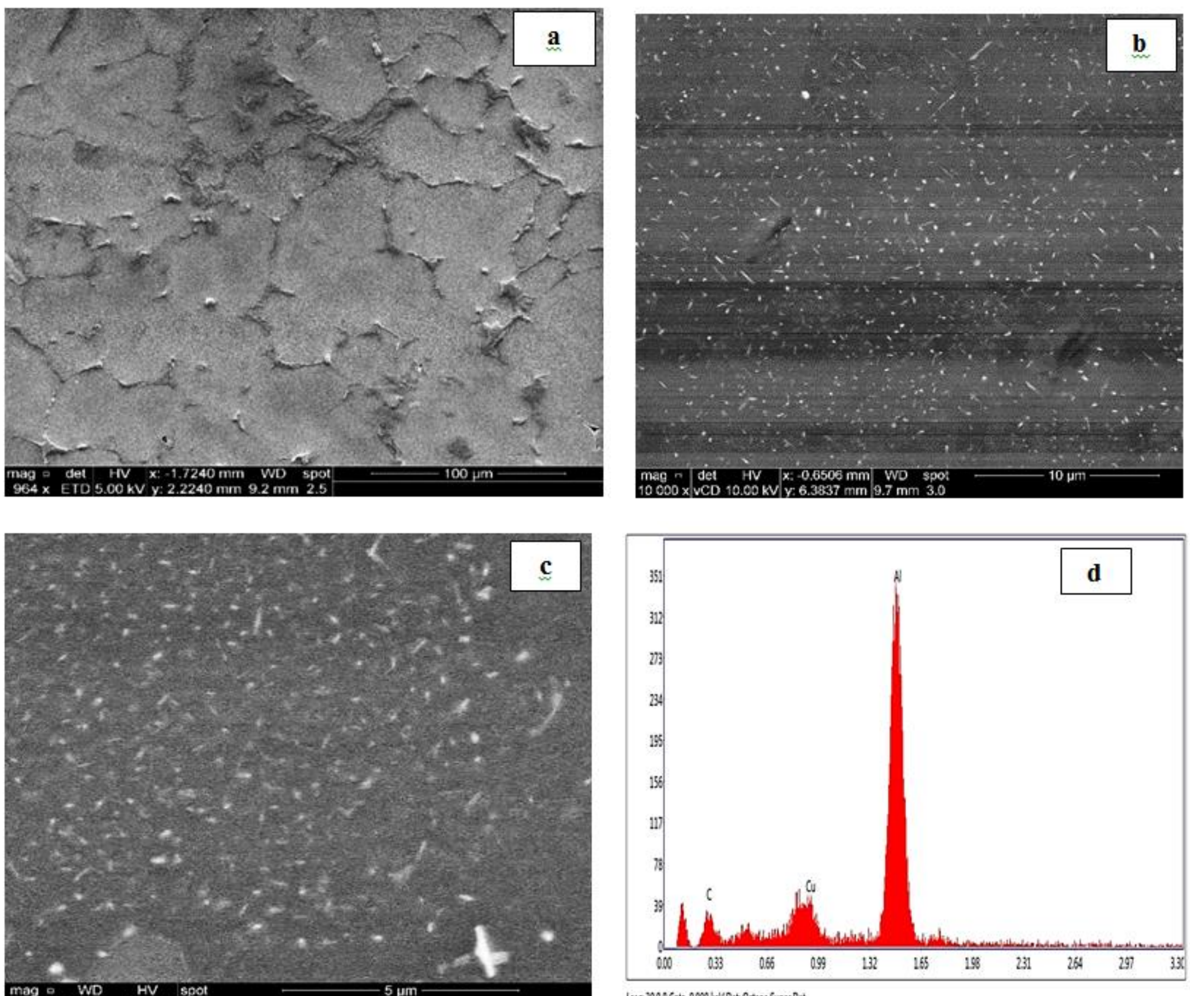

Figure 4-2 **Backscattered electron images showing precipitation in HT200 alloys: (a) alloy A, (b) alloy B, (c) alloy C, (d) EDS spectrum obtained from (c).**

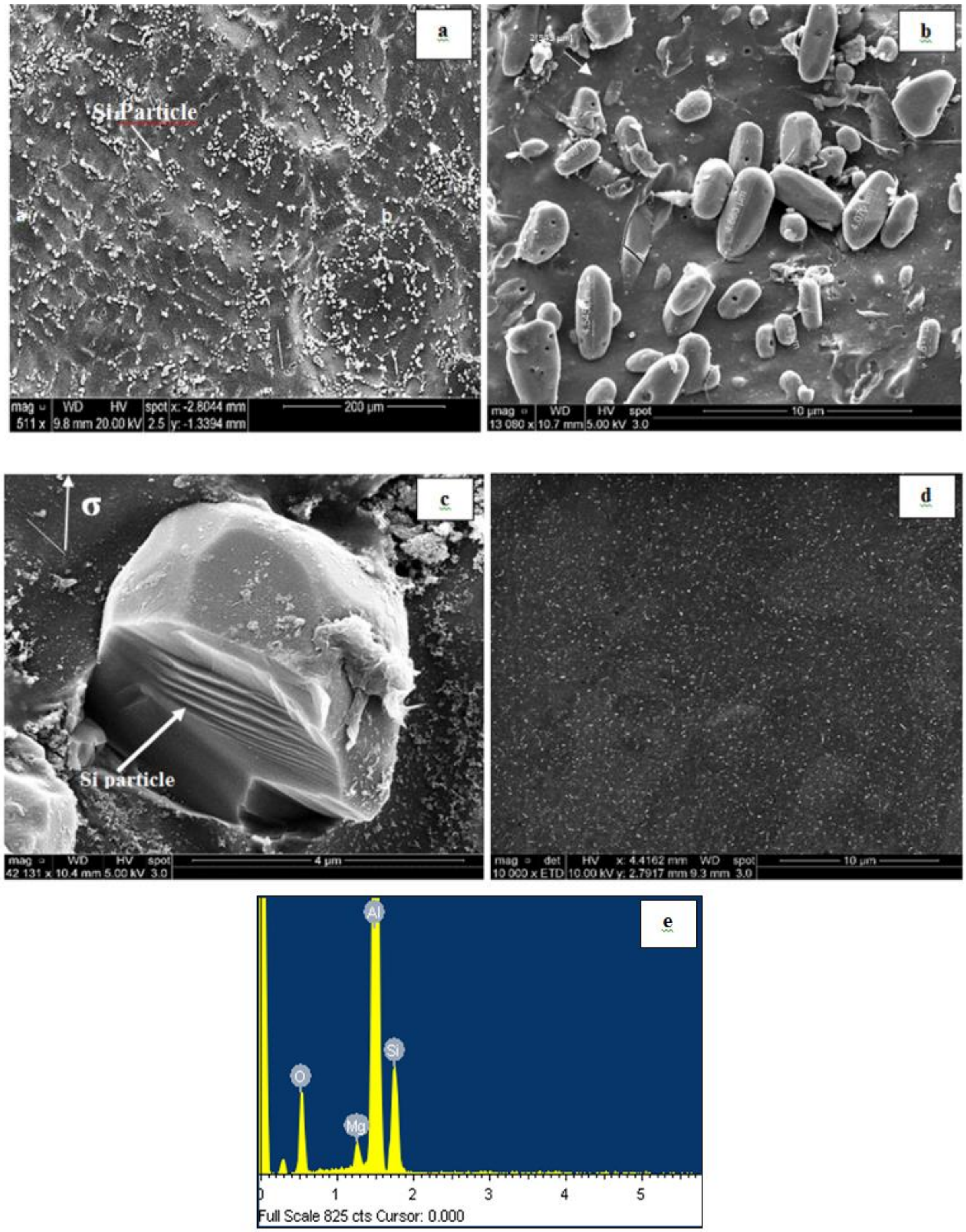

Figure 4-3 (a) Backscattered electron image showing precipitation of Si particles following solutionizing treatment, (b) a high magnification image of (a), (c) fracture of Si particles under tensile load, (d) ultra-fine Mg_2Si particles in alloy E in the T6 condition.

4.2.2. Cutting forces

A restricted criterion was designed for evaluating tool life for the drilling process. The criterion is to use one tool for each alloy to machine 2700 holes. Three conditions were considered to indicate tool failure: if the full margin width is worn in the outer corner, or flank wear achieves 0.375 mm, or the tool fails or gets broken [15]. Figure 4-5 shows a schematic presentation of a drilled block whereas Figure 4-6 reveals the wearing of the new tool displayed in Figure 4-6(a) after drilling 2700 holes (Figure 4-6(b)) using alloys A and E as an example. An important point noted about the surface of the cutting tool when drilling alloy E (see Figure 4-6(c)) - was that an initial deterioration and notches were observed on the tool surface but not with the HT200 alloys. In alloy E, this notch appeared after 900 holes, which indicates fast deterioration of the tool edge, which is to be expected, in keeping with the effect of high silicon content on the machinability in the case of the Al-Si alloys.

Initial results for forces were obtained by applying the algorithm methodology to the data recorded during the drilling process, as illustrated in Figure 4-7. The initial data included 12500 holes drilled for the five alloys; the data was filtered digitally using a 1000 Hz low pass filter to obtain the effect of rotation on the axial and resultant force, where the rotation frequency is almost 250 Hz. It should be noted that different filtration frequencies have only a slight effect on the axial force and resultant force, whereas it is vital to a study of the shear force over the cutting tool. This may be interpreted by the dominance of feed rate on the thrust force, while cutting speed is the main factor affecting shear force. This difference in filtration effect does not appear in the resultant because the main effect comes from the thrust force. The low frequency filtration for shear force indicates a repeated cycle, which may indicate the effect of formation and breakage of built-up edge. This assumption is supported by the fact that alloy B exhibits the highest shear forces and the highest BUE as well.

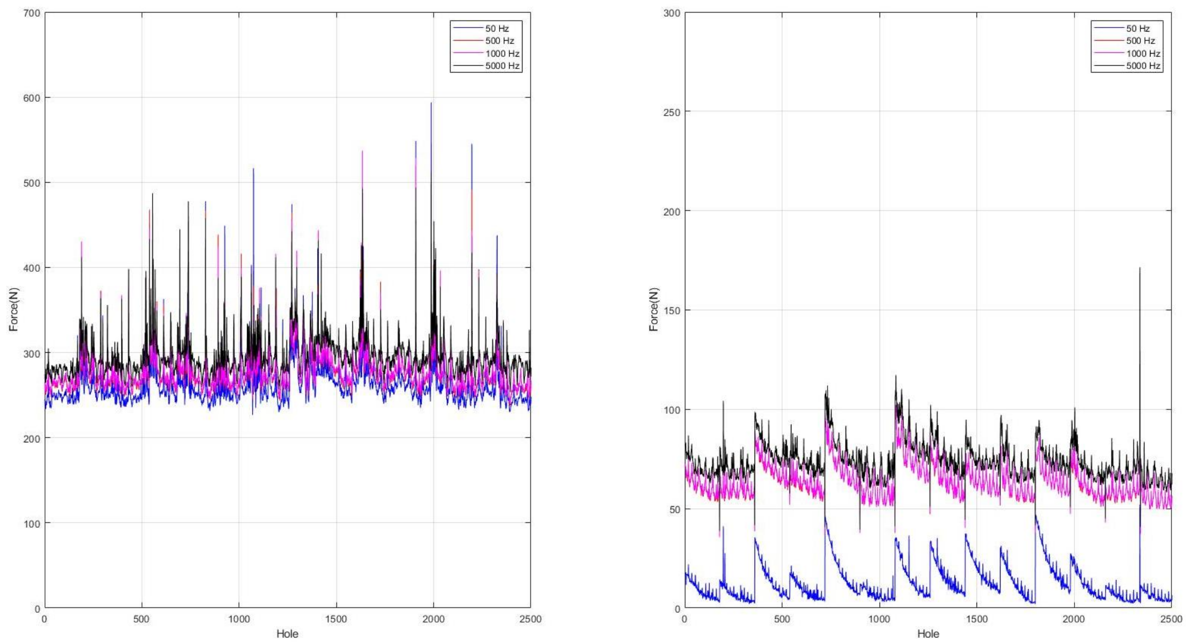

Figure 4-4 – The effect of different filtration frequencies on Fz (on the left) and Fs (On the right)

Figure 4-7 indicates the raw data of axial force and resultant force through 2500 holes for each alloy. Due to the large amount of data in Figure 4-7, which may mask the actual variation in the drilling forces (Fz), the results were replotted vs number of blocks in Figure 4-8, where each spot represents the average of 180 holes drilled per block.

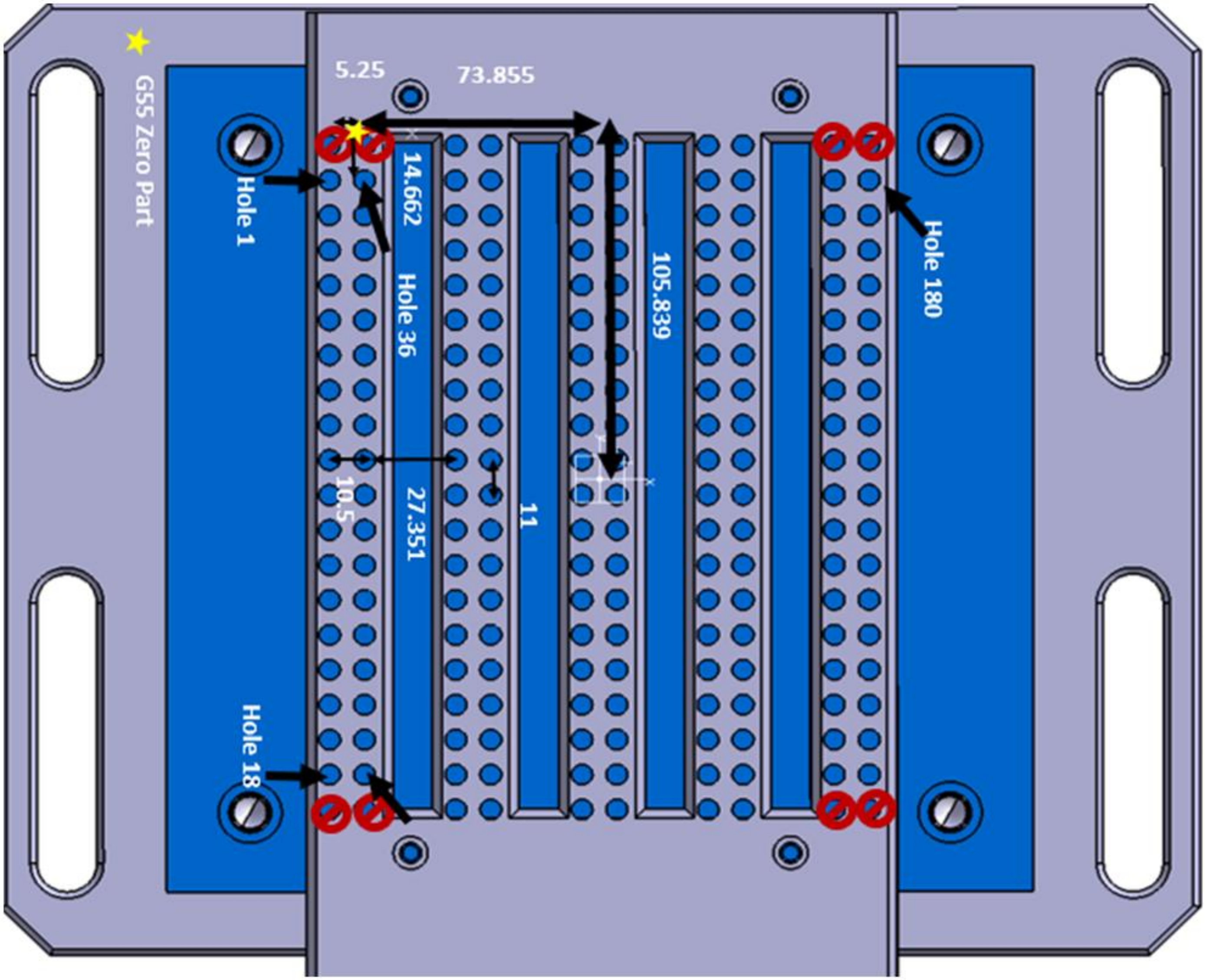
G55 Zero Part
5.25
73.855
14.662
105.839
Hole 1
Hole 36
Hole 180
10.5
27.351
11
Hole 18

(a)

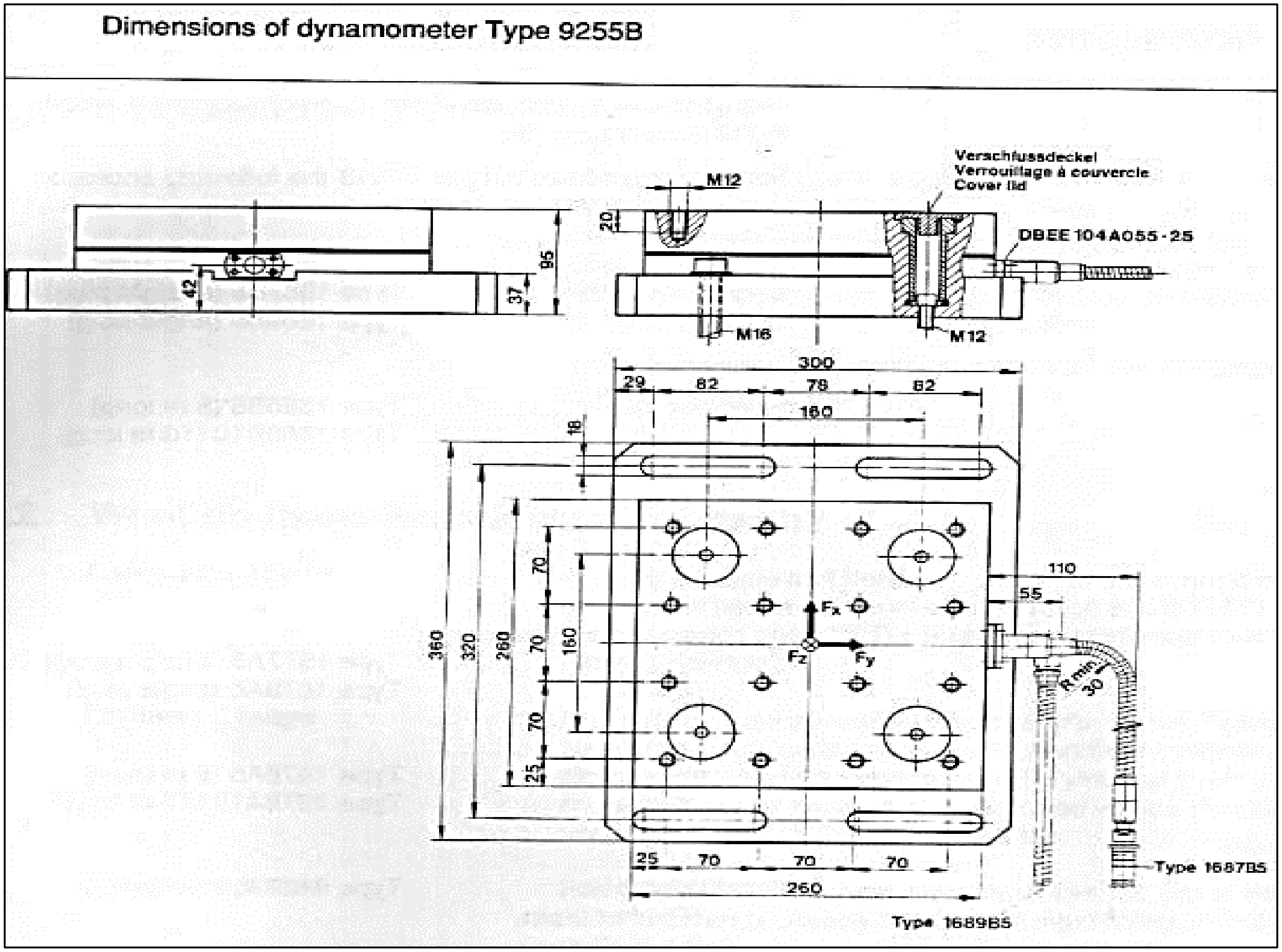

(b)

Figure 4-5 **(a) A schematic diagram showing a drilled block mounted on the drilling stage-180 holes drilled per block (dimensions are in mm), (b) Dynamometers positioning and dimension.**

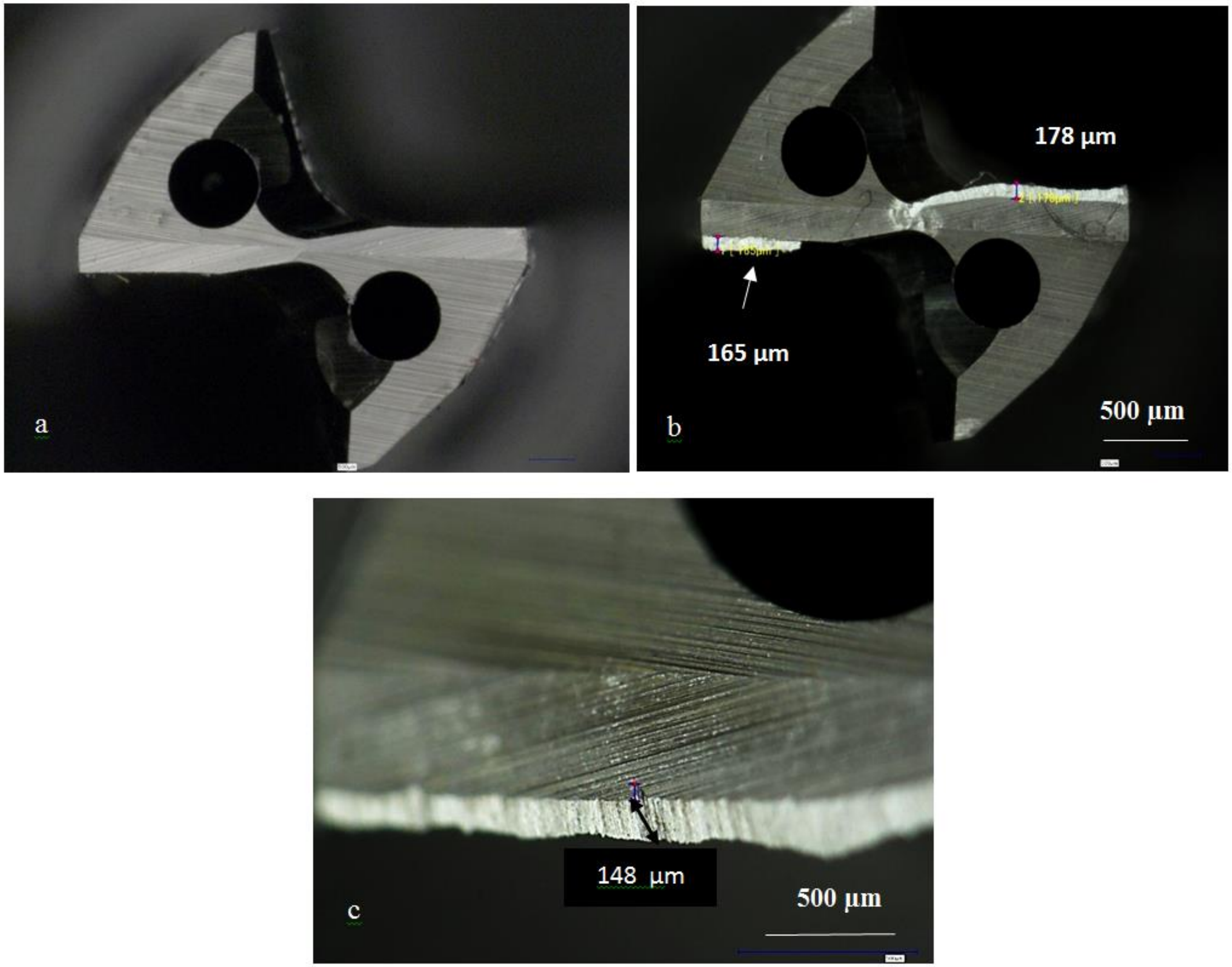

Figure 4-6 (a) New drill, (b) same tool after drilling 2700 holes in alloy A, showing signs of wear, (c) tool after drilling 900 holes in alloy E.

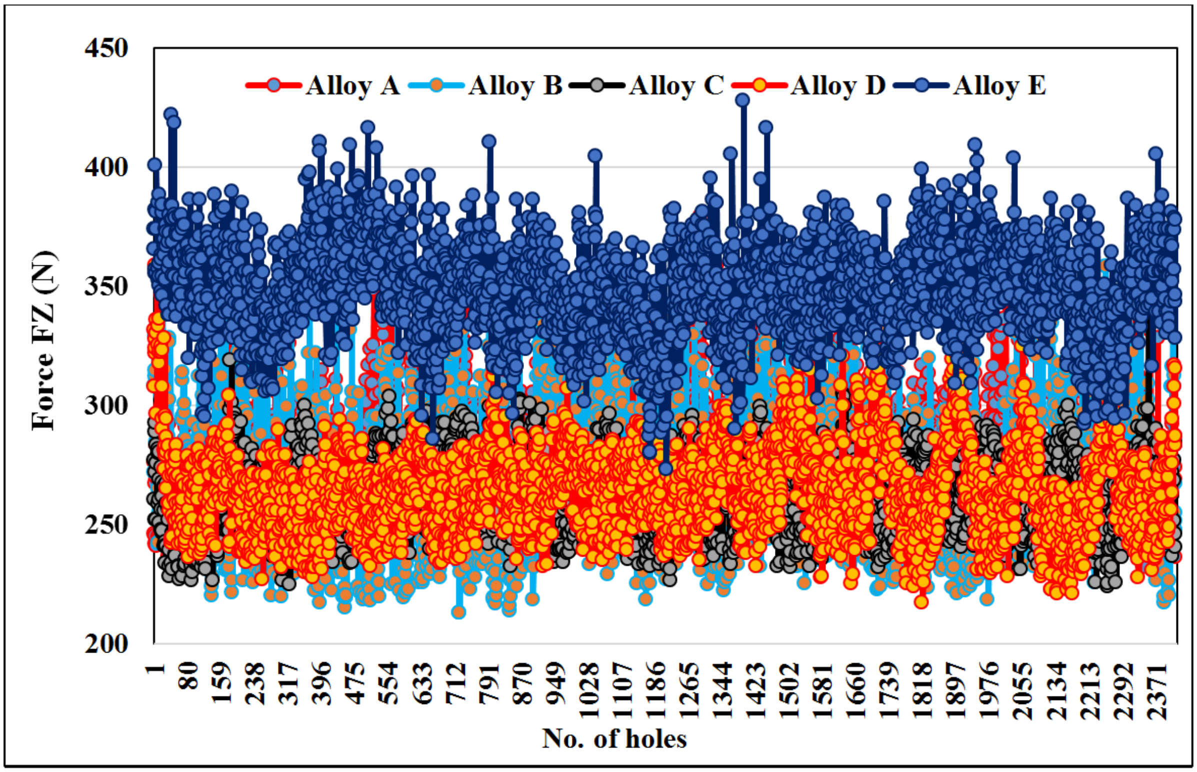

Figure 4-7 Axial cutting forces through different alloys vs number of drilled holes.

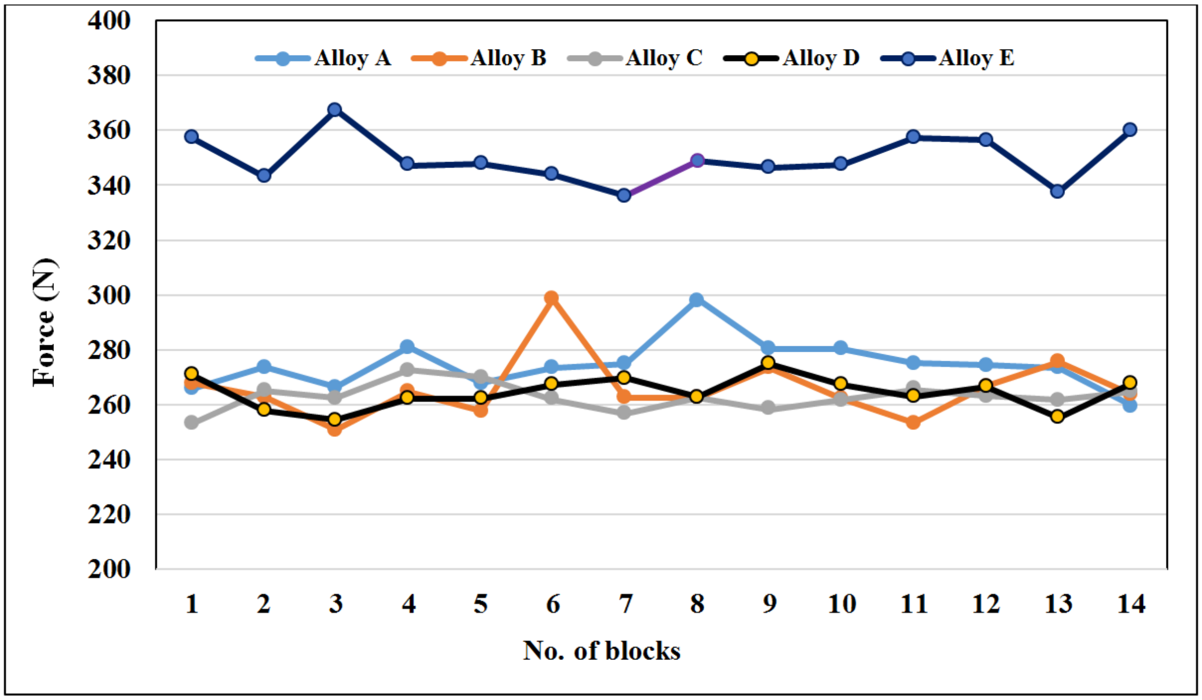

Figure 4-8 Average axial cutting forces through different alloys vs number of drilled blocks.

The main observation to be noted from Figure 4-8 is that alloy E shows the highest cutting forces for both axial and resultant components, which may be interpreted by the energy consumed to fragment silicon particles [16]. On the other hand, Alloy C shows the minimal cutting forces. In addition, the differences in average cutting forces between alloys B, C and D are small, although there is a wide difference in their mechanical properties. It can also be noted that T5 heat treatment of the HT200 alloy, as is the case for alloy B, reduces the necessary cutting forces in the drilling process somewhat, in comparison to the as-cast condition (alloy A). In addition, alloy B performed much better with respect to cutting forces compared to alloy E.

A slight tendency toward increase in the cutting forces with aging treatment was observed in the different alloys. This tendency can be noticed in the slight increase in the average force measured for each block for each alloy, and may be interpreted in terms of tool deterioration with the number of holes drilled. The average cutting forces are presented in Table 4-2. These average values were obtained over 180 holes drilled per block times 14 blocks drilled for each alloy.

Table 4-2 Average cutting forces for the alloys studied

Alloy	Average Fz (N)*	Average Fr (N)**
Alloy A	276 ± 23	284 ± 27
Alloy B	269 ± 28	276 ± 31
Alloy C	263 ± 15	269 ± 19
Alloy D	265 ± 20	272 ± 22
Alloy E	349 ± 21	354 ± 23

* Drilling direction, ** Resultant

2.2. Built Up Edge-Height and Width

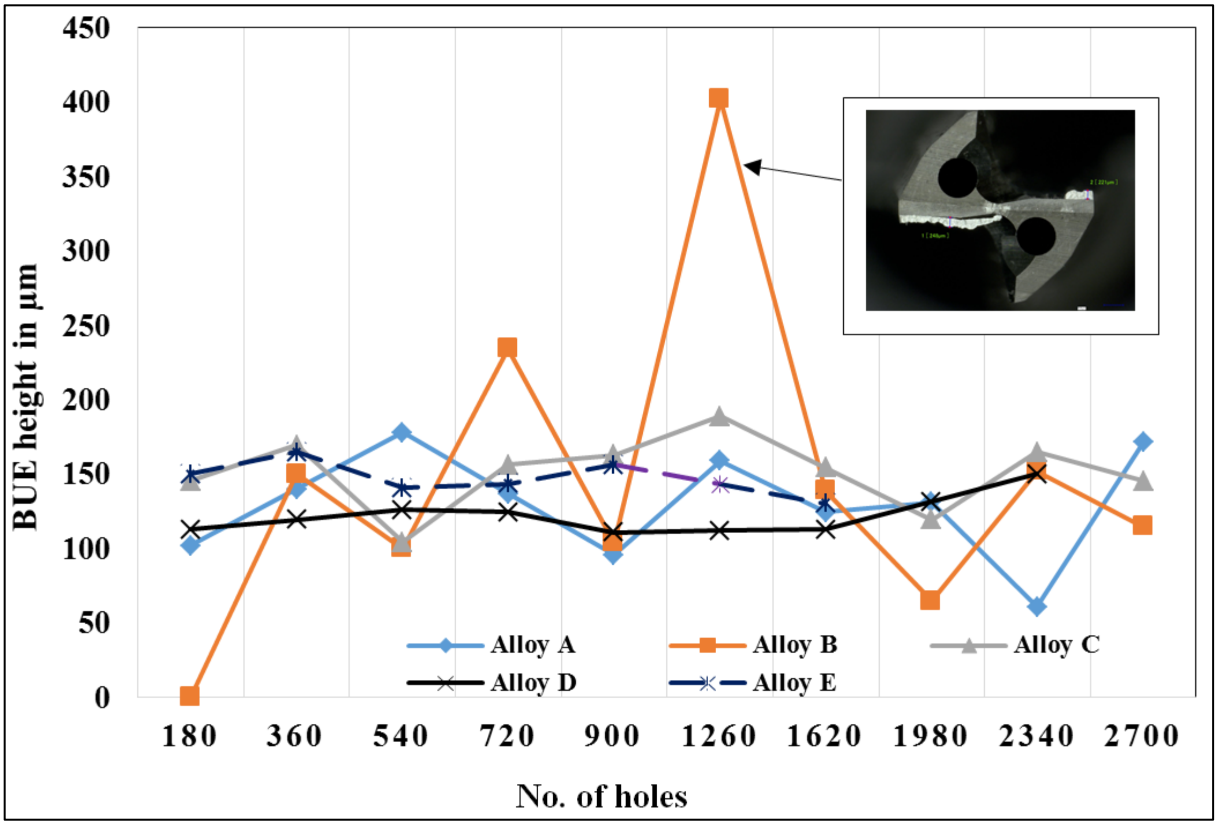

Figure 4-9 Built-up height during drilling.

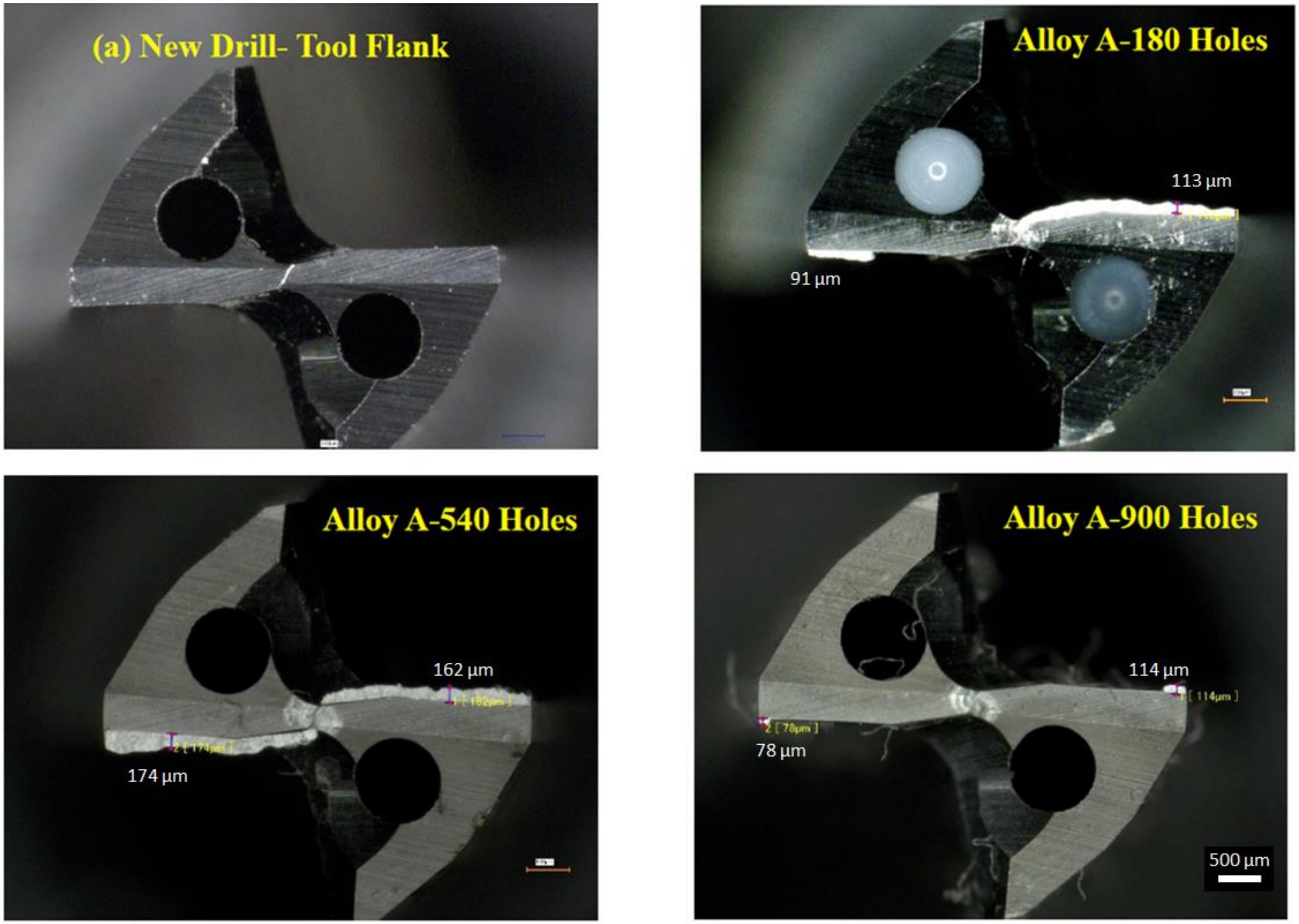
(a) New Drill- Tool Flank
Alloy A-180 Holes
113 µm
91 µm
Alloy A-540 Holes
162 µm
174 µm
Alloy A-900 Holes
114 µm
78 µm
500 µm

(a)

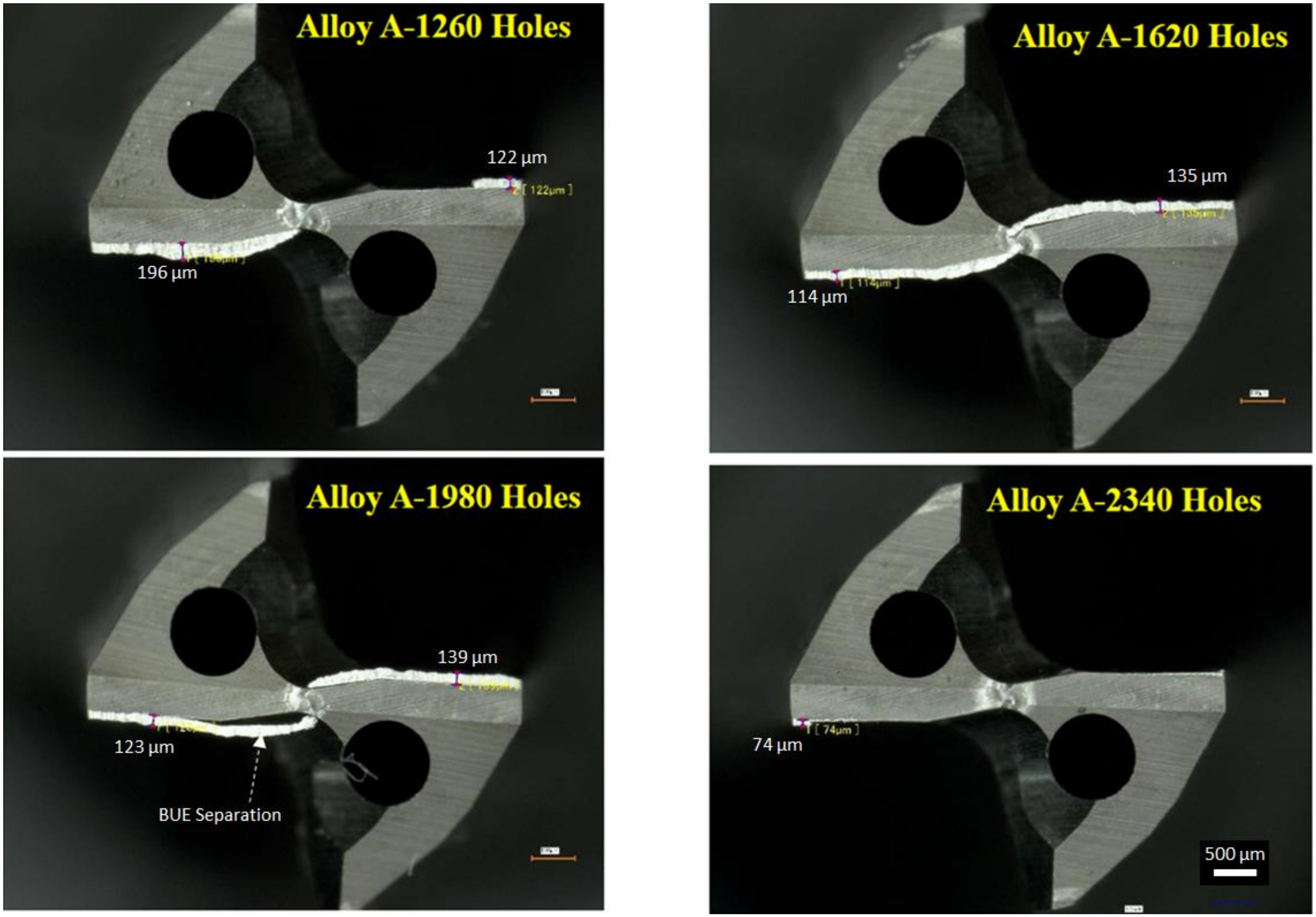
Alloy A-1260 Holes
122 µm
196 µm
Alloy A-1620 Holes
135 µm
114 µm
Alloy A-1980 Holes
139 µm
123 µm
BUE Separation
Alloy A-2340 Holes
74 µm
500 µm

(b)

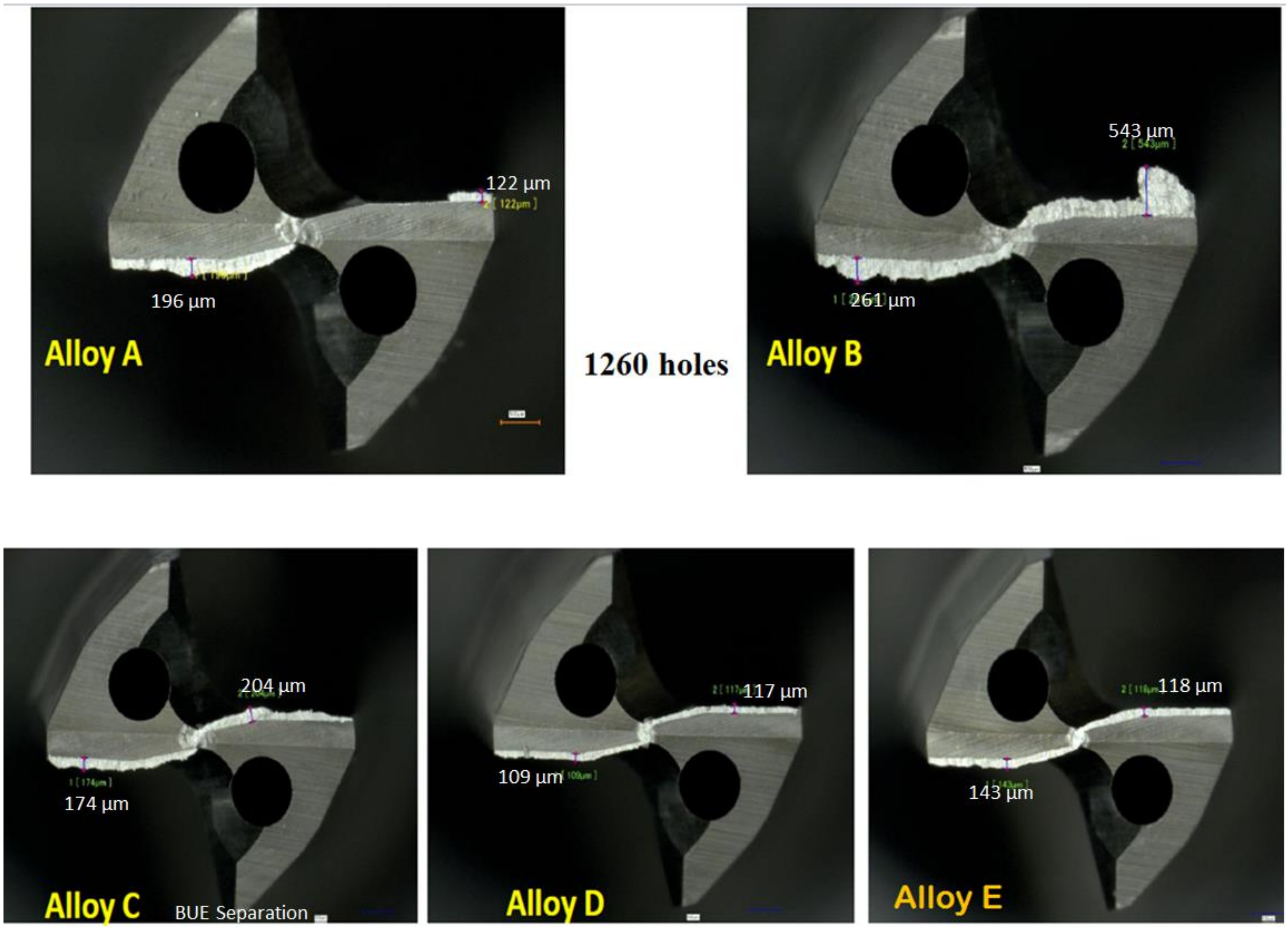

(c)

Figure 4-10 Examples of built up edge corresponding to different alloys after drilling different numbers of holes

Built up edge (BUE) is one of the major factors that affect the quality of the machining process, specifically in terms of surface roughness and hardness of the machined surface [12]. Parra [17] differentiates between the cause of built up edge and built-up layer (BUL). He interprets the BUE formation by a mechanical adhesion mechanism, while BUL forms due to thermo-mechanical causes. In general; Built up edge takes place because of heat generated due to friction, as some hardened particles from the metal flowing over the tool surface are welded to the tool edge because of the localized heat to form a new non-regular cutting edge. These chips start to accumulate over the cutting edge till it achieves the critical size to break. Although the mechanism is almost the same for all materials, the built-up edges formed in different alloys and cutting conditions vary widely in terms of size and shape [18]. The effect of heat built up edge on the machining process is significant with respect to different variables of the material removal process such as chip size, tool life, surface finish and dimensional control [7, 9]. In order to control the built-up edge process, various considerations are used when designing the machining process such as increasing the cutting speed and increasing the rake angle of the tool. Jomaa [19] reported that the built-up edge formation increases by an increase in the cutting feed rate, while increasing the cutting speed can reduce it and promote the formation of the built-up layer on the rake face. Selvam and Radhakrishnan [20] also reported that the extent of the built-up edge and the surface roughness decrease with increasing cutting speed, and that increase in the rake angle decreases side flow and the size of the built-up edge. As well, Azlan et al. [21] affirmed the effect of cutting medium on the formation of Built-up edge.

It can be noted from Figure 4-9 that after taking the measurements through the whole drilling process for the five alloys, the BUE over one side did not exceed 543μm in height -

as shown by the broken arrow in Figure 4-10, whereas the highest average was almost 400μm; both cases were noted for alloy B. In terms of height, alloy B showed a higher tendency to accumulate BUE during drilling, compared to the other alloys, which showed an average BUE within the range of 150 μm. The photograph of the cutting tool in Figure 4-11 reveals that separation of BUE starts to occur when its height is around 250 μm on one face. With respect to the built-up edge width, it can be noted from Figure 4-12(a) that alloy C had the highest effect on tool BUE accumulation. The average width for alloy C was about 600 μm in comparison to the other alloys with an average of about 300 μm. Alloy B also showed relatively higher average BUE width measurements than the rest of the alloys, but still lower than alloy C. Figure 4-13 displays examples of built up width corresponding to the different alloys used in the present study.

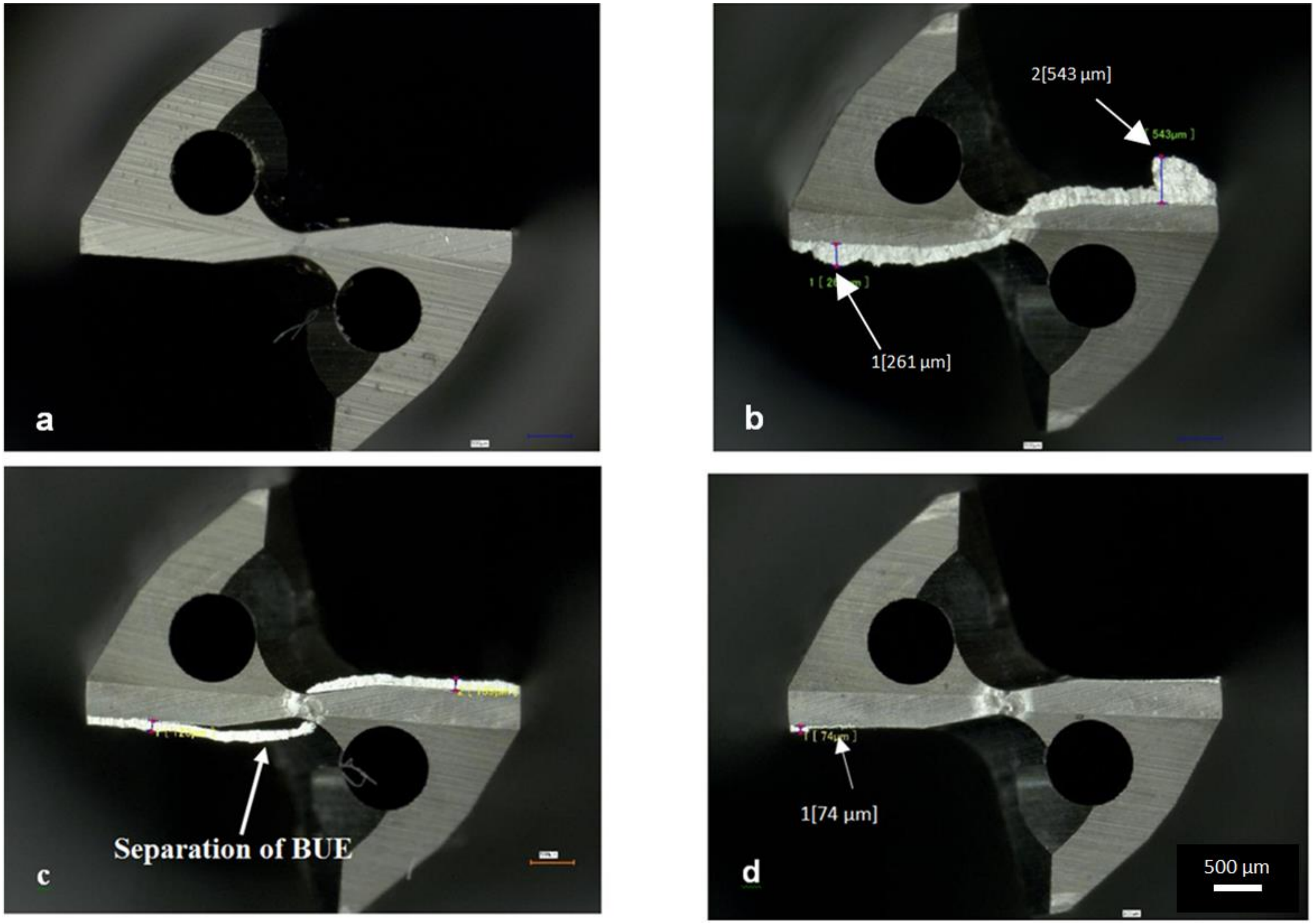

Figure 4-11 **Changes in the thickness of BUE in with the increase in number of drilled holes: (a) fresh tool, and after (b) 1260 holes (alloy B), (c) 1980 holes (alloy A), (d) 2700 holes (alloy A).**

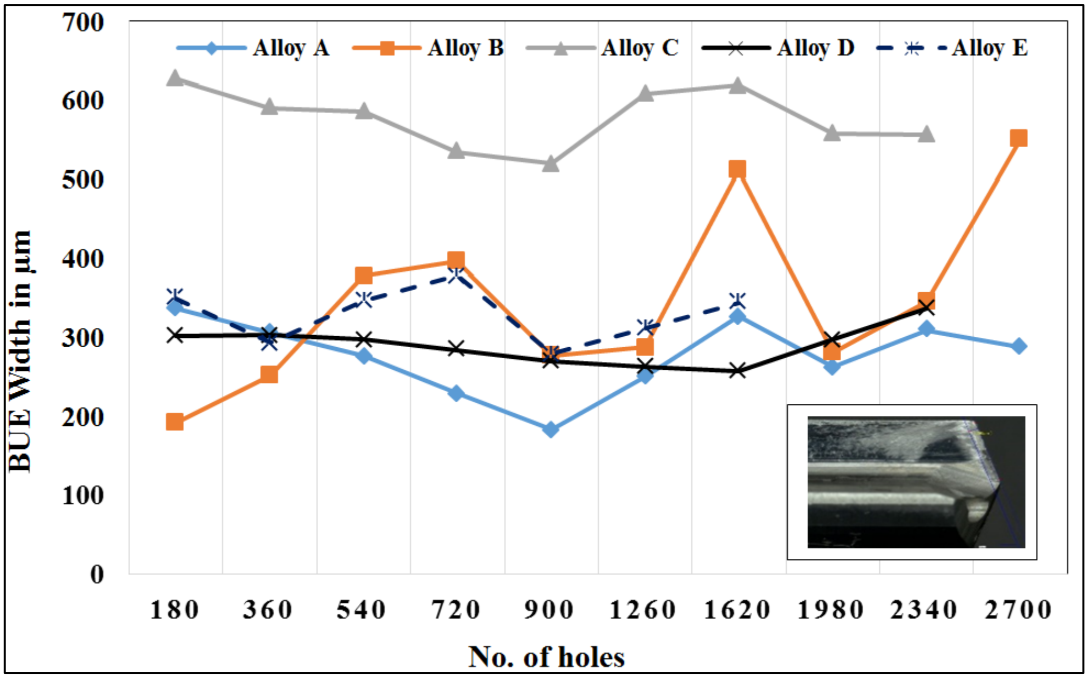

Figure 4-12 Built-up width in drilling- inset photo corresponds to alloy C.

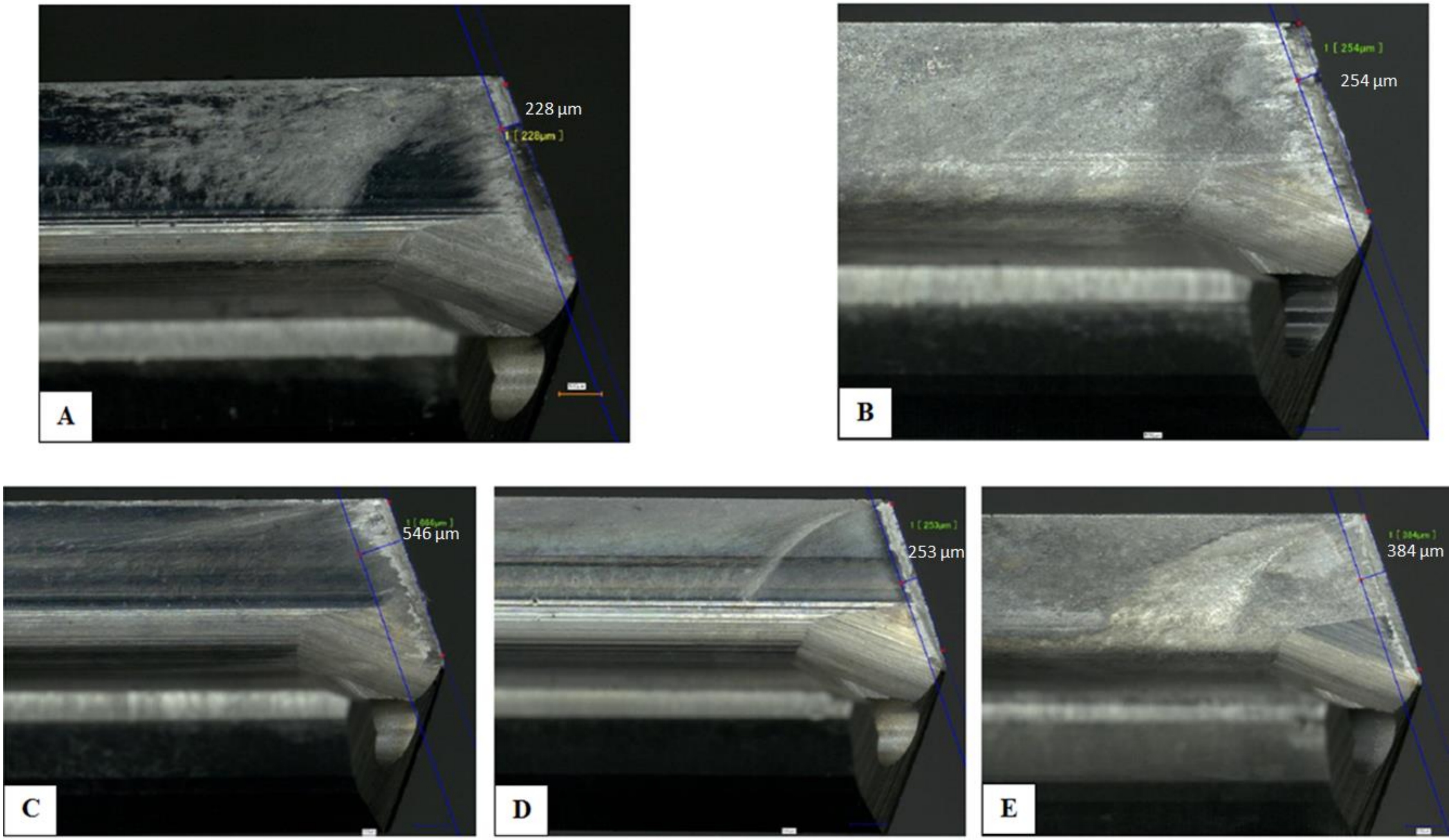

Figure 4-13 Examples of built up width corresponding to alloys A through E

4.2.3. Chip shape

Figure 4-14 illustrates the shape of the chips obtained from the last drilled block (approximately 2700 holes). It is evident from a comparison of Figure 4-14(a) and (b) that heat treatment of HT200 alloy has a marked effect on the shape of the chip. The chip morphology changes from cone in alloy A (area marked A), to a mix of straight, half-turn and full turn chips (area marked B). This can be interpreted by the improvement in the alloy ductility following the T7 treatment. This remark is supported by the work of Kouam et al. [22] that heat treatment can have a different effect on chip segmentation and morphology based on additive elements.

However, in both cases of Alloy A and B, the outer surfaces reveal feed markings caused by the depth of penetration, which may be interpreted by the higher tendency of BUE accumulation thus higher roughness values [16]. In addition, the surfaces appear to be relatively dull and the marking lines on the inner surfaces (drilling direction) are clearly in a direction opposite to those observed on the outer surfaces as indicated by the solid and broken arrows in Figure 4-14(a). Due to the very low Si content in the HT200 alloys, the surface markings are not smooth compared to those obtained from alloys D and E as demonstrated in Figure 4-14(c) and Figure 4-14(d), respectively, where the chips are conical or fan shaped. This may indicate poor breakability of the chips in HT200 alloys in comparison to Alloys D and E, thus lower surface integrity because of chip rotation with the flute [23]. This remark is consistent with the work of Gonçalves and da Silva [24] on the effect of copper content on machinability.

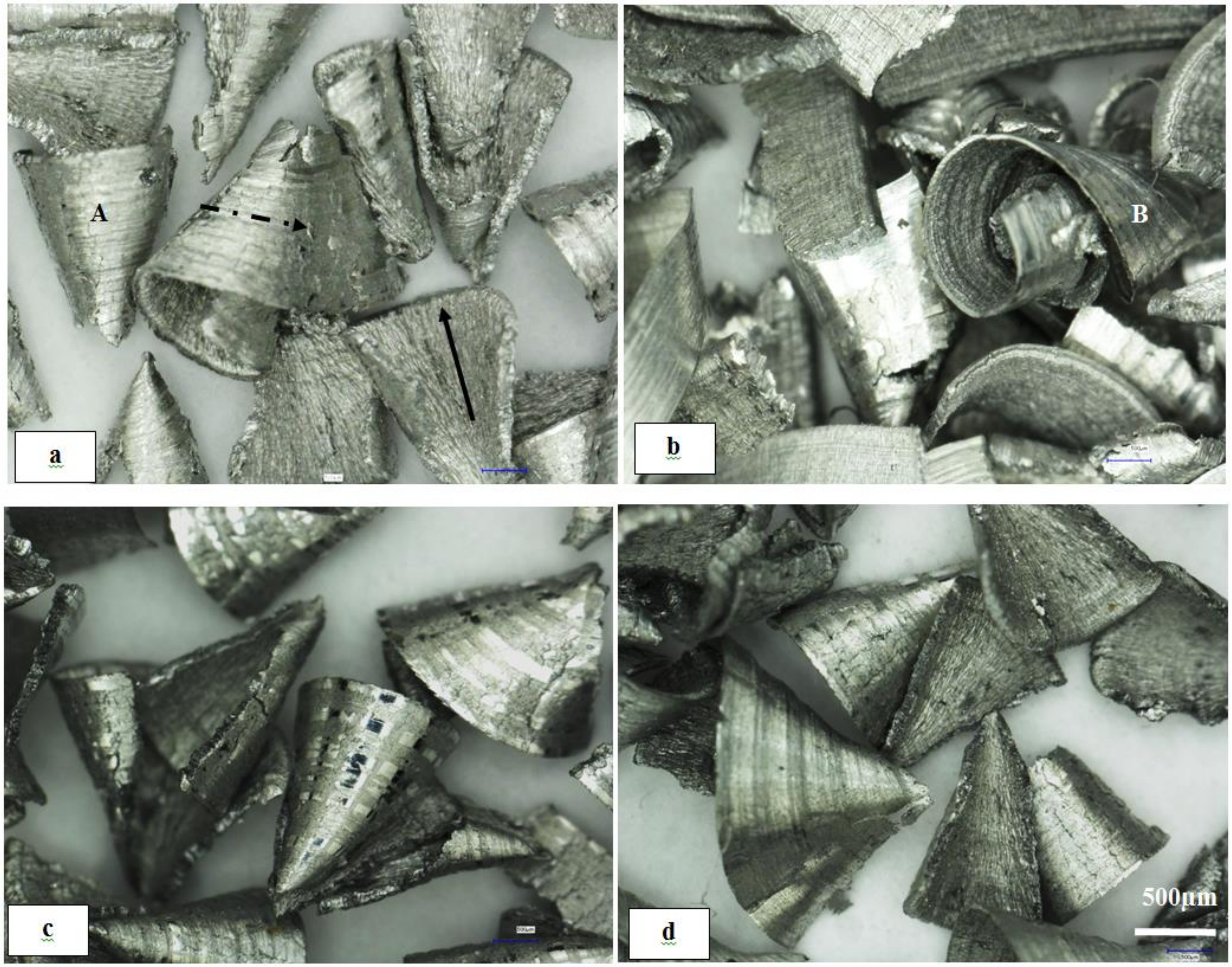

Figure 4-14 Shape of chips obtained from the alloys after drilling 2700 holes: (a) alloy A, (b) alloy C, (c) alloy D, (d) alloy E.

4.3. Tapping parameters

4.3.1. Introduction

Carvalho et al. [25] performed a study on the analysis of form threads using fluteless taps in cast magnesium alloy (AM60). The authors concluded that the best thread profile was achieved when uncoated tools and a forming speed of 100 m/min were used. Filho et al. [26] found that the variation in burr formation at the entrance was greater at the exit than the entrance and the initial diameter affected only the burr formation at the entrance based on an analysis of burr formation in form tapping in 7075 aluminum alloy. Thread forming taps are also known as fluteless taps, form taps, roll taps or cold forming taps. They form threads by displacing material without producing chips. Form taps are used on aluminum, brass, copper, lead, stainless steel, carbon steel, cast steel, leaded steel and zinc, as well as other mild steels and medium alloys. Thread forming advantages are summarized in Figure 4-15 :

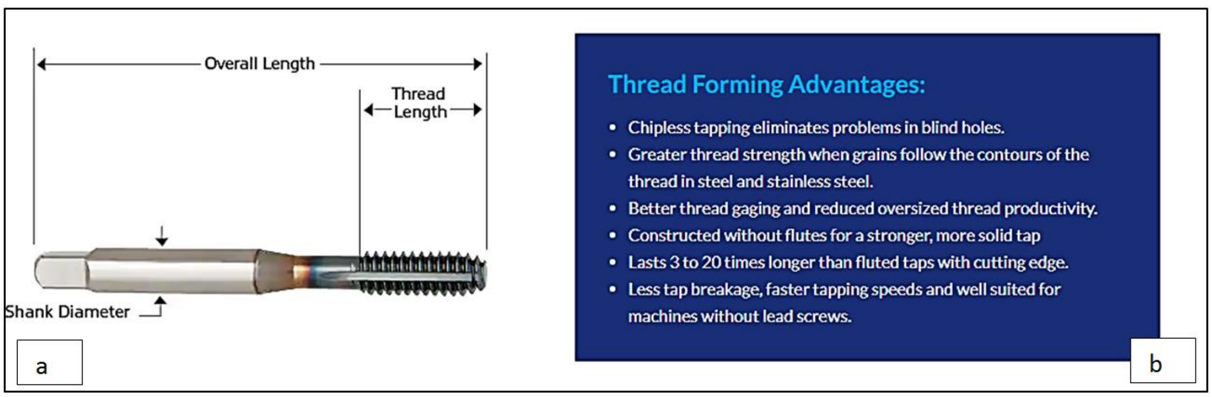

Figure 4-15 (a) Diagram of a thread-forming tap, (b) thread forming advantages

If the tap does not go any further or the desired depth has been reached, it is recommended to release pressure on the tap, as it has likely bottomed out, and to remove the tap from the hole. Applying any more pressure is likely to break the tap. The smaller the tap, the more likely it is to break.

4.3.2. Tapping forces

Tapping of the drilled holes was carried out using Guhring 971 H6 M6 6HX- Carbide taps (Figure 4-16). This tap series are classified as carbide tools, with a significant concentration of cobalt. This concentration enhances the wear resistance of the carbide taps and, more importantly, results in a longer than average tool life.

Figure 4-16 Shape and dimensions of the tapping tool used in the present study

According to Steininger et al [27], the dominant mechanism of wear in tapping is Built up edge because of low machining speed that is usually associated with this process. Thus he concluded that the minimum of the cutting torque is connected to a reduced tendency of BUE and BUL, and hence a longer tool life. Table 4-3 lists the number of drilled and tapped holes whereas Figure 4-17(a) and Figure 4-17(b) compare the tapping forces obtained. For similar tapping parameters, alloys D and E generate the highest cutting forces since these alloys have high silicon content (5-7%), which is consistent with the work of König and Erinski [28]. Note also that for alloy E, the breakage of a tap occurred after 1260 holes, which could indicate that the material is more difficult to machine. As well, the higher slope of the cutting force lines in alloys D and E give the same indication of machining difficulty and the upcoming failure of the tool. A second tapping test was performed for alloy E to validate this result and it was determined that it was possible to tap the same number of holes before tool failure.

Table 4-3 Number of drilled and tapped holes for the five alloys studied

Alloy	Drilling	Tapping
A	2700	2700
B	2700	2700
C	2520	2520
D	2520	2160
E	2340	1260

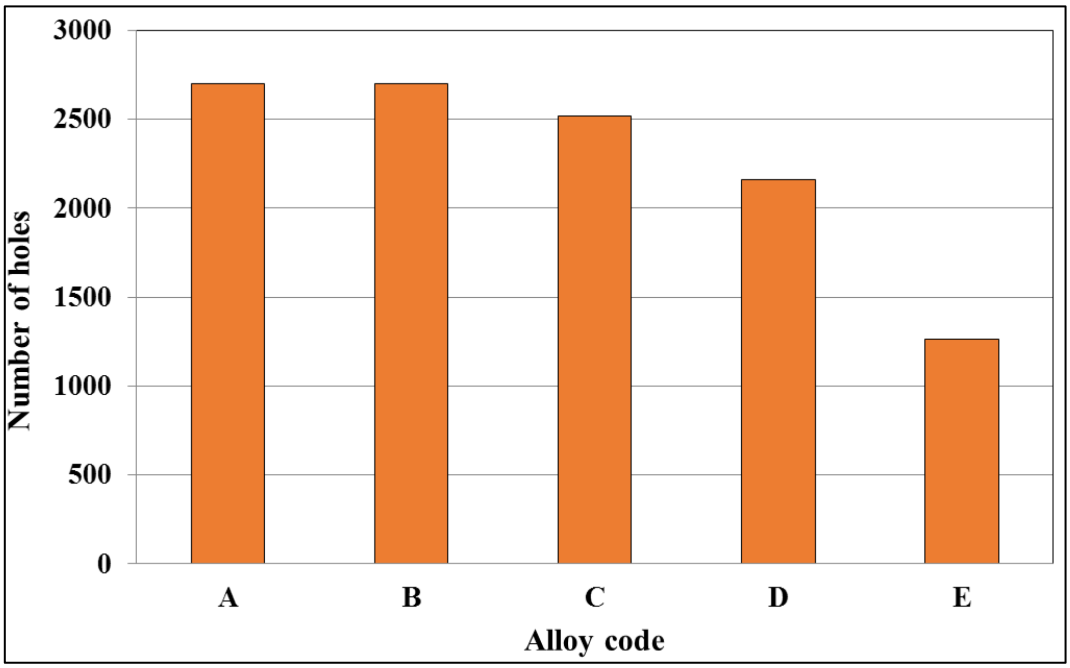

(a)

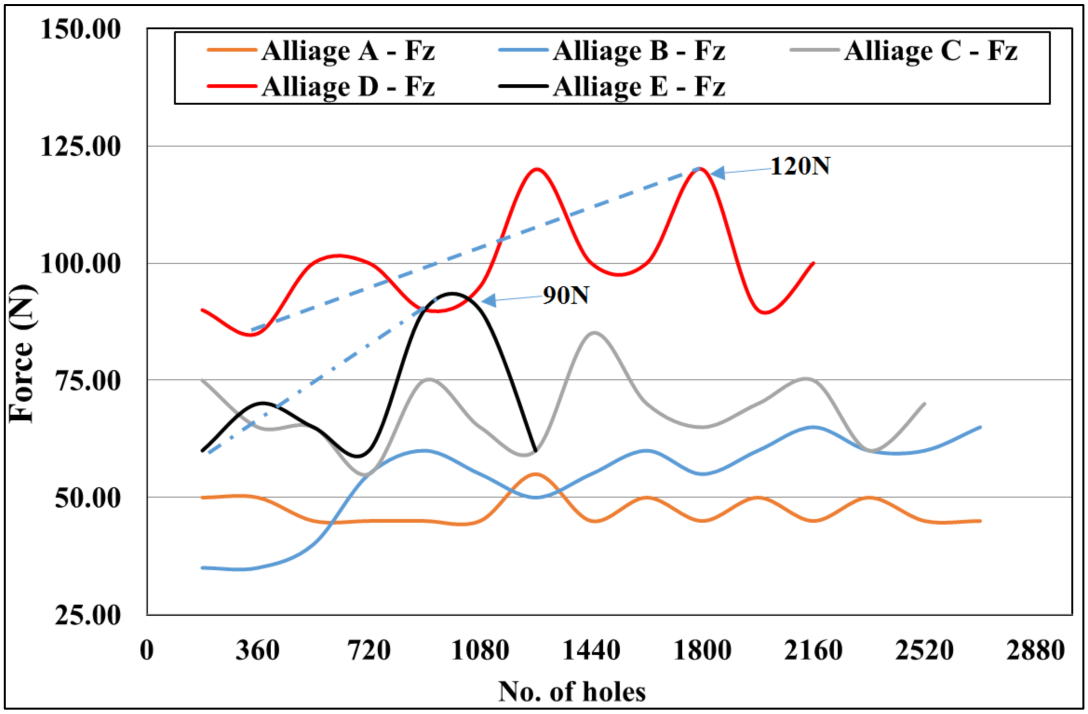

(b)

Figure 4-17 **Effect of alloy type and heat treatment on: (a) number of holes drilled before tool breakage, (b) tapping forces in the Z direction**

4.3.3. Tap wearing

During the microscopic inspection of the tapping tools, no wear could be detected. Figure 4-18 shows no trace of wear or material transfer that could stick on the tools. For this reason, no graph of wear or accumulation of build-up material could be produced. Figure Figure 4-19 illustrates wearing of alloys A, C, D and E at the end of the tapping process. This may indicate that fatigue stress was the main cause of failure, based on the work of Wang [29] and Zhou [30]. However, this would require further investigation, which is currently out of the scope of this thesis.

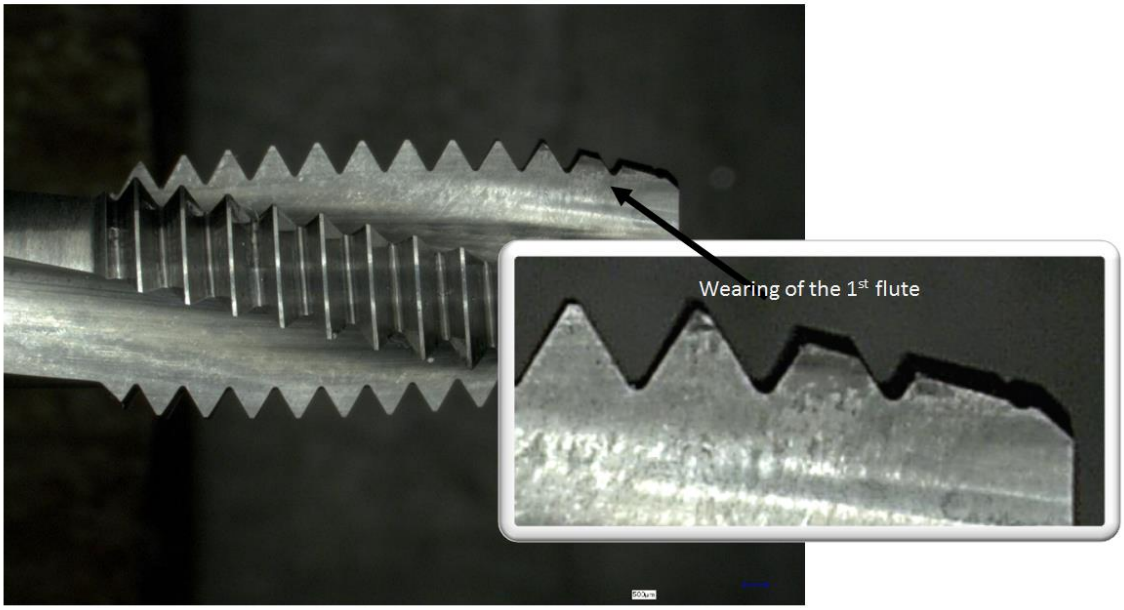

Figure 4-18 Wear of a tap

Figure 4-19 (a)   The photos below show the state of the tool used to tap the alloy A. After 2700 holes, no wear is visible on any of the three flutes.

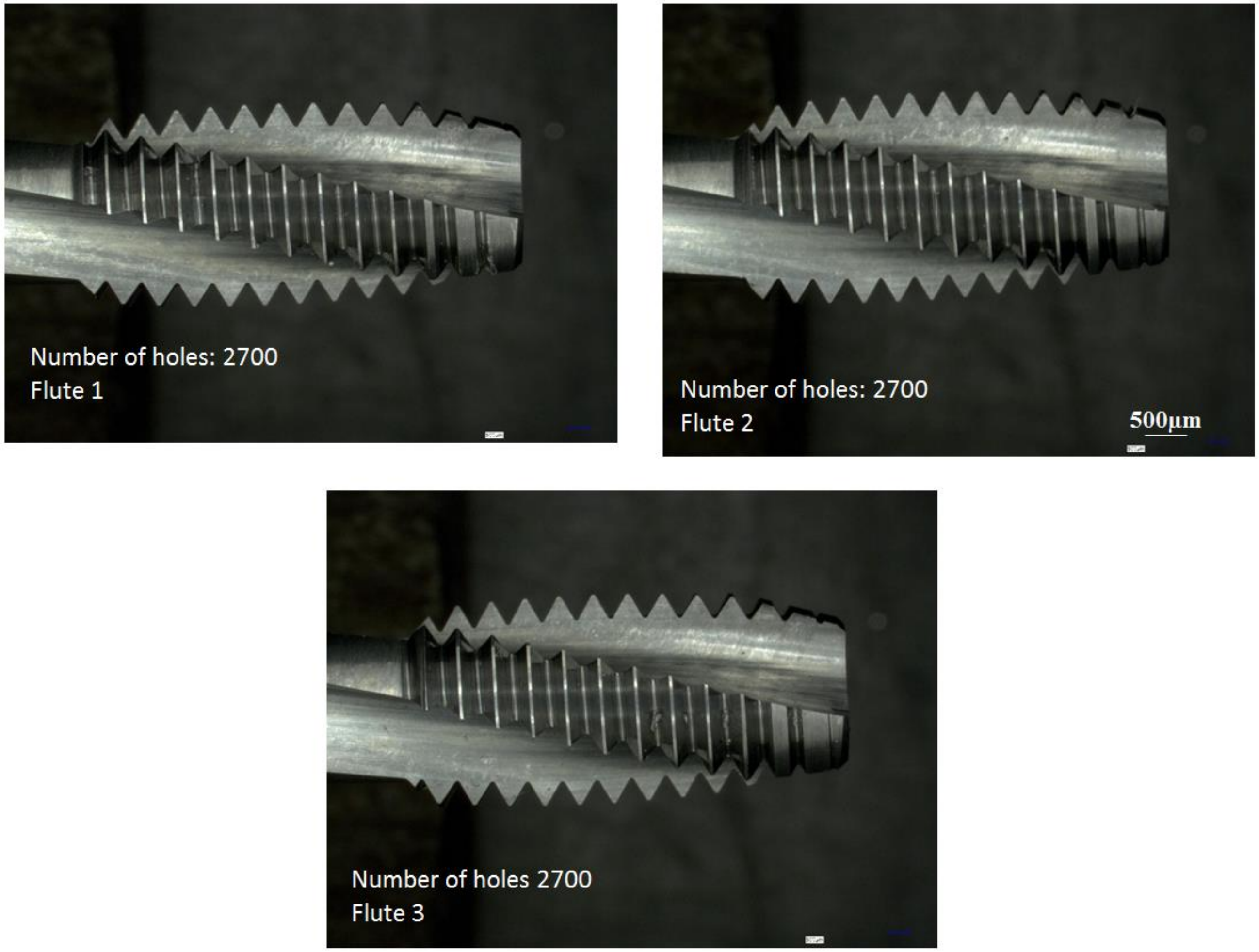

Figure 4-19 (b) **the photos below represent the state of the tool used to tap the C alloy. After 2340 holes, it is noted that there is no wear on any of the three flutes.**

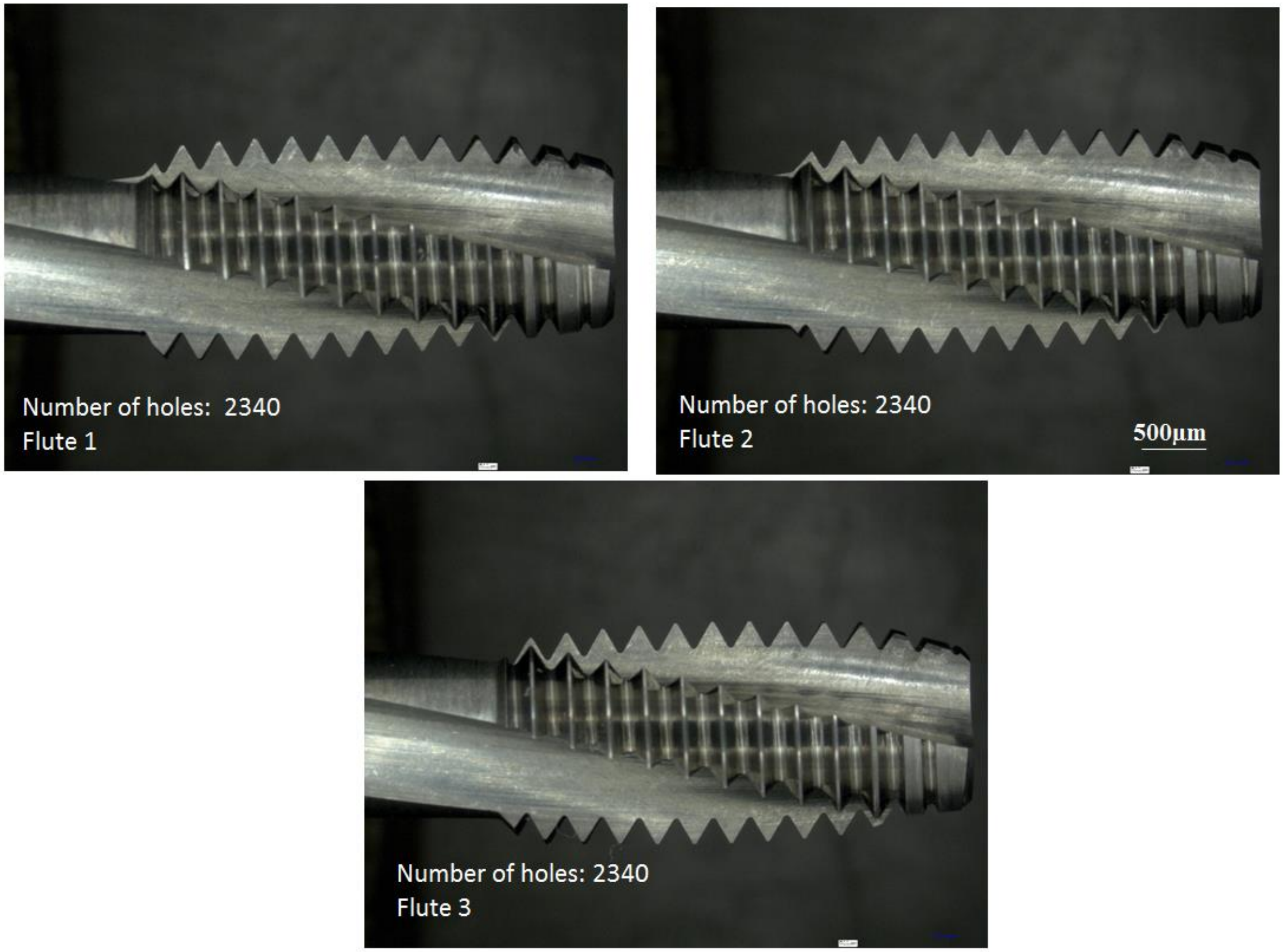

Figure 4-19 (c) The photos below represent the state of the tool used to tap alloy D. After 1620 holes, it is noted that there is no wear on any of the three flutes.

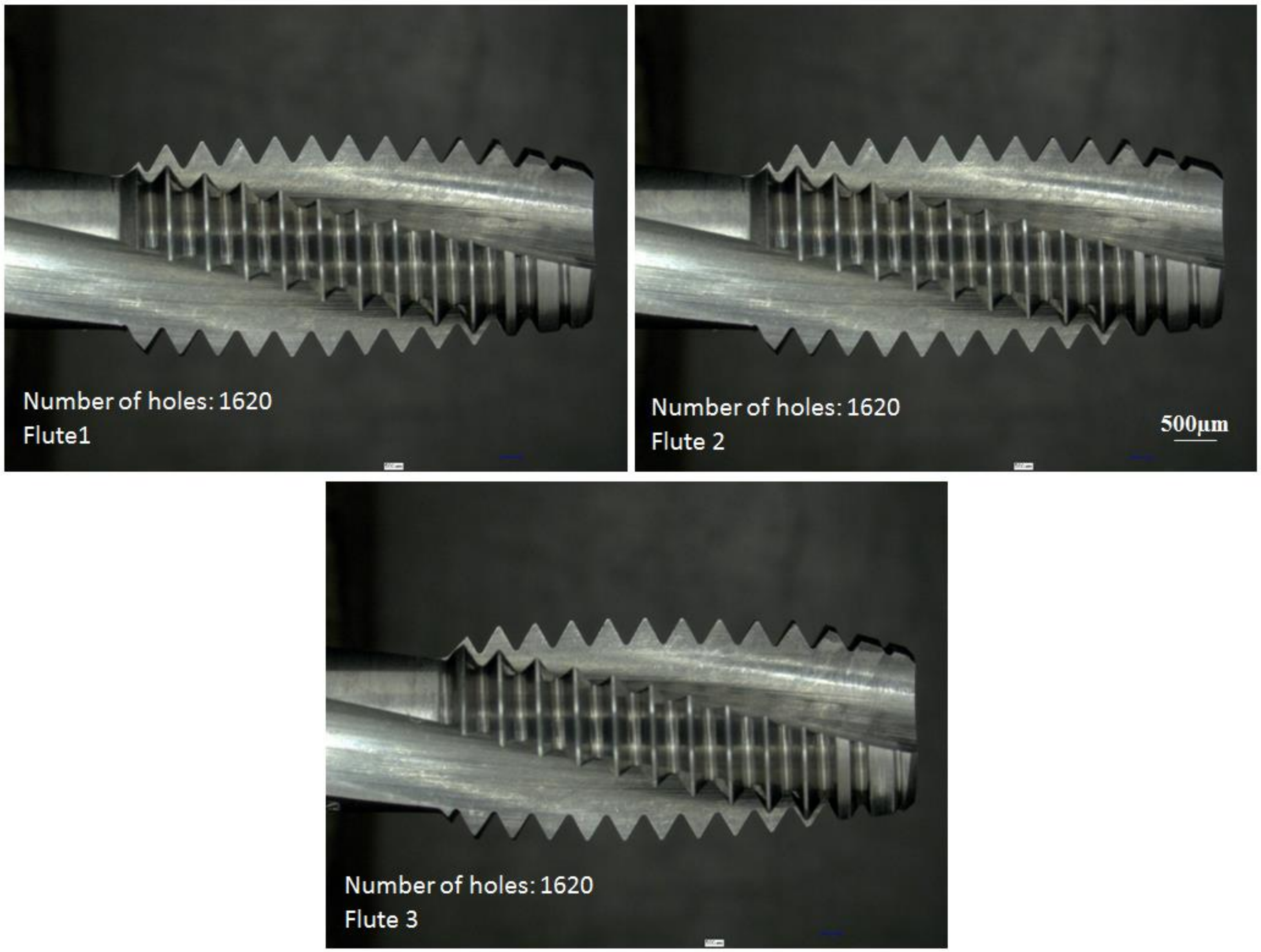

Figure 4-19 (d) The photos below represent the state of the tool used to tap the alloy E. After 1260 holes it is noted that there is no wear on any of the three flutes

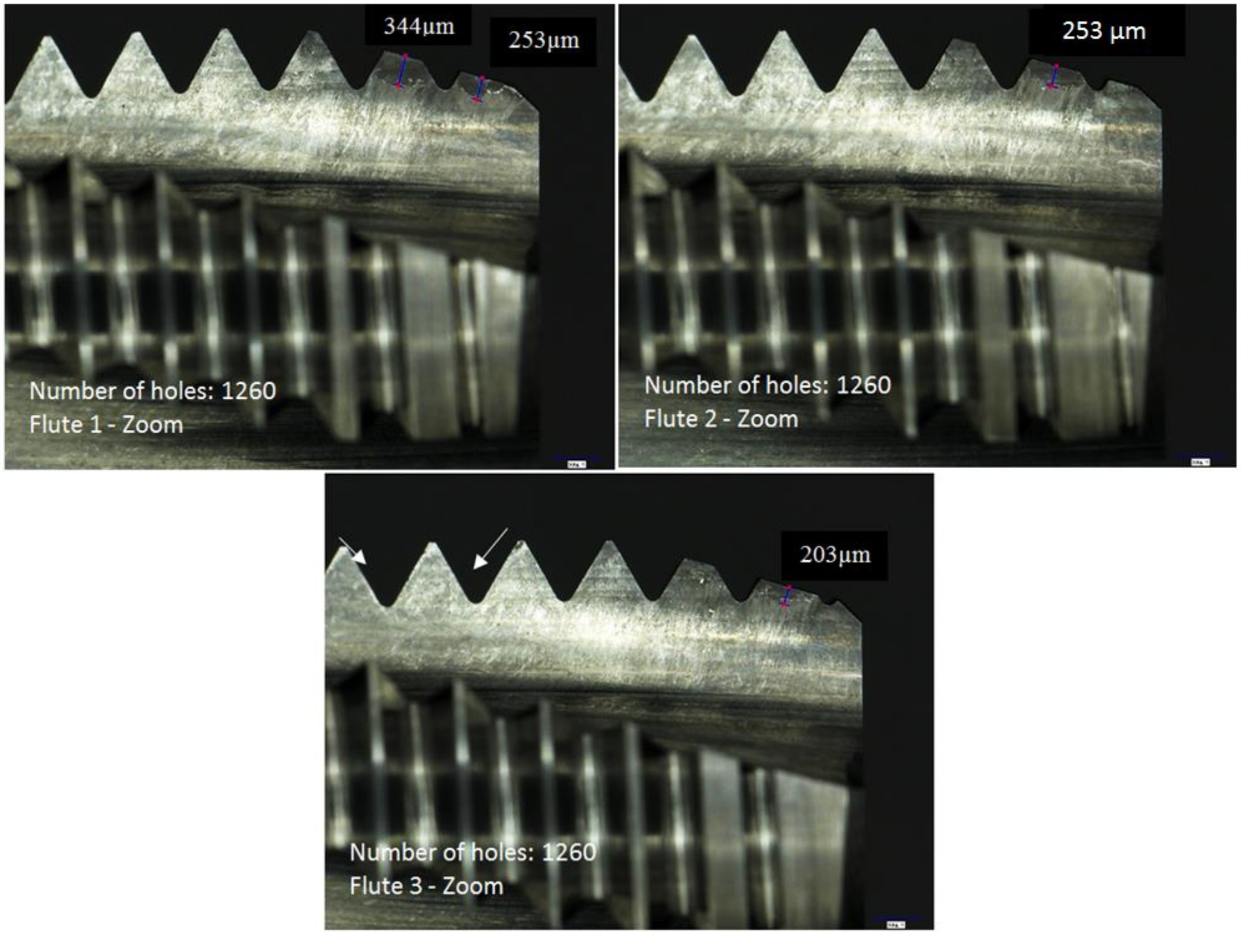

Figure 4-19 Wearing of tapping tools for alloys: (a) A, (b) C, (c) D, (d) E.

4.4. References

1. Kaufman, J.G. and E.L. Rooy, *Aluminum alloy castings : properties, processes, and applications*. 2004, Schaumburg, Ill. : AFS Materials Park, Ohio: ASM International. viii, 340 p.

2. Zedan, Y., *Machinability aspects of heat-treated Al-(6-11)%Si cast alloys : role of intermetallics and free-cutting elements*, in *Aspects de l'usinage des alliages de fonderie Al-(6-11)%Si traités thermiquement rôle des intermétalliques et des éléments de décolletage*. 2010, Université du Québec à Chicoutimi: Chicoutimi]. p. xiv, 217 f.

3. Fang, N. and Q. Wu, *The effects of chamfered and honed tool edge geometry in machining of three aluminum alloys.* International Journal of Machine Tools and Manufacture, 2005. **45**(10): p. 1178-1187.

4. Schneider, G. *Cutting Tool Applications*. 2002; Available from: www.toolingandproduction.com.

5. Soares, R., et al., *Comparison Between Cemented Carbide and PCD Tools on Machinability of a High Silicon Aluminum Alloy.* Journal of Materials Engineering and Performance, 2017. **26**(9): p. 4638-4657.

6. P. Johne, A.-Z.e.V., *TALAT Lecture 3100: Machining of Products*. 1994, European Aluminum Association, Brussels: Dusseldorf.

7. Garza Elizondo, G.H., *Machinability of Al-(7-11%)Si casting alloys : role of free-cutting elements*, in *Aspects de l'usinabilité des alliages de fonderie Al-(7-11)%Si*. 2010, Université du Québec à Chicoutimi: Chicoutimi]. p. xii, 151 f.

8. Mubaraki, B., et al., *Drilling studies of an Al 2 O 3 -Al metal matrix composite - Part I Drill wear characteristics.* Journal of Materials Science, 1995. **30**(24): p. 6273-6280.

9. Tash, M., *Effect of metallurgical parameters on the machining behavior of 356 and 319 alloys (drilling and tapping study)*. 2005, ProQuest Dissertations Publishing.

10. Girgis, A., *Parameters controlling the ambient and elevated temperature tensile properties of Al-Cu and Al-Si cast alloys*. 2018.

11. Samuel, A.M., et al., *New method of eutectic silicon modification in cast Al-Si alloys.* International Journal of Metalcasting, 2017. **11**(3): p. 475-493.

12. G. Pucella, A.M.S., F.H. Samuel, H.W. Doty, S. Valtierra, and American Foundry Society, *Sludge formation in Sr-modified Al-11.5 Wt% Si diecasting alloys.* AFS Transactions, 1999. **107**: p. p. 117-125.

13. Elsharkawi, E.A., F.H. Samuel, E. Simielli and G.K. Sigworth, *Influence of Solutionizing Time, Modification, and Cooling Rate on the Decomposition of Mg-Containing Iron Intermetallic Phase in 357 Alloys*, in *116th Metalcasting Congress*. 2012, Transactions of the American Foundry Society: Columbus, Ohio. p. p. 55-65..

14. Ahn, Y. and S.H. Lee, *Classification and prediction of burr formation in micro drilling of ductile metals.* International Journal of Production Research, 2017. **55**(17): p. 4833-4846.

15. Boothroyd, G. and W.A. Knight, *Fundamentals of machining and machine tools*. 3rd ed. ed. 2006, Boca Raton, Flor.: CRC/Taylor and Francis. 573 p.

16. Farid, A.A., S. Sharif, and M.H. Idris, *Surface integrity study of high-speed drilling of Al–Si alloy using HSS drill.* Proceedings of the Institution of Mechanical Engineers, Part B: Journal of Engineering Manufacture, 2011. **225**(7): p. 1001-1007.

17. Gómez-Parra, A., et al., *Analysis of the evolution of the Built-Up Edge and Built-Up Layer formation mechanisms in the dry turning of aeronautical aluminium alloys.* Wear, 2013. **302**(1-2): p. 1209-1218.

18. Bao, H. and M.G. Stevenson, *An investigation of built-up edge formation in the machining of aluminium.* International Journal of Machine Tool Design and Research, 1976. **16**(3): p. 165-178.

19. Jomaa, W., *Contributions to understanding the high speed machining effects on aeronautic part surface integrity*. 2015, ProQuest Dissertations Publishing.

20. Selvam, M.S. and V. Radhakrishnan, *Influence of side-flow and built-up edge on the roughness and hardness of the surface machined with a single point tool.* Wear, 1973. **26**(3): p. 393-403.

21. Azlan, U.A.A., et al., *Observation of Built-up Edge Formation on a Carbide Cutting Tool with Machining Aluminium Alloy under Dry and Wet Conditions.* MATEC Web of Conferences, 2017. **97**: p. <xocs:firstpage xmlns:xocs=""/>.

22. Kouam, J., et al., *ON CHIP FORMATION DURING DRILLING OF CAST ALUMINUM ALLOYS.* Machining Science and Technology, 2013. **17**(2): p. 228-245.

23. Liu, K., et al., *Investigation on chip morphology and properties in drilling aluminum and titanium stack with double cone drill.* The International Journal of Advanced Manufacturing Technology, 2018. **94**(5): p. 1947-1956.

24. Gonçalves, R.A. and M.B.D. Silva, *Influence of Copper Content on 6351 Aluminum Alloy Machinability.* Procedia Manufacturing, 2015. **1**(C): p. 683-695.

25. De Carvalho, A.O., et al., *Analysis of form threads using fluteless taps in cast magnesium alloy (AM60).* Journal of Materials Processing Technology, 2012. **212**(8): p. 1753-1760.

26. Moni Ribeiro Filho, S., et al., *Analysis of burr formation in form tapping in 7075 aluminum alloy*. The International Journal of Advanced Manufacturing Technology, 2016. **84**(5): p. 957-967.

27. Steininger, A., A. Siller, and F. Bleicher, *Investigations Regarding Process Stability Aspects in Thread Tapping Al-Si Alloys.* Procedia Engineering, 2015. **100**(January): p. 1124-1132.

28. König, W. and D. Erinski, *Machining and Machinability of Aluminium Cast Alloys.* CIRP Annals - Manufacturing Technology, 1983. **32**(2): p. 535-540.

29. Wang, X., et al., *Dynamic reliability sensitivity of cemented carbide cutting tool.* Chinese Journal of Mechanical Engineering, 2014. **27**(1): p. 79-85.

30. Zhou, L., J. Ni, and Q. He, *Study on failure mechanism of the coated carbide tool.* International Journal of Refractory Metals and Hard Materials, 2007. **25**(1): p. 1-5.

CHAPTER 5

CONCLUSIONS AND RECOMMENDATIONS

CHAPTER 5

CONCLUSIONS AND RECOMMENDATIONS

5.1 Conclusions

The present study was carried out to determine the machinability (drilling and tapping) characteristics and tensile properties of a new Al-Cu alloy HT200 and compare its performance with the commercially well-known Al-Si alloys A319.0 and A356.0. The effects of alloying additions and heat treatment were also incorporated. Five alloys were studied, namely HT200 alloy in the as-cast condition (coded A), and T5 and T7 heat treated conditions coded B and C), alloy A319.0 in the T7 condition (coded D), and alloy A356.0 in the T6 peak-aged condition (coded E). Based on the results obtained, the following conclusions may be drawn.

- Alloy HT200 containing 6.5% Cu exhibits comparable yield strength to the Al-Si-Cu A319.0 commercial alloy in T7 heat-treated condition with a higher percent elongation.
- Addition of 200ppm Sr to alloys D and E leads to modification of the eutectic Si particles, separation of the Al-Si eutectic from the Al-Cu eutectic in alloy D, precipitation of α-Fe phase particles within the α-Al network and coarse Mg_2Si particles in the form of Chinese script in alloy E.
- Pulling tensile bars of alloys D and E to failure leads to fracture of the hard brittle Si particles.

- Tool life in drilling tests on Al-Cu alloys regardless the heat treatment can last up to 2700 holes with no signs of failure. In contrast, the tools used for drilling the Al-Si alloys showed commencement of wearing of the cutting edges after 900 holes.
- Analysis of the cutting forces shows that alloy E revealed the highest cutting force in drilling with a significant difference in comparison to the other alloys which showed closed values in cutting forces.
- The cutting forces for each alloy retained more or less same value throughout all the 14 blocks used for each alloy.
- Since alloy D was treated in T7 condition, the cutting forces are close to those obtained from alloy C.
- Accumulation of built up edge showed significant increase in both height and width in alloy C, which may be interpreted by the increase in ductility of the HT200 alloy following heat treatment coupled with its low Si content, in comparison to alloys D and E.
- Alloy C also revealed maximum built up width (after 1200 holes) of about 666µm compared to 384µm obtained from alloy E under the same drilling conditions.
- In all cases, chips were having a conical shape. However, the surfaces of the chips obtained from Al-Cu alloys were somewhat dull compared to the bright surfaces in the case of the Al-Si alloy (alloy E).
- The HT200 alloys revealed excellent machinability with no tap wearing up to 2500-2700 holes. In contrast, for alloy E, the tool was damaged after 1260 holes (almost half those of HT200 alloys) whereas alloy D exhibited the highest machining force, about 120N compared to HT200 alloys (~75N).

- Due to presence of a large amount of hard Si particles (about 55000 particles/mm^2), the tapping tool was damaged after only 1260 holes, reaching 90N cutting force.

5.2 Recommendations for future work

The main aim of this study was to evaluate the machinability characteristics of Al-Cu alloys in comparison to Al-Si cast alloys used in the automotive industry, mainly because of machining problems caused by Silicon particles. The Al-Cu is represented by HT200 alloy and Al-Si is represented by A356 and A319 cast alloys. Generally, the machining aspects of Al-Cu cast alloys are not as well covered as those of Al-Si cast alloys. Thus, for the sake of completing this goal, the following recommendations may be good suggestions for further investigation.

- Studying the behavior of HT200 alloy with different tool materials, to investigate the compatibility of the alloy with different cutting tool materials.
- Investigating the performance of HT200 alloy under dry machining conditions.
- Studying wider aspects of machinability for the HT200 alloy, such as dust formation, heat generation, burr formation, vibration studies and microstructural changes due to cutting.
- Developing the current mathematical models of cutting to predict the cutting forces, and the variation of these forces during the machining cycle, to include engagement and disengagement dynamics using finite element techniques.
- Using artificial neural network techniques and genetic algorithms to predict and optimize the machining performance of HT200 alloys with data-based models.

CHAPTER 6

APPENDICES

6.1 Matlab code used in drilling force analysis

```
clc;
clear all;
close all ;

Fig_Counter =1;
Name = 'ABCDE';
Frequency_Filteration = [50,500,1000,5000];
for Frequency_Index = 1:length(Frequency_Filteration)

for Alloy=1:1
%%%%%%%%%%%%%%%%%%%DEFINING BASIC VARIABLES%%%%%%%%%%%%%%%%%%%%%%%
    Initial = 1;
    Old_Holes = 0;
    frequency = 10000;
    if Alloy ==2
        Final =15;
    else
        Final =14;
    end

    for Block=Initial:Final
%%%%%%%%%%%%%%%%%%%%%%LOADING & CLASSIFYING DATA%%%%%%%%%%%%%%%%%%
        [time,Fx12,Fx34,Fy14,Fy23,Fz1,Fz2,Fz3,Fz4] = Load_File(Name(Alloy),Block);

%%%%%%%%%%%%%%%%%% %%%CALCULATING FORCES%%%%%%%%%%%%%%%%%%%%%%%%%%
        Fx = Fx12 + Fx34;
        Fy = Fy14 + Fy23;
        Fz= Fz1+ Fz2 + Fz3 + Fz4;
        Fs = sqrt(Fx.*Fx + Fy.*Fy);
        Fr = sqrt(Fx.*Fx + Fy.*Fy + Fz.*Fz);

%%%%%%%%%%%%%%%%%%%%%%%%STANDARDIZATION%%%%%%%%%%%%%%%%%%%%%%%%%%%
        [Std_Cycle] = Cycle_Recognition(Fz);
        Peak_Std(1,Block) = (length(Std_Cycle)-1)/2;
        History(Alloy,Block) = (length(Std_Cycle)-1)/2;

        figure()
        plot(time,Fz,'b');
        hold on
        for i=1:length(Std_Cycle)
            line([Std_Cycle(i,2)/frequency Std_Cycle(i,2)/frequency],[ylim])
        end
        title('Fz');
        x=input('Number Of Holes Manual\n');
        fprintf('Manual Result for Alloy %c Block %d is %d Cycle, While Cycle Function Recognized %d Cycle\n',Name(Alloy),Block,x,Peak_Std(1,Block));

        if x ==   Peak_Std(1,Block)
```

```
            Err_fn(Alloy,Block,1) = 1;
        else
            Err_fn(Alloy,Block,1) = -1;
        end

%%%%%%%%%%%%%%%%%%%%%FREQUENCY ANALYSIS%%%%%%%%%%%%%%%%%%%%%%%%%%%
        [Res_x] = Frequency_Analysis(Fx,frequency);
        [Res_y] = Frequency_Analysis(Fy,frequency);
        [Res_z] = Frequency_Analysis(Fz,frequency);

        figure()
        plot(Res_x(:,1),Res_x(:,2))
        title('Fx')

        figure()
        plot(Res_y(:,1),Res_y(:,2))
        title('Fy')

        figure()
        plot(Res_z(:,1),Res_z(:,2))
        title('Fz')

%%%%%%%%%%%%%%%%%%%%%%%%%%FILTERATION%%%%%%%%%%%%%%%%%%%%%%%%%%%%%
        Hx = Fx;
        Hy = Fy;
        Hz = Fz;
        if Frequency_Filteration(Frequency_Index)==5000
            FFx = Fx;
            FFy = Fy;
            FFz = Fz;
        else
            while 1
                Sort = 1;%input('Determine the type of Filteration [1-Digital, 2-Dynamic Avr , 3-Svtsky Gly , 4-Median] \n');

                if Sort ~= 1 && Sort ~= 2 && Sort ~= 3 && Sort ~= 4
                    fprintf('\n Wrong Type \n');
                    continue;
                end

                Nx = Frequency_Filteration(Frequency_Index);%input('\n Frequency Demain Of Filteration of Fx = ');
                Ny = Frequency_Filteration(Frequency_Index);%input('\n Frequency Demain Of Filteration of Fy = ');
                Nz = Frequency_Filteration(Frequency_Index);%input('\n Frequency Demain Of Filteration of Fz = ');

                Loopx = 1;%input('\n Number of Loops Of Filteration of Fx = ');
```

```
                Loopy = 1;%input('\n Number of Loops Of Filteration of Fy = ');
                Loopz = 1;%input('\n Number of Loops Of Filteration of Fz = ');

                [FFx] = Flexible_Filteration(Hx,Sort,Nx,Loopx);
                [FFy] = Flexible_Filteration(Hy,Sort,Ny,Loopy);
                [FFz] = Flexible_Filteration(Hz,Sort,Nz,Loopz);

                figure()
                plot(time,Fx,'b',time,FFx,'r')
                title('Filteration of Fx')
                legend('Fx','FFx')

                figure()
                plot(time,Fy,'b',time,FFy,'r')
                title('Filteration of Fy')
                legend('Fy','FFy')

                figure()
                plot(time,Fz,'b',time,FFz,'r')
                title('Filteration of Fz')
                legend('Fz','FFz')

                xx = input('\n Does The Filteration Of The Forces Suitable?? [1,-1] \n');
                if xx == 1 || Frequency_Filteration(Frequency_Index) == 5000
                    %close all
                    break;
                else
                    xx = input('\n Do you want To Filter The Filtered Signal Or the Original Signal?? [Filtered 1, Original -1] \n');
                    if xx == 1
                        Hx = FFx;
                        Hy = FFy;
                        Hz = FFz;
                    else
                        continue;
                    end
                end
            end
        end

%%%%%%%%%%%%%%%%%%%%%%%%%%%%CORRECTION%%%%%%%%%%%%%%%%%%%%%%%%%%%%
        [Cor_FFx] = FFx;
        [Cor_FFy] = FFy;

        while 1
            limit = 15;%input('\n Demain of Filteration for Origin Correction = ');
            [Origin] = Flexible_Filteration(Fz,1,limit,10);

```

```
            figure()
            plot(time,FFz,'b',time,Origin,'r')
            title('Fz')

            Question = input('Does the Origin fit Logically?? [1,-1] \n');
            if Question ~= 1
                continue;
            end

            [Cor_FFz] = Force_Correction(FFz,Std_Cycle,Origin,0.25);
            Cor_FFz = transpose(Cor_FFz);

            figure()
            plot(time,FFz,'b',time,Cor_FFz,'r')
            title('Fz')
            hold on
            line([xlim],[0,0])
            for i=1:length(Std_Cycle)
                line([Std_Cycle(i,2)/frequency Std_Cycle(i,2)/frequency],[ylim])
            end

            x=input('Does The Corrected Cycle fits Logically for Fz??[1,-1] \n');
            if x ==      1
                close all;
                break;
            else
                fprintf('\n Non Logical Correction\n');
            end
        end

        Cor_FFs = sqrt(Cor_FFx.*Cor_FFx + Cor_FFy.*Cor_FFy);
        Cor_FFr = sqrt(Cor_FFx.*Cor_FFx + Cor_FFy.*Cor_FFy + Cor_FFz.*Cor_FFz);

%%%%%%%%%%%%%%%%%%%%DESIGNING PEAK CRITERIA%%%%%%%%%%%%%%%%%%%%%%%
%This function is designed in order to design peak extraction criteria as a
%percentage of maximum peak of a very filtered signal

        limit = 0.5;%input('\n Filteration For Maximum Peak Calculation = ');
        FFz_01 = Flexible_Filteration(Fz,1,limit,10);
        FFz_00 = Flexible_Filteration(FFz_01,3,701,10);
        [Cor_FFz_00] = Force_Correction(FFz_00,Std_Cycle,Origin,0.25);

        Cor_FFr_01 = Flexible_Filteration(Cor_FFr,1,limit,10);
        Cor_FFr_00 = Flexible_Filteration(Cor_FFr_01,3,701,10);

        Cor_FFx_01 = Flexible_Filteration(Cor_FFx,1,limit,10);
```

```
        Cor_FFx_00 = Flexible_Filteration(Cor_FFx_01,3,701,10);

        Cor_FFy_01 = Flexible_Filteration(Cor_FFy,1,limit,10);
        Cor_FFy_00 = Flexible_Filteration(Cor_FFy_01,3,701,10);

        Cor_FFs_01 = Flexible_Filteration(Cor_FFs,1,limit,10);
        Cor_FFs_00 = Flexible_Filteration(Cor_FFs_01,3,701,10);

        figure()
        plot(time,Cor_FFz,'b',time,Cor_FFz_00,'r')
        title('Fz  As A Peak Criteria')

%%%%%%%%%%%%%%%%%%%%%%%%PEAK EXTRACTION%%%%%%%%%%%%%%%%%%%%%%%%%%%
        while 1
            Percent = input('\n Minimum Peak Percentage of Max Height for Fx = \n');
            for n=3:2:length(Std_Cycle)
                limit = Percent* max(abs(Cor_FFx_00(Std_Cycle(n-2,2):Std_Cycle(n,2)-1)));
                [Peak_Fx(:,1),Peak_Fx(:,2)] = findpeaks(abs(Cor_FFx(Std_Cycle(n-2,2):Std_Cycle(n,2)-1)),'MinPeakDistance',200,'MinPeakProminence',0,'MinPeakHeight',limit,'Threshold',0);

                Final_Peak_Fx((n-1)/2,1) = mean(Peak_Fx(:,1));
                Final_Peak_Fx((n-1)/2,2) = max(Peak_Fx(:,1));
                Final_Peak_Fx((n-1)/2,3) = Std_Cycle(n-1,2);

                clear Peak_Fx
            end

            figure();
plot(time,Fx,'y',time,Cor_FFx,'b',Final_Peak_Fx(:,3)/frequency,Final_Peak_Fx(:,1),'r',Final_Peak_Fx(:,3)/frequency,Final_Peak_Fx(:,2),'m')
            title('Fx');
            x=input('Does The Peak Extraction fits Logically for Fx??[1,-1]\n');
            if x ==      1
                %close all
                break;
            else
                clear Final_Peak_Fx
            end
        end

        while 1
            Percent = input('\n Minimum Peak Percentage of Max Height for Fy = \n');
            for n=3:2:length(Std_Cycle)
                limit = Percent* max(abs(Cor_FFy_00(Std_Cycle(n-2,2):Std_Cycle(n,2)-1)));
```

```
                [Peak_Fy(:,1),Peak_Fy(:,2)] = findpeaks(abs(Cor_FFy(Std_Cycle(n-2,2):Std_Cycle(n,2)-1)),'MinPeakDistance',200,'MinPeakProminence',0,'MinPeakHeight',limit,'Threshold',0);

                Final_Peak_Fy((n-1)/2,1) = mean(Peak_Fy(:,1));
                Final_Peak_Fy((n-1)/2,2) = max(Peak_Fy(:,1));
                Final_Peak_Fy((n-1)/2,3) = Std_Cycle(n-1,2);

                clear Peak_Fy
            end

            figure();
plot(time,Fy,'y',time,Cor_FFy,'b',Final_Peak_Fy(:,3)/frequency,Final_Peak_Fy(:,1),'r',Final_Peak_Fy(:,3)/frequency,Final_Peak_Fy(:,2),'m')
            title('Fy');
            x=input('Does The Peak Extraction fits Logically for Fy??[1,-1]\n');
            if x ==      1
                %close all
                break;
            else
                clear Final_Peak_Fy
            end
        end

        while 1
            Percent = input('\n Minimum Peak Percentage of Max Height for Fz = \n');
            for n=3:2:length(Std_Cycle)
                limit = Percent* max(Cor_FFz_00(Std_Cycle(n-2,2):Std_Cycle(n,2)-1));
                [Peak_Fz(:,1),Peak_Fz(:,2)] = findpeaks(Cor_FFz(Std_Cycle(n-2,2):Std_Cycle(n,2)-1),'MinPeakDistance',200,'MinPeakProminence',0,'MinPeakHeight',limit,'Threshold',0);

                Final_Peak_Fz((n-1)/2,1) = mean(Peak_Fz(:,1));
                Final_Peak_Fz((n-1)/2,2) = max(Peak_Fz(:,1));
                Final_Peak_Fz((n-1)/2,3) = Std_Cycle(n-1,2);

                clear Peak_Fz
            end

            figure();
plot(time,Fz,'y',time,Cor_FFz,'b',Final_Peak_Fz(:,3)/frequency,Final_Peak_Fz(:,1),'r',Final_Peak_Fz(:,3)/frequency,Final_Peak_Fz(:,2),'m')
            title('Fz');
            x=input('Does The Peak Extraction fits Logically for Fz??[1,-1]\n');
```

```
        if x ==      1
            %close all
            break;
        else
            clear Final_Peak_Fz
        end
    end

    while 1
        Percent = input('\n Minimum Peak Percentage of Max Height for Fs = \n');
        for n=3:2:length(Std_Cycle)
            limit = Percent* mean(abs(Cor_FFs_00(Std_Cycle(n-2,2):Std_Cycle(n,2)-1)));
            [Peak_Fs(:,1),Peak_Fs(:,2)] = findpeaks(abs(Cor_FFs(Std_Cycle(n-2,2):Std_Cycle(n,2)-1)),'MinPeakDistance',200,'MinPeakProminence',0,'MinPeakHeight',limit,'Threshold',0);

            Final_Peak_Fs((n-1)/2,1) = mean(Peak_Fs(:,1));
            Final_Peak_Fs((n-1)/2,2) = max(Peak_Fs(:,1));
            Final_Peak_Fs((n-1)/2,3) = Std_Cycle(n-1,2);

            clear Peak_Fs
        end

        figure();
plot(time,Fs,'y',time,Cor_FFs,'b',Final_Peak_Fs(:,3)/frequency,Final_Peak_Fs(:,1),'r',Final_Peak_Fs(:,3)/frequency,Final_Peak_Fs(:,2),'m')
        title('Fs');
        x=input('Does The Peak Extraction fits Logically for Fs??[1,-1]\n');
        if x ==      1
            %close all
            break;
        else
            clear Final_Peak_Fs
        end
    end

    while 1
        Percent = input('\n Minimum Peak Percentage of Max Height for Fr = \n');
        for n=3:2:length(Std_Cycle)
            limit = Percent* max(Cor_FFr_00(Std_Cycle(n-2,2):Std_Cycle(n,2)-1));
            [Peak_Fr(:,1),Peak_Fr(:,2)] = findpeaks(Cor_FFr(Std_Cycle(n-2,2):Std_Cycle(n,2)-1),'MinPeakDistance',200,'MinPeakProminence',0,'MinPeakHeight',limit,'Threshold',0);

            Final_Peak_Fr((n-1)/2,1) = mean(Peak_Fr(:,1));
```

```
                Final_Peak_Fr((n-1)/2,2) = max(Peak_Fr(:,1));
                Final_Peak_Fr((n-1)/2,3) = Std_Cycle(n-1,2);

                clear Peak_Fr
            end

            figure();
plot(time,Fr,'y',time,Cor_FFr,'b',Final_Peak_Fr(:,3)/frequency,Final_Peak_Fr(:,1),'r',Final_Peak_Fr(:,3)/frequency,Final_Peak_Fr(:,2),'m')
            title('Fr')
            x=input('Does The Peak Extraction fits Logically for Fr??[1,-1]\n');
            if x ==      1
                %close all
                break;
            else
                clear Peak_Fr
            end
        end

%%%%%%%%%%%%%%%%%%%%%%%BLOCK FORCE AVARAGE%%%%%%%%%%%%%%%%%%%%%%%
        Peak_Std(2,Block) = mean(Final_Peak_Fx(:,1));
        Peak_Std(3,Block) = mean(Final_Peak_Fy(:,1));
        Peak_Std(4,Block) = mean(Final_Peak_Fz(:,1));
        Peak_Std(5,Block) = mean(Final_Peak_Fs(:,1));
        Peak_Std(6,Block) = mean(Final_Peak_Fr(:,1));

        Peak_Std(7,Block) = mean(Final_Peak_Fx(:,2));
        Peak_Std(8,Block) = mean(Final_Peak_Fy(:,2));
        Peak_Std(9,Block) = mean(Final_Peak_Fz(:,2));
        Peak_Std(10,Block) = mean(Final_Peak_Fs(:,2));
        Peak_Std(11,Block) = mean(Final_Peak_Fr(:,2));

%%%%%%%%%%%%%%%%%%%%%%%%%%DATA MERGING%%%%%%%%%%%%%%%%%%%%%%%%%%%
        Holes = Old_Holes + (length(Std_Cycle)-1)/2;
        for i=Old_Holes + 1: Holes
            Final_Force(i,1) = i;
            Final_Force(i,2) = Final_Peak_Fx(i-Old_Holes,1);
            Final_Force(i,3) = Final_Peak_Fy(i-Old_Holes,1);
            Final_Force(i,4) = Final_Peak_Fz(i-Old_Holes,1);
            Final_Force(i,5) = Final_Peak_Fs(i-Old_Holes,1);
            Final_Force(i,6) = Final_Peak_Fr(i-Old_Holes,1);

            Final_Force(i,7) = Final_Peak_Fx(i-Old_Holes,2);
            Final_Force(i,8) = Final_Peak_Fy(i-Old_Holes,2);
            Final_Force(i,9) = Final_Peak_Fz(i-Old_Holes,2);
            Final_Force(i,10) = Final_Peak_Fs(i-Old_Holes,2);
            Final_Force(i,11) = Final_Peak_Fr(i-Old_Holes,2);
        end
        Old_Holes = Holes;

```

```
        clearvars -except Alloy Block Name Peak_Std Holes Old_Holes Initial Final Final_Force frequency Err_fn History Frequency_Filteration Frequency_Index
    end

%%%%%%%%%%%%%%%%%%%%%%%%%%FORM OF OUTPUT%%%%%%%%%%%%%%%%%%%%%%%%%%
    Row_Header = {'Hole','mean_Fx','mean_Fy','mean_Fz','mean_Fs','mean_Fr','max_Fx','max_Fy','max_Fz','max_Fs','max_Fr'};

    xlswrite(['C:\Users\p2-1020.LABORATOIRE\Desktop\Results\Summerized Force_Final_',num2str(Frequency_Filteration(Frequency_Index)),'.xls'], Peak_Std, Name(Alloy), 'A1')
    xlswrite(['C:\Users\p2-1020.LABORATOIRE\Desktop\Results\Force_Final_',num2str(Frequency_Filteration(Frequency_Index)),'.xls'], Row_Header, Name(Alloy), 'A1')
    xlswrite(['C:\Users\p2-1020.LABORATOIRE\Desktop\Results\Force_Final_',num2str(Frequency_Filteration(Frequency_Index)),'.xls'], Final_Force, Name(Alloy), 'A2')

%%%%%%%%%%%%%%%%%%%%%%%%%%%%%%%%%%%%%%%%%%%%%%%%%%%%%%%%%%%%%%%%%%%
    clearvars -except Alloy Block Name Err_fn History Frequency_Filteration Frequency_Index
end

clear Final_Force
end

%%%%%%%%%%%%%%%%%%%%%%%%%%%%%%%%%%%%%%%%%%%%%%%%%%%%%%%%%%%%%%%%%%%
%%%%%%%%%%%%%%%%%%%%%%DATA LOADING FUNCTION%%%%%%%%%%%%%%%%%%%%%%
%%%%%%%%%%%%%%%%%%%%%%%%%%%%%%%%%%%%%%%%%%%%%%%%%%%%%%%%%%%%%%%%%%%

function [time,Fx12,Fx34,Fy14,Fy23,Fz1,Fz2,Fz3,Fz4] = Load_File(Alloy,Block)

if Block < 10
    filename = (['D:\Master Data\1-Drilling\Alliage_',Alloy,'\',Alloy,'_Plaque_0',num2str(Block),'\', Alloy,'_Plaque_0',num2str(Block),'.mdt']);
    load (filename);
    filename_01 = eval([Alloy,'_Plaque_0',num2str(Block)]);
else
    filename = (['D:\Master Data\1-Drilling\Alliage_',Alloy,'\',Alloy,'_Plaque_',num2str(Block),'\',Alloy,'_Plaque_',num2str(Block),'.mdt']);
    load (filename);
    filename_01 = eval([Alloy,'_Plaque_',num2str(Block)]);
end

time = filename_01(:,1);
Fx12 = filename_01(:,2);
```

```
Fx34 = filename_01(:,3);
Fy14 = filename_01(:,4);
Fy23 = filename_01(:,5);
Fz1 =  filename_01(:,6);
Fz2 =  filename_01(:,7);
Fz3 =  filename_01(:,8);
Fz4 =  filename_01(:,9);

end

%%%%%%%%%%%%%%%%%%%%%%%%%%%%%%%%%%%%%%%%%%%%%%%%%%%%%%%%%%%%%%%%%%
%%%%%%%%%%%%%%%%%%%%%FREQUENCY ANALYSIS FUNCTION%%%%%%%%%%%%%%%%%%
%%%%%%%%%%%%%%%%%%%%%%%%%%%%%%%%%%%%%%%%%%%%%%%%%%%%%%%%%%%%%%%%%%

function [Result] = Frequency_Analysis(Process,frequency)
 NS_Process = fft(Process);
 NSR_Process = fftshift(NS_Process);
 f = linspace(-frequency/2,frequency/2,length(Process));
 Result(:,1) = f(:);
 Result(:,2) = abs(NSR_Process(:));
end

%%%%%%%%%%%%%%%%%%%%%%%%%%%%%%%%%%%%%%%%%%%%%%%%%%%%%%%%%%%%%%%%%%
%%%%%%%%%%%%%%%%%%%%%%%%%FILTERATION FUNCTIONS%%%%%%%%%%%%%%%%%%%%
%%%%%%%%%%%%%%%%%%%%%%%%%%%%%%%%%%%%%%%%%%%%%%%%%%%%%%%%%%%%%%%%%%

function [F_Process] = Flexible_Filteration(Process,type,Range,Loop)
History = Process;

%%Type of filteration
if type == 1
%%%%%%%%%%%%%%%% Using Digital Filter Techniques%%%%%%%%%%%%%%%%%%
    Fil_01 = designfilt('lowpassiir', 'PassbandFrequency', Range, 'StopbandFrequency', Range + 5, 'PassbandRipple', 1, 'StopbandAttenuation', 2, 'SampleRate', 10000);
    F_Process = filtfilt(Fil_01,Process);

elseif type == 2
%%%%%%%%%%%%%%%% Smoothing Using Dynamic Avrage%%%%%%%%%%%%%%%%%%
    Dyn_avrrate = Range;
    Dyn_Coeff = ones(1, Dyn_avrrate)/Dyn_avrrate;

    for i=1:Loop
        F_Process = filter(Dyn_Coeff, 1, Process);
        Process = F_Process;
    end

elseif type == 3
%%%%%%%%%%%%%% Smoothing Using Savitzky-Golay%%%%%%%%%%%%%%%%%%%
    for i=1:Loop
        F_Process = sgolayfilt(Process,5,Range);
        Process = F_Process;
    end
```

```
elseif type == 4
%%%%%%%%%% Spiking Removal using Median Filter Technique%%%%%%%%%
    for i=1:Loop
        F_Process = medfilt1(Process,Range);
        Process = F_Process;
    end
end
end

%%%%%%%%%%%%%%%%%%%%%%%%%%%%%%%%%%%%%%%%%%%%%%%%%%%%%%%%%%%%%%%%%
%%%%%%%%%%%%%%%%%%CYCLE RECOGNITION FUNCTION%%%%%%%%%%%%%%%%%%%
%%%%%%%%%%%%%%%%%%%%%%%%%%%%%%%%%%%%%%%%%%%%%%%%%%%%%%%%%%%%%%%%%

function [Std_Cycle] = Cycle_Recognition(Fz)
%%%%%%%%%%%%%%%%%%%%%STANDARDIZATION%%%%%%%%%%%%%%%%%%%%%%%%%%%%%%
frequency = 10000;
Fil_01 = designfilt('lowpassiir', 'PassbandFrequency', 1,
'StopbandFrequency', 1.1, 'PassbandRipple', 1,
'StopbandAttenuation', 2, 'SampleRate', 10000);
F_Process = filtfilt(Fil_01,Fz);

%%%%%%%%%%%%%%%%%%%DIFFERENTIAL METHOD%%%%%%%%%%%%%%%%%%%%%%%%%%%
    Dif_FProcess = diff(F_Process)*1000;
    Dif_FProcess(length(F_Process))=
Dif_FProcess(length(F_Process)-1);
    Diff_FProcess = diff(Dif_FProcess)*1000;
    Diff_FProcess(length(F_Process))=
Diff_FProcess(length(F_Process)-1);

    Peak_Counter = 1;
    Bot_Counter = 2;

    DM_Bottom(1,1) = 0;
    DM_Bottom(1,2) = 1;

    for i=2:length(F_Process)
        if Diff_FProcess(i) <= 0 && ((Dif_FProcess(i)>=0 &&
Dif_FProcess(i-1)<0) || (Dif_FProcess(i)<0 && Dif_FProcess(i-
1)>=0)) && F_Process(i) > 50
            DM_Peak(Peak_Counter,1) = F_Process(i);
            DM_Peak(Peak_Counter,2) = i;
            Peak_Counter = Peak_Counter+1;
        elseif Diff_FProcess(i) > 0 && ((Dif_FProcess(i)>=0 &&
Dif_FProcess(i-1)<0) || (Dif_FProcess(i)<0 && Dif_FProcess(i-
1)>=0)) && F_Process(i) < 30
            DM_Bottom(Bot_Counter,1) = F_Process(i);
            DM_Bottom(Bot_Counter,2) = i;
            Bot_Counter = Bot_Counter+1;
        end
    end
    DM_Bottom(Bot_Counter,1) = 0;
    DM_Bottom(Bot_Counter,2) = length(F_Process);

```

```
%%%%%%%%%%%%%%%%%%CONDITIONAL PEAK METHOD%%%%%%%%%%%%%%%%%%%%%%%
    [Bottom(:,1), Bottom(:,2)] = findpeaks(-1*F_Process,'MinPeakHeight',-30,'MinPeakDistance',7000);
    [CPM_Peak(:,1), CPM_Peak(:,2)] = findpeaks(F_Process,'MinPeakHeight',50,'MinPeakDistance',7000);
    Bottom(:,1) = -1*Bottom(:,1);

for i=1:length(Bottom)
    CPM_Bottom(i+1,1) = Bottom(i,1);
    CPM_Bottom(i+1,2) = Bottom(i,2);
end
CPM_Bottom(1,1) = 0;
CPM_Bottom(1,2) = 1;
CPM_Bottom(length(Bottom)+2,1) = 0;
CPM_Bottom(length(Bottom)+2,2) = length(F_Process);

%%%%%%%%%%%%%%%%%%ERROR CHECKING PROCEDURE%%%%%%%%%%%%%%%%%%%%%%
if length(CPM_Peak)~= length(DM_Peak)
    error('Peak Number Does not Match Whereas CPM Recognise %d and DM Recognise %d',length(CPM_Peak),length(DM_Peak));
elseif CPM_Peak(:,2) - DM_Peak(:,2) > 2000
    error('Deviation In Peak Recognition');
elseif length(CPM_Peak) >= length(CPM_Bottom)
    error('Bottom Number Does not Match for CPM Calculations');
elseif length(DM_Peak) >= length(DM_Bottom)
    error('Bottom Number Does not Match for DM Calculations');
end

for i=1:length(CPM_Peak)-1
    CPM_Pointer = 0;
    for j=1:length(CPM_Bottom)
        if CPM_Bottom(j,2) < CPM_Peak(i+1,2) && CPM_Bottom(j,2) > CPM_Peak(i,2)
            CPM_Pointer = 1;
            break;
        end
    end
    if CPM_Pointer == 0
        error('Missing Bottom Between Peak %d & %d in CPM Method',i, i+1);
    end
end

for i=1:length(DM_Peak)-1
    DM_Pointer = 0;
    for j=1:length(DM_Bottom)
        if DM_Bottom(j,2) < DM_Peak(i+1,2) && DM_Bottom(j,2) > DM_Peak(i,2)
            DM_Pointer = 1;
            break;
        end
    end
    if DM_Pointer == 0
```

```
        error('Missing Bottom Between Peak %d & %d in DM Method',i, i+1);
    end
end

%%%%%%%%%%%%%%%%%%CREATING STANDARD CYCLE MATRIX%%%%%%%%%%%%%%%%%%
n=1;
for i=1:length(CPM_Peak)
    for j=length(CPM_Bottom):-1:1
        if i==1 && CPM_Bottom(j,2) < CPM_Peak(i,2)
            CPM_Std_Cycle(n,1) = CPM_Bottom(j,1);
            CPM_Std_Cycle(n,2) = CPM_Bottom(j,2);
            CPM_Std_Cycle(n+1,1) = CPM_Peak(i,1);
            CPM_Std_Cycle(n+1,2) = CPM_Peak(i,2);
            n=n+2;
            break;
        elseif CPM_Bottom(j,2) < CPM_Peak(i,2) && CPM_Bottom(j,2) > CPM_Peak(i-1,2)
            CPM_Std_Cycle(n,1) = CPM_Bottom(j,1);
            CPM_Std_Cycle(n,2) = CPM_Bottom(j,2);
            CPM_Std_Cycle(n+1,1) = CPM_Peak(i,1);
            CPM_Std_Cycle(n+1,2) = CPM_Peak(i,2);
            n=n+2;
            break;
        end
    end
end
CPM_Std_Cycle(n,1) = 0;
CPM_Std_Cycle(n,2) = length(F_Process);

n=1;
for i=1:length(DM_Peak)
    for j=length(DM_Bottom):-1:1
        if i==1 && DM_Bottom(j,2) < DM_Peak(i,2)
            DM_Std_Cycle(n,1) = DM_Bottom(j,1);
            DM_Std_Cycle(n,2) = DM_Bottom(j,2);
            DM_Std_Cycle(n+1,1) = DM_Peak(i,1);
            DM_Std_Cycle(n+1,2) = DM_Peak(i,2);
            n=n+2;
            break;
        elseif DM_Bottom(j,2) < DM_Peak(i,2) && DM_Bottom(j,2) > DM_Peak(i-1,2)
            DM_Std_Cycle(n,1) = DM_Bottom(j,1);
            DM_Std_Cycle(n,2) = DM_Bottom(j,2);
            DM_Std_Cycle(n+1,1) = DM_Peak(i,1);
            DM_Std_Cycle(n+1,2) = DM_Peak(i,2);
            n=n+2;
            break;
        end
    end
end
DM_Std_Cycle(n,1) = 0;
DM_Std_Cycle(n,2) = length(F_Process);

```

```
for i=1: length(DM_Std_Cycle)
    Difference(i,1) = i;
    Difference(i,2) = DM_Std_Cycle(i,2) - CPM_Std_Cycle(i,2);
end

for i=1: length(DM_Std_Cycle)
    Std_Cycle(i,1) = (DM_Std_Cycle(i,1) + CPM_Std_Cycle(i,1))/2;
    Std_Cycle(i,2) = (DM_Std_Cycle(i,2) + CPM_Std_Cycle(i,2))/2;
end
end

%%%%%%%%%%%%%%%%%%%%%%%%%%%%%%%%%%%%%%%%%%%%%%%%%%%%%%%%%%%%%%%%%%
%%%%%%%%%%%%%%%%DATA DIVISION INTO CYCLES FUNCTION%%%%%%%%%%%%%%%%
%%%%%%%%%%%%%%%%%%%%%%%%%%%%%%%%%%%%%%%%%%%%%%%%%%%%%%%%%%%%%%%%%%

function [Output] = Data_Devision(Input,Std_Cycle)
for n=3:2:length(Std_Cycle)
    for i = Std_Cycle(n-2,2):Std_Cycle(n,2)-1
        Output(i-Std_Cycle(n-2,2)+1,(n-1)/2) = Input(i);
    end
end
Output(Std_Cycle(length(Std_Cycle),2)-Std_Cycle(length(Std_Cycle)-2,2),(length(Std_Cycle)-1)/2) = Input(Std_Cycle(length(Std_Cycle),2));
end

%%%%%%%%%%%%%%%%%%%%%%%%%%%%%%%%%%%%%%%%%%%%%%%%%%%%%%%%%%%%%%%%%%
%%%%%%%%%%%%%%%%%%%%%%%CORRECTION FUNCTION%%%%%%%%%%%%%%%%%%%%%%%%
%%%%%%%%%%%%%%%%%%%%%%%%%%%%%%%%%%%%%%%%%%%%%%%%%%%%%%%%%%%%%%%%%%

function [Cor_Force] = Force_Correction(Force,Std_Cycle,Origin,Threshold)
if Threshold <1
    Lim = Threshold*max(Force);
    for n=3:2:length(Std_Cycle)
        if Origin(Std_Cycle(n-2,2)) > Lim
            Origin(Std_Cycle(n-2,2))=0;
        end
    end
end

n=3;
for i=1: length(Force)
    if i < Std_Cycle(n,2)
        Cor_Force(i) = Force(i) - Origin(Std_Cycle(n-2,2));
    elseif i== length(Force)
        Cor_Force(i) = Force(i) - Origin(Std_Cycle(n-2,2));
    else
        n=n+2;
        Cor_Force(i) = Force(i) - Origin(Std_Cycle(n-2,2));
    end
end
end
```

6.2 Matlab code used in tapping force analysis

```
clc;
clear all;
close all ;

Fig_Counter =1;
Name = 'ABCDE';
Frequency_Filteration = [50,500,1000,5000];
for Frequency_Index = 1:length(Frequency_Filteration)

    for Alloy=1:5
%%%%%%%%%%%%%%%%DEFINING BASIC VARIABLES%%%%%%%%%%%%%%%%%%%%%%%%%
        Old_Holes = 0;
        frequency = 10000;

        Initial = 1;
        if Alloy == 1 || Alloy == 2
            Final = 15;
        elseif Alloy == 3
            Final = 14;
        elseif Alloy == 4
            Final = 12;
        else
            Final = 7;
        end

        for Block=Initial:Final
%%%%%%%%%%%%%%%%%%%LOADING & CLASSIFYING DATA%%%%%%%%%%%%%%%%%%%%%
            First =1;
            if Alloy == 1 && (Block == 2 || Block == 3 || Block == 4)
                Middle = 1;
            elseif Alloy == 4 && Block == 12
                Middle = 1;
            elseif Alloy == 5 && Block == 7
                Middle = 1;
            elseif Alloy == 5 && Block == 1
                Middle = 1;
            else
                Middle =2;
            end

            for part=First:Middle
                [time,Fx12,Fx34,Fy14,Fy23,Fz1,Fz2,Fz3,Fz4] = Load_File(Name(Alloy),Block,part);

%%%%%%%%%%%%%%%%%%%%%%CALCULATING FORCES%%%%%%%%%%%%%%%%%%%%%%%%%%
                Fx = Fx12 + Fx34;
                Fy = Fy14 + Fy23;
                AFx = abs(Fx);
                AFy = abs(Fy);
                Fz= Fz1+ Fz2 + Fz3 + Fz4;
```

```
                Fs = sqrt(Fx.*Fx + Fy.*Fy);
                Fr = sqrt(Fx.*Fx + Fy.*Fy + Fz.*Fz);

                x = input('\n Do you want to plot row data?? [1,-1] \n');
                if x==1
                    figure()
                    subplot(2,3,1)
                    plot(time,abs(Fx),'b')
                    title(sprintf('Fx for Block %d Part %d alloy %c', Block, part, Name(Alloy)))
                    subplot(2,3,2)
                    plot(time,abs(Fy),'b')
                    title(sprintf('Fy for Block %d Part %d alloy %c', Block, part, Name(Alloy)))
                    subplot(2,3,3)
                    plot(time,abs(Fz),'b')
                    title(sprintf('Fz for Block %d Part %d alloy %c', Block, part, Name(Alloy)))
                    subplot(2,3,4)
                    plot(time,Fs,'b')
                    title(sprintf('Fs for Block %d Part %d alloy %c', Block, part, Name(Alloy)))
                    subplot(2,3,5)
                    plot(time,Fr,'b')
                    title(sprintf('Fr for Block %d Part %d alloy %c', Block, part, Name(Alloy)))
                    subplot(2,3,6)
plot(time,Fx,'b',time,Fy,'r',time,Fz,'k',time,Fs,'m',time,Fr,'g')
                    title(sprintf('Fx, Fy, Fz, Fs, Fr for Block %d Part %d alloy %c', Block, part, Name(Alloy)))
                end

%%%%%%%%%%%%%%%%%%%%%%FREQUENCY ANALYSIS%%%%%%%%%%%%%%%%%%%%%%%%%%
                [Res_x] = Frequency_Analysis(Fx,frequency);
                [Res_y] = Frequency_Analysis(Fy,frequency);
                [Res_z] = Frequency_Analysis(Fz,frequency);

                x = input('\n Do you want to get Frequency Analysis?? [1,-1] \n');
                if x==1
                    figure()
                    plot(Res_x(:,1),Res_x(:,2))
                    title('Fx')

                    figure()
                    plot(Res_y(:,1),Res_y(:,2))
                    title('Fy')

                    figure()
                    plot(Res_z(:,1),Res_z(:,2))
                    title('Fz')
                end
```

```
%%%%%%%%%%%%%%%%%%%%%%%%STANDARDIZATION%%%%%%%%%%%%%%%%%%%%%%%%%%
                [Std_Cycle] = Cycle_Recognition(Fy);
                Peak_Std(1,part+(Block-1)*2) = (length(Std_Cycle)-1)/2;
                History(Alloy,Block,part) = (length(Std_Cycle)-1)/2;

                x= input('Number Of Holes Manual\n');
                fprintf('Manual Result for Alloy %c Block %d is %d Cycle, While Cycle Function Recognized %d Cycle\n',Name(Alloy),Block,x,Peak_Std(1,part+(Block-1)*2));

                figure()
                plot(time,Fz,'b');
                hold on
                for i=1:length(Std_Cycle)
                    line([Std_Cycle(i,2)/frequency Std_Cycle(i,2)/frequency],[ylim])
                end
                title('Fz');

                if x ==   Peak_Std(1,part+(Block-1)*2)
                    Err_fn(Alloy,part+(Block-1)*2,1) = 1;
                else
                    Err_fn(Alloy,part+(Block-1)*2,1) = -1;
                end
%%%%%%%%%%%%%%%%%%%%%%%%%%%FILTERATION%%%%%%%%%%%%%%%%%%%%%%%%%%%
                Hx = Fx;
                Hy = Fy;
                Hz = Fz;
                if Frequency_Filteration(Frequency_Index)==5000
                    FFx = Fx;
                    FFy = Fy;
                    FFz = Fz;
                else
                    while 1
                        Sort = 1;%input('Determine the type of Filteration [1-Digital, 2-Dynamic Avr , 3-Svtsky Gly , 4-Median] \n');

                        if Sort ~= 1 && Sort ~= 2 && Sort ~= 3 && Sort ~= 4
                            fprintf('\n Wrong Type \n');
                            continue;
                        end

                        Nx = Frequency_Filteration(Frequency_Index);%input('\n Frequency Demain Of Filteration of Fx = ');
                        Ny = Frequency_Filteration(Frequency_Index);%input('\n Frequency Demain Of Filteration of Fy = ');
```

```
                Nz = Frequency_Filteration(Frequency_Index);%input('\n Frequency Demain Of Filteration of Fz = ');

                Loopx = 1;%input('\n Number of Loops Of Filteration of Fx = ');
                Loopy = 1;%input('\n Number of Loops Of Filteration of Fy = ');
                Loopz = 1;%input('\n Number of Loops Of Filteration of Fz = ');

                [FFx] = Flexible_Filteration(Hx,Sort,Nx,Loopx);
                [FFy] = Flexible_Filteration(Hy,Sort,Ny,Loopy);
                [FFz] = Flexible_Filteration(Hz,Sort,Nz,Loopz);

                figure()
                plot(time,Fx,'b',time,FFx,'r')
                title('Filteration of Fx')
                legend('Fx','FFx')

                figure()
                plot(time,Fy,'b',time,FFy,'r')
                title('Filteration of Fy')
                legend('Fy','FFy')

                figure()
                plot(time,Fz,'b',time,FFz,'r')
                title('Filteration of Fz')
                legend('Fz','FFz')

                xx = input('\n Does The Filteration Of The Forces Suitable?? [1,-1] \n');
                if xx == 1 || Frequency_Filteration(Frequency_Index) == 5000
                    %close all
                    break;
                else
                    xx = input('\n Do you want To Filter The Filtered Signal Or the Original Signal?? [Filtered 1, Original -1] \n');
                    if xx == 1
                        Hx = FFx;
                        Hy = FFy;
                        Hz = FFz;
                    else
                        continue;
                    end
                end
            end
        end

```

```
%%%%%%%%%%%%%%%%%%%%%%%%%%%CORRECTION%%%%%%%%%%%%%%%%%%%%%%%%%%%%%
                limit = 10;
                [Originx] = Flexible_Filteration(Fx,1,limit,10);
                [Originy] = Flexible_Filteration(Fy,1,limit,10);
                [Originz] = Flexible_Filteration(Fz,1,limit,10);

                [Cor_FFx] = Force_Correction(FFx,Std_Cycle,Originx,0.25);
                Cor_FFx = transpose(Cor_FFx);
                [Cor_FFy] = Force_Correction(FFy,Std_Cycle,Originy,0.25);
                Cor_FFy = transpose(Cor_FFy);
                [Cor_FFz] = Force_Correction(FFz,Std_Cycle,Originz,0.25);
                Cor_FFz = transpose(Cor_FFz);

                Cor_FFs = sqrt(Cor_FFx.*Cor_FFx + Cor_FFy.*Cor_FFy);
                Cor_FFr = sqrt(Cor_FFx.*Cor_FFx + Cor_FFy.*Cor_FFy + Cor_FFz.*Cor_FFz);

                figure()
                plot(time,Fx,'y',time,FFx,'b',time,Cor_FFx,'r')
                title('Fx Before and After Correction')

                figure()
                plot(time,Fy,'y',time,FFy,'b',time,Cor_FFy,'r')
                title('Fy Before and After Correction')

                figure()
                plot(time,Fz,'y',time,FFz,'b',time,Cor_FFz,'r')
                title('Fz Before and After Correction')

%%%%%%%%%%%%%%%%%%%%DESIGNING PEAK CRITERIA%%%%%%%%%%%%%%%%%%%%%%%
%This function is designed in order to design peak extraction criteria as a
%percentage of maximum peak of a very filtered signal

        limit = 15;%input('\n Filteration For Maximum Peak Calculation = ');

        Cor_FFz_00 = Flexible_Filteration(Cor_FFz,1,limit,10);
        Cor_FFx_00 = Flexible_Filteration(Cor_FFx,1,limit,10);
        Cor_FFy_00 = Flexible_Filteration(Cor_FFy,1,limit,10);
        Cor_FFs_00 = Flexible_Filteration(Cor_FFs,1,limit,10);
        Cor_FFr_00 = Flexible_Filteration(Cor_FFr,1,limit,10);

%%%%%%%%%%%%%%%%%%%%%%%%PEAK EXTRACTION%%%%%%%%%%%%%%%%%%%%%%%%%%%
        while 1
            Percent = input('\n Minimum Peak Percentage of Max Height for Fx = \n');
            for n=3:2:length(Std_Cycle)
                limit = Percent* max(abs(Cor_FFx_00(Std_Cycle(n-2,2):Std_Cycle(n,2)-1)));
```

```
            [Peak_Fx(:,1),Peak_Fx(:,2)] = findpeaks(abs(Cor_FFx(Std_Cycle(n-2,2):Std_Cycle(n,2)-1)),'MinPeakDistance',200,'MinPeakProminence',0,'MinPeakHeight',limit,'Threshold',0);

            Final_Peak_Fx((n-1)/2,1) = mean(Peak_Fx(:,1));
            Final_Peak_Fx((n-1)/2,2) = max(Peak_Fx(:,1));
            Final_Peak_Fx((n-1)/2,3) = Std_Cycle(n-1,2);

            clear Peak_Fx
        end

        figure();
        plot(time,Fx,'y',time,Cor_FFx,'b',Final_Peak_Fx(:,3)/frequency,Final_Peak_Fx(:,1),'r',Final_Peak_Fx(:,3)/frequency,Final_Peak_Fx(:,2),'m')
        title('Fx');
        x=input('Does The Peak Extraction fits Logically for Fx??[1,-1]\n');
        if x ==      1
            close all
            break;
        else
            clear Final_Peak_Fx
        end
    end

    while 1
        Percent = input('\n Minimum Peak Percentage of Max Height for Fy = \n');
        for n=3:2:length(Std_Cycle)
            limit = Percent* max(abs(Cor_FFy_00(Std_Cycle(n-2,2):Std_Cycle(n,2)-1)));
            [Peak_Fy(:,1),Peak_Fy(:,2)] = findpeaks(abs(Cor_FFy(Std_Cycle(n-2,2):Std_Cycle(n,2)-1)),'MinPeakDistance',200,'MinPeakProminence',0,'MinPeakHeight',limit,'Threshold',0);

            Final_Peak_Fy((n-1)/2,1) = mean(Peak_Fy(:,1));
            Final_Peak_Fy((n-1)/2,2) = max(Peak_Fy(:,1));
            Final_Peak_Fy((n-1)/2,3) = Std_Cycle(n-1,2);

            clear Peak_Fy
        end

        figure();
        plot(time,Fy,'y',time,Cor_FFy,'b',Final_Peak_Fy(:,3)/frequency,Final_Peak_Fy(:,1),'r',Final_Peak_Fy(:,3)/frequency,Final_Peak_Fy(:,2),'m')
        title('Fy');
        x=input('Does The Peak Extraction fits Logically for Fy??[1,-1]\n');
```

```
            if x == 1
                %close all
                break;
            else
                clear Final_Peak_Fy
            end
        end

        while 1
            Percent = input('\n Minimum Peak Percentage of Max Height for Fz = \n');
            for n=3:2:length(Std_Cycle)
                limit = Percent* max(abs(Cor_FFz_00(Std_Cycle(n-2,2):Std_Cycle(n,2)-1)));
                [Peak_Fz(:,1),Peak_Fz(:,2)] = findpeaks(abs(Cor_FFz(Std_Cycle(n-2,2):Std_Cycle(n,2)-1)),'MinPeakDistance',200,'MinPeakProminence',0,'MinPeakHeight',limit,'Threshold',0);

                Final_Peak_Fz((n-1)/2,1) = mean(Peak_Fz(:,1));
                Final_Peak_Fz((n-1)/2,2) = max(Peak_Fz(:,1));
                Final_Peak_Fz((n-1)/2,3) = Std_Cycle(n-1,2);

                clear Peak_Fz
            end

            figure();
plot(time,Fz,'y',time,Cor_FFz,'b',Final_Peak_Fz(:,3)/frequency,Final_Peak_Fz(:,1),'r',Final_Peak_Fz(:,3)/frequency,Final_Peak_Fz(:,2),'m')
            title('Fz');
            x=input('Does The Peak Extraction fits Logically for Fz??[1,-1]\n');
            if x ==      1
                %close all
                break;
            else
                clear Final_Peak_Fz
            end
        end

        while 1
            Percent = input('\n Minimum Peak Percentage of Max Height for Fs = \n');
            for n=3:2:length(Std_Cycle)
                limit = Percent* mean(abs(Cor_FFs_00(Std_Cycle(n-2,2):Std_Cycle(n,2)-1)));
                [Peak_Fs(:,1),Peak_Fs(:,2)] = findpeaks(abs(Cor_FFs(Std_Cycle(n-2,2):Std_Cycle(n,2)-1)),'MinPeakDistance',200,'MinPeakProminence',0,'MinPeakHeight',limit,'Threshold',0);

                Final_Peak_Fs((n-1)/2,1) = mean(Peak_Fs(:,1));
```

```
                Final_Peak_Fs((n-1)/2,2) = max(Peak_Fs(:,1));
                Final_Peak_Fs((n-1)/2,3) = Std_Cycle(n-1,2);

                clear Peak_Fs
            end

            figure();
            plot(time,Fs,'y',time,Cor_FFs,'b',Final_Peak_Fs(:,3)/frequency,Final_Peak_Fs(:,1),'r',Final_Peak_Fs(:,3)/frequency,Final_Peak_Fs(:,2),'m')
            title('Fs');
            x=input('Does The Peak Extraction fits Logically for Fs??[1,-1]\n');
            if x ==      1
                %close all
                break;
            else
                clear Final_Peak_Fs
            end
        end

        while 1
            Percent = input('\n Minimum Peak Percentage of Max Height for Fr = \n');
            for n=3:2:length(Std_Cycle)
                limit = Percent* max(Cor_FFr_00(Std_Cycle(n-2,2):Std_Cycle(n,2)-1));
                [Peak_Fr(:,1),Peak_Fr(:,2)] = findpeaks(Cor_FFr(Std_Cycle(n-2,2):Std_Cycle(n,2)-1),'MinPeakDistance',200,'MinPeakProminence',0,'MinPeakHeight',limit,'Threshold',0);

                Final_Peak_Fr((n-1)/2,1) = mean(Peak_Fr(:,1));
                Final_Peak_Fr((n-1)/2,2) = max(Peak_Fr(:,1));
                Final_Peak_Fr((n-1)/2,3) = Std_Cycle(n-1,2);

                clear Peak_Fr
            end

            figure();
            plot(time,Fr,'y',time,Cor_FFr,'b',Final_Peak_Fr(:,3)/frequency,Final_Peak_Fr(:,1),'r',Final_Peak_Fr(:,3)/frequency,Final_Peak_Fr(:,2),'m')
            title('Fr')
            x=input('Does The Peak Extraction fits Logically for Fr??[1,-1]\n');
            if x ==      1
                %close all
                break;
            else
                clear Peak_Fr
            end
```

```
        end

%%%%%%%%%%%%%%%%%%%%%%BLOCK FORCE AVARAGE%%%%%%%%%%%%%%%%%%%%%%%%%
        Peak_Std(2,part+(Block-1)*2) = mean(Final_Peak_Fx(:,1));
        Peak_Std(3,part+(Block-1)*2) = mean(Final_Peak_Fy(:,1));
        Peak_Std(4,part+(Block-1)*2) = mean(Final_Peak_Fz(:,1));
        Peak_Std(5,part+(Block-1)*2) = mean(Final_Peak_Fs(:,1));
        Peak_Std(6,part+(Block-1)*2) = mean(Final_Peak_Fr(:,1));

        Peak_Std(7,part+(Block-1)*2) = mean(Final_Peak_Fx(:,2));
        Peak_Std(8,part+(Block-1)*2) = mean(Final_Peak_Fy(:,2));
        Peak_Std(9,part+(Block-1)*2) = mean(Final_Peak_Fz(:,2));
        Peak_Std(10,part+(Block-1)*2) = mean(Final_Peak_Fs(:,2));
        Peak_Std(11,part+(Block-1)*2) = mean(Final_Peak_Fr(:,2));

%%%%%%%%%%%%%%%%%%%%%%%%%%%DATA MERGING%%%%%%%%%%%%%%%%%%%%%%%%%%%%
        Holes = Old_Holes + (length(Std_Cycle)-1)/2;
        for i=Old_Holes + 1: Holes
            Final_Force(i,1) = i;
            Final_Force(i,2) = (Block-1)*180 + (part-1)*90 + (i-Old_Holes);
            Final_Force(i,3) = Final_Peak_Fx(i-Old_Holes,1);
            Final_Force(i,4) = Final_Peak_Fy(i-Old_Holes,1);
            Final_Force(i,5) = Final_Peak_Fz(i-Old_Holes,1);
            Final_Force(i,6) = Final_Peak_Fs(i-Old_Holes,1);
            Final_Force(i,7) = Final_Peak_Fr(i-Old_Holes,1);

            Final_Force(i,8) = Final_Peak_Fx(i-Old_Holes,2);
            Final_Force(i,9) = Final_Peak_Fy(i-Old_Holes,2);
            Final_Force(i,10) = Final_Peak_Fz(i-Old_Holes,2);
            Final_Force(i,11) = Final_Peak_Fs(i-Old_Holes,2);
            Final_Force(i,12) = Final_Peak_Fr(i-Old_Holes,2);
        end
        Old_Holes = Holes;
        clearvars -except Alloy Block part Name Peak_Std Holes Old_Holes Initial Final First Middle Final_Force frequency Err_fn History Frequency_Filteration Frequency_Index
            end
        end

%%%%%%%%%%%%%%%%%%%%%%%%%%FORM OF OUTPUT%%%%%%%%%%%%%%%%%%%%%%%%%%
    Row_Header = {'Hole','Hole Number','mean_Fx','mean_Fy','mean_Fz','mean_Fs','mean_Fr','max_Fx','max_Fy','max_Fz','max_Fs','max_Fr'};

    xlswrite(['C:\Users\p2-1020.LABORATOIRE\Desktop\Results\Summerized Tapping Force_',num2str(Frequency_Filteration(Frequency_Index)),'.xls'], Peak_Std, Name(Alloy), 'A1')
    xlswrite(['C:\Users\p2-1020.LABORATOIRE\Desktop\Results\Tapping Force_',num2str(Frequency_Filteration(Frequency_Index)),'.xls'], Row_Header, Name(Alloy), 'A1')
```

```
    xlswrite(['C:\Users\p2-1020.LABORATOIRE\Desktop\Results\Tapping Force_',num2str(Frequency_Filteration(Frequency_Index)),'.xls'], Final_Force, Name(Alloy), 'A2')

    clearvars -except Alloy Block part Name Initial Final First Middle Frequency_Filteration Frequency_Index History

    end
end

%%%%%%%%%%%%%%%%%%%%%%%%%%%%%%%%%%%%%%%%%%%%%%%%%%%%%%%%%%%%%%%%%%%%
%%%%%%%%%%%%%%%%%%%%%%%%DATA LOADING FUNCTION%%%%%%%%%%%%%%%%%%%%%
%%%%%%%%%%%%%%%%%%%%%%%%%%%%%%%%%%%%%%%%%%%%%%%%%%%%%%%%%%%%%%%%%%%%
function [time,Fx12,Fx34,Fy14,Fy23,Fz1,Fz2,Fz3,Fz4] = Load_File(Alloy,Block, part)
if part ==1
    if Block < 10
        filename = (['D:\Master Data\2-Tapping\Alliage_',Alloy,'\',Alloy,'_Plaque_0',num2str(Block),'\',Alloy,'_Plaque_0',num2str(Block),'.mdt']);
        load (filename);
        filename_01 = eval([Alloy,'_Plaque_0',num2str(Block)]);
    else
        filename = (['D:\Master Data\2-Tapping\Alliage_',Alloy,'\',Alloy,'_Plaque_',num2str(Block),'\',Alloy,'_Plaque_',num2str(Block),'.mdt']);
        load (filename);
        filename_01 = eval([Alloy,'_Plaque_',num2str(Block)]);
    end
else
    if Block < 10
        filename = (['D:\Master Data\2-Tapping\Alliage_',Alloy,'\',Alloy,'_Plaque_0',num2str(Block),'_Middle\',Alloy,'_Plaque_0',num2str(Block),'_Middle.mdt']);
        load (filename);
        filename_01 = eval([Alloy,'_Plaque_0',num2str(Block),'_Middle']);
    else
        filename = (['D:\Master Data\2-Tapping\Alliage_',Alloy,'\',Alloy,'_Plaque_',num2str(Block),'_Middle\',Alloy,'_Plaque_',num2str(Block),'_Middle.mdt']);
        load (filename);
        filename_01 = eval([Alloy,'_Plaque_',num2str(Block),'_Middle']);
    end
end

time = filename_01(:,1);
Fx12 = filename_01(:,2);
Fx34 = filename_01(:,3);
Fy14 = filename_01(:,4);
Fy23 = filename_01(:,5);
Fz1 =  filename_01(:,6);
```

```
Fz2 =  filename_01(:,7);
Fz3 =  filename_01(:,8);
Fz4 =  filename_01(:,9);
end

%%%%%%%%%%%%%%%%%%%%%%%%%%%%%%%%%%%%%%%%%%%%%%%%%%%%%%%%%%%%%%%%%
%%%%%%%%%%%%%%%%%%%FREQUENCY ANALYSIS FUNCTION%%%%%%%%%%%%%%%%%%%
%%%%%%%%%%%%%%%%%%%%%%%%%%%%%%%%%%%%%%%%%%%%%%%%%%%%%%%%%%%%%%%%%
function [Result] = Frequency_Analysis(Process,frequency)
 NS_Process = fft(Process);
 NSR_Process = fftshift(NS_Process);
 f = linspace(-frequency/2,frequency/2,length(Process));
 Result(:,1) = f(:);
 Result(:,2) = abs(NSR_Process(:));
end

%%%%%%%%%%%%%%%%%%%%%%%%%%%%%%%%%%%%%%%%%%%%%%%%%%%%%%%%%%%%%%%%%
%%%%%%%%%%%%%%%%%%%%%FILTERATION FUNCTIONS%%%%%%%%%%%%%%%%%%%%%%%
%%%%%%%%%%%%%%%%%%%%%%%%%%%%%%%%%%%%%%%%%%%%%%%%%%%%%%%%%%%%%%%%%
function [F_Process] = Flexible_Filteration(Process,type,Range,Loop)
History = Process;

%%Type of filteration
if type == 1
%%%%%%%%%%%%%%%%% Using Digital Filter Techniques%%%%%%%%%%%%%%%%
    Fil_01 = designfilt('lowpassiir', 'PassbandFrequency', Range, 'StopbandFrequency', Range + 5, 'PassbandRipple', 1, 'StopbandAttenuation', 2, 'SampleRate', 10000);
    F_Process = filtfilt(Fil_01,Process);

elseif type == 2
%%%%%%%%%%%%%%% Smoothing Using Dynamic Avrage%%%%%%%%%%%%%%%%%%%
    Dyn_avrrate = Range;
    Dyn_Coeff = ones(1, Dyn_avrrate)/Dyn_avrrate;

    for i=1:Loop
        F_Process = filter(Dyn_Coeff, 1, Process);
        Process = F_Process;
    end

elseif type == 3
%%%%%%%%%%%%%%% Smoothing Using Savitzky-Golay%%%%%%%%%%%%%%%%%%%
    for i=1:Loop
        F_Process = sgolayfilt(Process,5,Range);
        Process = F_Process;
    end

elseif type == 4
%%%%%%%%% Spiking Removal using Median Filter Technique%%%%%%%%%%
    for i=1:Loop
        F_Process = medfilt1(Process,Range);
        Process = F_Process;
    end
```

```
end
end

%%%%%%%%%%%%%%%%%%%%%%%%%%%%%%%%%%%%%%%%%%%%%%%%%%%%%%%%%%%%%%%%%%%%
%%%%%%%%%%%%%%%%%%%%%CYCLE RECOGNITION FUNCTION%%%%%%%%%%%%%%%%%%%%%
%%%%%%%%%%%%%%%%%%%%%%%%%%%%%%%%%%%%%%%%%%%%%%%%%%%%%%%%%%%%%%%%%%%%
function [Std_Cycle] = Cycle_Recognition(Process)
%%%%%%%%%%%%%%%%%%%%%%%%%%%%STANDARDIZATION%%%%%%%%%%%%%%%%%%%%%%%%%
frequency = 10000;
Type = 'F';
Range = 1;
Loop = 1;
Fil_01 = designfilt('lowpassiir', 'PassbandFrequency', Range,
'StopbandFrequency', Range+2, 'PassbandRipple', 1,
'StopbandAttenuation', 2, 'SampleRate', 10000);
F_Process = filtfilt(Fil_01,Process);
F_Process = F_Process.*F_Process;
%%%%%%%%%%%%%%%%%%%%%%CONDITIONAL PEAK METHOD%%%%%%%%%%%%%%%%%%%%%%%
[CPM_Peak(:,1), CPM_Peak(:,2)] =
findpeaks(F_Process,'MinPeakHeight',250,'MinPeakDistance',8000);

CPM_Bottom(1,1) = 0;
CPM_Bottom(1,2) = 1;
for i=1:length(CPM_Peak)-1
    CPM_Bottom(i+1,2) = ceil((CPM_Peak(i,2)+CPM_Peak(i+1,2))/2);
    CPM_Bottom(i+1,1) = 0;
end

CPM_Bottom(length(CPM_Peak)+2,1) = 0;
CPM_Bottom(length(CPM_Peak)+2,2) = length(F_Process);

%%%%%%%%%%%%%%%%CREATING STANDARD CYCLE MATRIX%%%%%%%%%%%%%%%%%%%%%%
n=1;
for i=1:length(CPM_Peak)
    for j=length(CPM_Bottom):-1:1
        if i==1 && CPM_Bottom(j,2) < CPM_Peak(i,2)
            CPM_Std_Cycle(n,1) = CPM_Bottom(j,1);
            CPM_Std_Cycle(n,2) = CPM_Bottom(j,2);
            CPM_Std_Cycle(n+1,1) = CPM_Peak(i,1);
            CPM_Std_Cycle(n+1,2) = CPM_Peak(i,2);
            n=n+2;
            break;
        elseif CPM_Bottom(j,2) < CPM_Peak(i,2) && CPM_Bottom(j,2)
> CPM_Peak(i-1,2)
            CPM_Std_Cycle(n,1) = CPM_Bottom(j,1);
            CPM_Std_Cycle(n,2) = CPM_Bottom(j,2);
            CPM_Std_Cycle(n+1,1) = CPM_Peak(i,1);
            CPM_Std_Cycle(n+1,2) = CPM_Peak(i,2);
            n=n+2;
            break;
        end
    end
end
CPM_Std_Cycle(n,1) = 0;
```

```
CPM_Std_Cycle(n,2) = length(F_Process);

Std_Cycle = CPM_Std_Cycle;
Std_Cycle(1,2) = 1;
end

%%%%%%%%%%%%%%%%%%%%%%%%%%%%%%%%%%%%%%%%%%%%%%%%%%%%%%%%%%%%%%%%%%
%%%%%%%%%%%%%%%DATA DIVISION INTO CYCLES FUNCTION%%%%%%%%%%%%%%
%%%%%%%%%%%%%%%%%%%%%%%%%%%%%%%%%%%%%%%%%%%%%%%%%%%%%%%%%%%%%%%%%%

function [Output] = Data_Devision(Input,Std_Cycle)
for n=3:2:length(Std_Cycle)
    for i = Std_Cycle(n-2,2):Std_Cycle(n,2)-1
        Output(i-Std_Cycle(n-2,2)+1,(n-1)/2) = Input(i);
    end
end
Output(Std_Cycle(length(Std_Cycle),2)-Std_Cycle(length(Std_Cycle)-2,2),(length(Std_Cycle)-1)/2) = Input(Std_Cycle(length(Std_Cycle),2));
end

%%%%%%%%%%%%%%%%%%%%%%%%%%%%%%%%%%%%%%%%%%%%%%%%%%%%%%%%%%%%%%%%%%
%%%%%%%%%%%%%%%%%%%%%%%%CORRECTION FUNCTION%%%%%%%%%%%%%%%%%%%%%%
%%%%%%%%%%%%%%%%%%%%%%%%%%%%%%%%%%%%%%%%%%%%%%%%%%%%%%%%%%%%%%%%%%

function [Cor_Force] = Force_Correction(Force,Std_Cycle,Origin,Threshold)
if Threshold <1
    Lim = Threshold*max(Force);
    for n=3:2:length(Std_Cycle)
        if Origin(Std_Cycle(n-2,2)) > Lim
            Origin(Std_Cycle(n-2,2))=0;
        end
    end
end

n=3;
for i=1: length(Force)
    if i < Std_Cycle(n,2)
        Cor_Force(i) = Force(i) - Origin(Std_Cycle(n-2,2));
    elseif i== length(Force)
        Cor_Force(i) = Force(i) - Origin(Std_Cycle(n-2,2));
    else
        n=n+2;
        Cor_Force(i) = Force(i) - Origin(Std_Cycle(n-2,2));
    end
end
end
```